Resonance Raman Study on a Mechanism of Quaternary Structural Change of Human Hemoglobin A

NAGATOMO Shigenori

Part I

Part II

Publications

Main papers

1. UV Resonance Raman Studies of α-Nitrosyl Hemoglobin Derivatives: Relation between the α_1-β_2 Subunit Interface Interactions and the Fe-Histidine Bonding of α heme

Nagatomo, S., Nagai, M., Tsuneshige, A., T. Yonetani, T., and Kitagawa, T.
Biochemistry 38, 9659-9666 (1999)

2. Differences in Changes of the α1-β2 Subunit Contacts between Ligand Binding to the α and β Subunits of Hemoglobin A: UV Resonance Raman Analysis Using Ni-Fe Hybrid Hemoglobin

Nagatomo, S., Nagai, M., Shibayama, N., and Kitagawa, T.
*Biochemistry 41***,** 10010 –10020 (2002).

3. Changes in the Abnormal α-Subunit upon CO-Binding to the Normal β-Subunit of Hb M Boston: Resonance Raman, EPR, and CD Study

Nagatomo, S., Jin, Y., Nagai, M., Hori, H., and Kitagawa, T.
Biophysical Chemistry 98, 217-232 (2002).

4. Resonance Raman Revisit to Influences of Strong Allosteric Effectors, on Quaternary Structure Changes of Hemoglobin

Nagatomo, S., Nagai, M., Mizutani, Y., Yonetani, T., and Kitagawa, T.
To be submitted.

5. Coordination Geometry of Cu-porphyrin in Cu(II)-Fe(II) Hybrid Hemoglobins Studied by Q-band EPR and Resonance Raman Spectroscopies

Venkatesh, B., Hori, H., Miyazaki, G., **Nagatomo, S.,** Kitagawa, T., and Morimoto, H.
J. Inorg. Biochemistry 88, 310-315 (2002).

6. Heme Structure of Hemoglobin M Iwate [α87(F8)His→Tyr]: A UV and Visible Resonance Raman Study

Nagai, M., Aki, M., Li, R., Jin, Y., Sakai, H., **Nagatomo, S.,** and Kitagawa, T.
Biochemistry 39, 13093-13105 (2000).

7. Quaternary Structure Sensitive Tyrosine Residues in Human Hemoglobin: UV Resonance Raman Studies of Mutants at α140, β35, and β145 Tyrosine
Nagai, M., Wajcman, H., Lahary, A., Nakatsukasa, T., **Nagatomo, S.,** and Kitagawa, T.
Biochemistry 38, 1243-1251 (1999).

8. Functional Regulation of Myoglobin by Iron Corrphycene
Neya, S., Funasaki, N., Hori, H., Imai, K., **Nagatomo, S.,** Iwase, T., and Yonetani, T.
Chem. Lett. 1999, 989-990.

9. Iron Hemiporphycene as a Functional Prosthetic Group for Myoglobin
Neya, S., Imai, K., Hori, H., Ishikawa, H., Ishimori, K., Okuno, D., **Nagatomo, S.,** Hoshino, T., Hata, M., and Funasaki, N.
Inorg. Chem. in press.

Related papers

10. UV Resonance Raman and NMR Spectroscopic Studies on the pH Dependent Metal Ion Release from Pseudoazurin
Sato, K., **Nagatomo, S.,** Dennison, C., Niizeki, T., Kitagawa, T., and Kohzuma, T.
Inorg. Chim. Acta 339, 383-392 (2002).

11. A Bis(μ-oxo)dicopper(III) Complex with Aromatic Nitrogen Donors: Structural Characterization and Reversible Conversion between Copper(I) and Bis(μ-oxo)dicopper(III) Species
Hayashi, H., Fujinami, S., **Nagatomo, S.,** Ogo, S., Suzuki, M., Uehara, A., Watanabe, Y., and Kitagawa, T.
J. Am. Chem. Soc. 122, 2124-2125 (2002).

12. Fine-Tuning of Copper(I)-Dioxygen Reactivity by 2-(2-Pyridyl)ethylamine Bidentate Ligands
Taki, M., Teramae, S., **Nagatomo, S.,** Tachi, Y., Kitagawa, T., Itoh, S., and Fukuzumi, S.
J. Am. Chem. Soc. 124, 6367-6377 (2002).

13. A New Mononuclear Iron(III) Complex Containing a Peroxocarbonate Ligand
Hashimoto, K., **Nagatomo, S.,** Fujinami, S., Furutachi, F., Ogo, S., Suzuki, M., Uehara, A., Maeda, Y., Watanabe, Y., and Kitagawa, T.
Angew. Chem., Int. Ed. 41, 1202-1205 (2002).

14. Low-Temperature Stopped-Flow Studies on the Reactions of Copper(II) Complexes and H_2O_2: The First Detection of a Mononuclear Copper(II)-Peroxo Intermediate
Osako, T., **Nagatomo, S.,** Tachi, Y., Kitagawa, T., and Itoh, S.
Angew. Chem., Int. Ed. 41, 4325-4328 (2002).

15. Modulation of the Copper-Dioxygen Reactivity by Stereochemical Effect of Tetradentate Tripodal Ligands
Hayashi, H., Uozumi, K., Fujinami, S., **Nagatomo, S.,** Shiren, K., Furutachi, H., Suzuki, M., Uehara, A., and Kitagawa, T.

Chem. Lett. 2002, 416-417.

16. Reactivity of Hydroperoxide Bound to a Mononuclear Non-Heme Iron Site
Wada, A., Ogo, S., **Nagatomo, S.,** Kitagawa, T., Watanabe, Y., Jitsukawa, K., and Masuda, H.
Inorg. Chem. 41, 616-618 (2002).

17. Effects of Metal Ions on Physicochemical Properties and Redox Reactivity of Phenolates and Phenoxyl Radicals: Mechanistic Insight into Hydrogen Atom Abstraction by Phenoxyl Radical-Metal Complexes
Itoh, S., Kumei, H., **Nagatomo, S.,** Kitagawa, T., and Fukuzumi, S.
J. Am. Chem. Soc. 123, 2165-2175 (2001).

18. Oxygenation of Phenols to Catechols by A (μ^2:η^2-Peroxo)dicopper(II) Complex: Mechanistic Insight into the Phenolase Activity of Tyrosinase
Itoh, S., Kumei, H., Taki, M., **Nagatomo, S.,** Kitagawa, T., and Fukuzumi, S.
J. Am. Chem. Soc. 123, 6708-6709 (2001).

19. Formation, Characterization, and Reactivity of Bis(μ-oxo)dinickel(III) Complexes Supported by A Series of Bis[2-(2-pyridyl)ethyl]amine Ligands
Itoh, S., Bandoh, H., Nakagawa, M., **Nagatomo, S.,** Kitagawa, T., Karlin, K. D., and Fukuzumi, S.
J. Am. Chem. Soc. 123, 11168-11178 (2001).

20. Identification of Tyrosine Residues Involved in Ligand Recognition by the Phosphatidylinositol 3-Kinase Src Homology 3 Domain: Circular Dichroism and UV Resonance Raman Studies
Okishio, N., Tanaka, T., Nagai, M., Fukuda, R., **Nagatomo, S.,** and Kitagawa, T.
Biochemistry 40, 15797-15804 (2001).

21. Characterization of Imidazolate-Bridged Dinuclear and Mononuclear Hydroperoxo Complexes
Ohtsu, H., Itoh, S., **Nagatomo, S.,** Kitagawa, T., Ogo, S., Watanabe, Y., and Fukuzumi, S.
Inorg. Chem. 40, 3200-3207 (2001).

22. Effects of Metal Ions on the Electronic, Redox, and Catalytic Properties of Cofactor TTQ of Quinoprotein Amine Dehydrogenases

Itoh, S., Taniguchi, M., Takada, N., **Nagatomo, S.,** Kitagawa, T., and Fukuzumi, S.
J. Am. Chem. Soc. 122, 12087-12097 (2000).

23. Model Complexes for the Active Form of Galactose Oxidase. Physicochemical Properties of Cu(II)- and Zn(II)-Phenoxyl Radical Complexes

Itoh, S., Taki, M., Kumei, H., Takayama, S., **Nagatomo, S.,** Kitagawa, T., Sakurada, N., Arakawa, R., and Fukuzumi, S.
Inorg. Chem. 39, 3708-3711 (2000).

24. A novel Diiron Complex as a Functional Model for Hemerythrin

Arii, H., **Nagatomo, S.,** Kitagawa, T., Miwa, T., Jitsukawa, K., Einaga, H., and Masuda, H.
J. Inorg. Biochemistry 82, 153-162 (2000).

25. Interactions of Phosphatidylinositol 3-Kinase Src Homology 3 Domain with Its Ligand Peptide Studied by Absorption, Circular Dichroism, and UV Resonance Raman Spectroscopies

Okishio, N., Nagai, M., Fukuda, R., **Nagatomo, S.,** and Kitagawa, T.
Biopolymers 57, 208-217 (2000).

26. Active Site Models for Galactose Oxidase Containing Two Different Phenol Groups

Taki, M., Kumei, H., **Nagatomo, S.,** Kitagawa, T., Itoh, S., and Fukuzumi, S.
Inorg. Chim. Acta 300, 622-632 (2000).

27. Characterization of Imidazolate-Bridged Cu(II)-Zn(II) Heterodinuclear and Cu(II)-Cu(II) Homodinuclear Hydroperoxo Complexes as Reaction Intermediate Models of Cu,Zn-SOD

Ohtsu, H., Itoh, S., **Nagatomo, S.,** Kitagawa, T., Ogo, S., Watanabe, Y., and Fukuzumi, S.
Chem. Commun. 2000, 1051-1052.

28. Oxidation of Benzyl Alcohol with Cu^{II} and Zn^{II} Complexes of the Phenoxyl Radical as a Model of the Reaction of Galactose Oxidase

Itoh, S., Taki, M., Takayama, S., **Nagatomo, S.,** Kitagawa, T., Sakurada, N., and Arakawa, R., and Fukuzumi, S.
Angew Chem., Int. Ed. 38, 2774-2776 (1999).

29. The Structure and Unusual pH Dependence of Plastocyanin from the Fern *Dryopteris Crassirhizoma*
The Protonation of an Active Site Histidine is Hindered by π-π interactions
Kohzuma, T., Inoue, T., Yoshizaki, F., Sasakawa, Y., Onodera, K., **Nagatomo, S.,** Kitagawa, T., Uzawa, S., Isobe, Y., Sugimura, Y., Gotowda, M., and Kai, Y.
J. Biol. Chem. 274, 11817-11823 (1999).

30. Aliphatic Hydroxylation by a Bis(μ-oxo)dinickel(III) Complex
Itoh, S., Bandoh, H., **Nagatomo, S.,** Kitagawa, T., and Fukuzumi, S.
J. Am. Chem. Soc. 121, 8945-8946 (1999).

31. Tyrosine Phosphorylation-Induced Changes in Absorption and UV Resonance Raman Spectra of Src-Peptides
Okishio, N., Fukuda, R., Nagai, M., Nagai, Y., **Nagatomo, S.,** and Kitagawa, T.
J. Raman Spectrosc. 29, 31-39 (1998).

32. Spectroscopic Characterization and Kinetic Studies of a Novel Plastocyanin from the Green Alga *Ulva Pertusa*
Sasakawa, Y., Onodera, K., Karasawa, M., Im, S.-C., Suzuki, E., Yoshizaki, F., Sugimura, Y., Shibata, N., Inoue, T., Kai, Y., **Nagatomo, S.,** Kitagawa, T., and Kohzuma, T.
Inorg. Chim. Acta 283, 184-192 (1998).

Other paper

33. Hydrogen Bonds in Crystalline Imidazoles Studied by N-15 NMR and *ab initio* MO Calculations
Ueda, T., **Nagatomo, S.,** Masui, H., Nakamura, N., and Hayashi, S.
Z. Naturforsch. 54a, 437-442 (1999).

Summary The quaternary structural change of human hemoglobin A (Hb A) was studied by resonance Raman spectroscopy. The quaternary structural change of Hb A occurs upon ligand (oxygen, carbon monoxide (CO) and nitric oxide (NO)) binding to hemes and has a close correlation with oxygen affinity and cooperativity. It is known that no ligand-bound form of Hb A (deoxyHb A) adopts T (tense) structure with the low affinity extreme and that fully ligand-bound form of Hb A (COHb A) adopts R (relaxed) structure with the high affinity extreme. The most important problem to be answered for the quaternary structural change of Hb is when and how it occurs. However, generally it is difficult to detect a partially ligand-bound form of Hb A in a solution condition, because most of Hb A molecules are present in either no ligand-bound form or fully ligand-bound form. Therefore, in this study were selected the following Hbs in which a partially ligand-bound form can be stabilized in solution conditions: NOHb, Ni-Fe hybrid Hb, and Hb M Boston.

In Part I the results from ultraviolet resonance Raman (UVRR) studies on NOHb ($\alpha^{NO}\beta^{deoxy}$), Ni-Fe hybrid Hb ($\alpha^{Ni}\beta^{CO}$ and $\alpha^{CO}\beta^{Ni}$), and Hb M Boston ($(\alpha^{Mmet}\beta^{CO})$ will be discussed. NOHb has the property that NO binds heme more strongly than CO. As the dissociation rate of NO is quite different between the α-heme and β-heme, it is possible to prepare a stable intermediate in which NO is bound only to α-heme. In this case, a condition of the Fe-His bond can be controlled by pH or addition of IHP: the heme can be made five- or six-coordinate state. Therefore the author can investigate the effect of the Fe-His bond of α-heme on the quaternary structural change of tetramer. Ni-Fe hybrid Hb has the property that CO does not bind to the Ni-heme. In this case, the author can investigate the quaternary structure of a half ligand-bound form. Hb M Boston has the property that CO does not bind to ferric α-abnormal chain. Hb M Boston is not exactly the same as Hb A owing to the difference in a distal residue of α-chain. Recently it is reported that Hb M Boston has cooperativity at high pH (pH = 9). This suggests that Hb M Boston may induce a quaternary structural change. The quaternary structure of Hb M Boston in a partially

ligand-bound form can be studied. The largest structural differences between the T and R structures, revealed by X-ray crystallographic analysis, are located in the α1-β2 subunit interface. In this study an amount of the T and R structures in the intermediate states of quaternary structural change was estimated from UVRR spectral changes of the bands of tyrosine (Tyr) and tryptophan (Trp) residues. The quaternary structural change from T structure (deoxyHb A) to R structure (COHb A) results in the lower frequency shifts of Y8a and Y9a bands of tyrosine and intensity reduction of W3, W16, W18 bands of tryptophan.

The results from the measurements of the three Hbs are as follows. The quaternary structures of partially ligand-bound forms in NOHb ($\alpha^{NO}\beta^{deoxy}$), Ni-Fe hybrid Hb ($\alpha^{Ni}\beta^{CO}$) and ($\alpha^{CO}\beta^{Ni}$), and Hb M Boston ($\alpha^{Mmet}\beta^{CO}$) depend on pH and the absence or presence of IHP (inositol-hexakis-phosphate), and cannot be described by superimposition of only T and R structures which are limiting structures. Generally the ligand (CO not NO) binding to α-heme causes both lower frequency shifts of the special bands of tyrosine and intensity reduction of the special bands of tryptophan, but the ligand binding to β heme causes only the intensity reduction of the special bands of tryptophan, although the ligand binding to either α−, or β−heme at lower pH (pH 6.3~6.7) in the presence of IHP apparently causes no spectral change. This suggests that the roles of α-heme and β-heme (their Fe-His bonds) in the quaternary structural change are different. Binding of NO and CO to α-heme yields clear difference between the two ligands. Although the special bands of both tyrosine and tryptophan changed in the case of CO, the special bands of neither tyrosine nor tryptophan changed by NO even at pH 8.8 in the absence of IHP. This suggests that the difference in coordination ability between CO and NO influences the proximal His-Fe bond in α-heme, which reflects the large difference in the quaternary structural change.

On the other hand, the ligand binding to β-heme can be discussed from another views when $\alpha^{Ni}\beta^{CO}$ and Hb M Boston ($\alpha^{Mmet}\beta^{CO}$) are compared with $\alpha^{NO}\beta^{NO}$, because $\alpha^{NO}\beta^{deoxy}$ showed T structure at even higher pH (pH = 8.8) in the absence of IHP. But $\alpha^{NO}\beta^{NO}$ showed the

R characteristics including both the lower frequency shifts of special bands of tyrosine and intensity reduction of special bands of tryptophan. It is different from the case of $\alpha^{Ni}\beta^{CO}$ (or $\alpha^{Mmet}\beta^{CO}$) that the NO (or CO) binding to β-heme in $\alpha^{NO}\beta^{deoxy}$ causes the lower frequency shifts of the special bands of tyrosine at lower pH and in the presence of IHP. The most important difference between $\alpha^{Ni}\beta^{CO}$ (or $\alpha^{Mmet}\beta^{CO}$) and $\alpha^{NO}\beta^{NO}$ is whether the sixth coordination site of α-heme is occupied by a ligand (NO) or not. This suggests that the quaternary structural change caused by the CO (NO) binding to β-heme depends on the coordination state in α-heme. The network involving the distal histidine such as Fe-NO---His in α-heme may also have a close connection with the change of tyrosine.

In conclusion of Part I, the change of tryptophan and tyrosine upon the quaternary structural change due to ligand (CO) binding to α-heme or β-heme can be summarized in the following way. CO binding to α-heme causes changes of both tryptophan and tyrosine and the changes do not depend on the state of β-heme. On the other hand, CO binding to β-heme causes a change of tryptophan only, but the change of tyrosine strongly depends on the state of α-heme. Thus, CO binding to α-heme seems to induce the quaternary structural change more strongly than that to β-heme.

In Part II, the relation between the function and structure of Hb which has very low affinity and apparently no cooperativity is treated. This type of Hb can be prepared under low pH in the presence of strong allosteric effector such as bezafibrate (BZF). Generally it has been considered that binding of ligands to Hb causes a quaternary structural change. However it is reported that ligand binding of Hb occurs with no cooperativity but that judging from the ^{1}H NMR signal, the quaternary structural change takes place. To investigate the relation between quaternary structure and cooperativity, this type of Hb is examined with resonance Raman spectroscopy

The quaternary structural change upon ligand (CO) binding was also observed by resonance Raman spectroscopy for Hb which has very low affinity and apparently no cooperativity due to the

strong allosteric effector. The R structure in the presence of the strong allosteric effector was not spectrally different from the R structure of normal HbA.

The effects of strong allosteric effector appeared in a rate of structural relaxation after CO photodissociation, which is usually of microsecond order. In the presence of allosteric effector, the structural change from R-structure to T-structure becomes faster. The Fe-His stretching frequency at 13 μs after CO photodissociation at pH 6.4 in the presence of IHP and BZF was lower by 5 cm^{-1} than that observed in the absence of the effectors, for which the number of CO molecules remaining on hemes was estimated to be 2.8. When the number of CO molecules bound to hemes was changed, the degree of the quaternary structural change from R-structure to T-structure was also changed. At pH 6.4 in the presence of IHP and BZF the quaternary structural change from R-structure to T-structure has finished at 4 μs after CO photodissociation, even if the number of CO molecules remaining on hemes is 3.5. However, at pH 8.8 in the absence of the effectors the quaternary structural change from R-structure to T-structure has not been completed at 13 μs, even if the number of CO molecules bound to hemes is 2.8. This suggests that the quaternary structural change from R-structure to T-structure occurs between R_4 and T_3 at pH 6.4 in the presence of IHP and BZF, and that at pH 8.8 in the absence of the effectors quaternary structural change from R-structure to T-structure has not been completed yet in 13 μs after CO photodissociation or that T structure cannot be maintained when the number of CO molecules bound to hemes is 2.8. This indicates that mixed allosteric effector, IHP and BZF, shifts the transition point of the quaternary structure from $T_2 \rightarrow R_3$ to $T_3 \rightarrow R_4$.

CHAPTER 1

Hemoglobin: Its Physiological Property and Investigation by Resonance Raman Spectroscopy

1.1 Overview of Hemoglobin (Hb)

Human Hemoglobin A (HbA) is contained in red blood corpuscles, and functions as an oxygen carrier in human body. HbA is composed of two kinds of subunits, which form $\alpha_2\beta_2$ tetramer structure, and its molecular weight is about 65 kDa (Figure 1.1). The numbers of amino

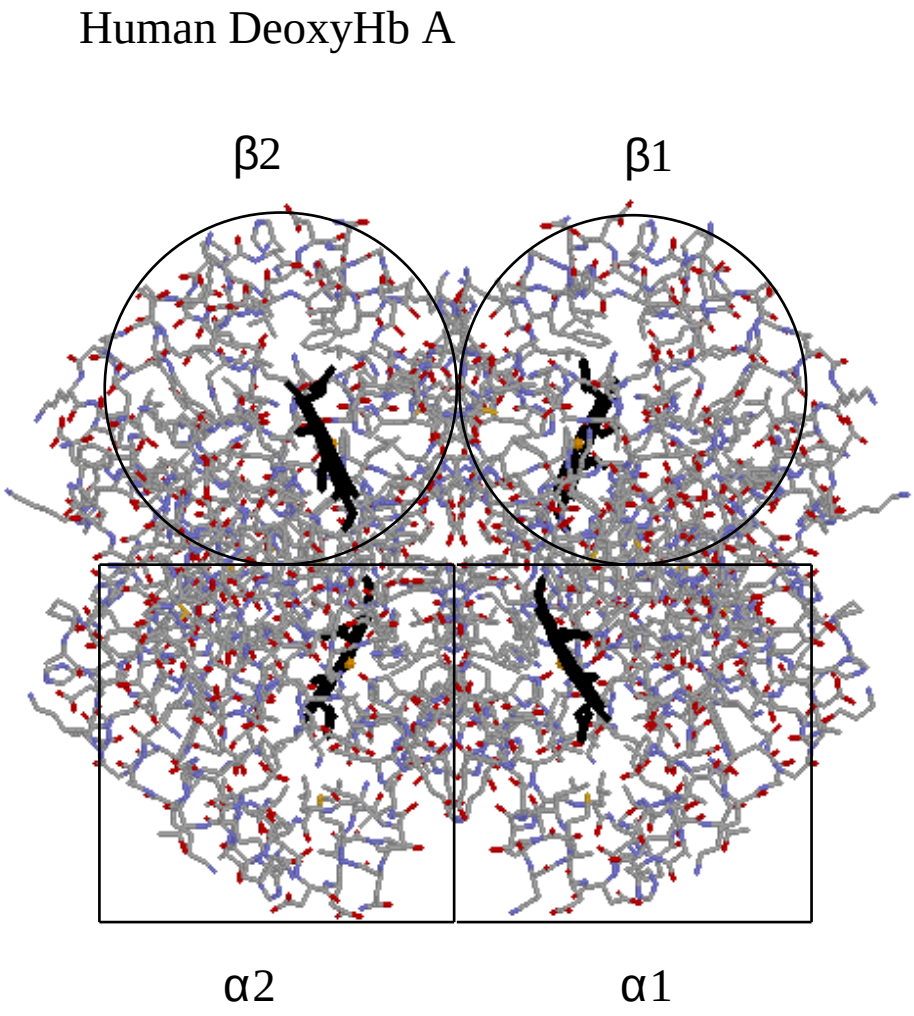

Figure 1.1 G. Fermi et al., *J. Mol. Biol.*, **175,** 159 (1984).

acid residues in α-, and β-subunits are 141 and 146, respectively. One of the most important characteristics in Hb A is that Hb A has cooperativity on oxygen binding process (Figure 1.2) (1).

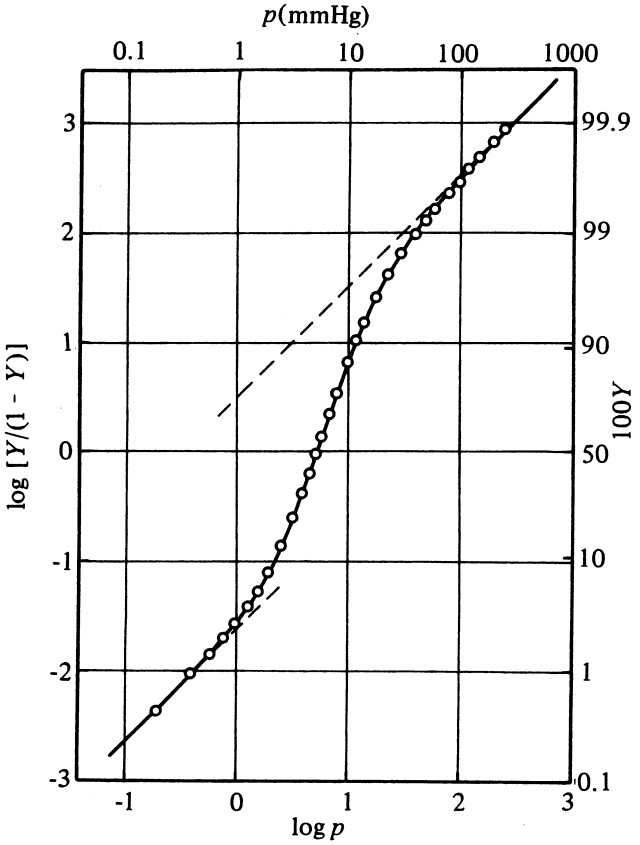

Figure 1.2 Hill plot of the model data. Straight broken lines are the asymptotes which were fitted to the data points by eye. The solid line was constructed from the best-fit Adair constants which were evaluated by the least-squares method.
(ref.1 Imai, K., "Allosteric Effects in Haemoglobin" Cambridge University Press, Cambridge (1982) p.93.)

This cooperativity in Hb A makes it possible to transport oxygen effectively from lung to tissue. The reason is explained in a following way. Figure 1.3 shows oxygen equilibrium curves of Hb and Myoglobin (Mb) (1). Mb is a monomer whose amino acid sequence is similar to the α- and β-subunits of HbA. Mb also binds oxygen similar to Hb, but Mb has no cooperativity, that is distinct from Hb. This difference in Figure 1.3 between Hb and Mb provides Hb with superiority than Mb in oxygen transport. At lower oxygen pressure Hb can bind less oxygen than Mb, but at higher

pressure Hb can bind as much oxygen as Mb does. Therefore when we compare oxygen transportation of Hb with that of Mb between 40 and 100 mmHg of oxygen pressure, we see that oxygen corresponding to 23% saturation difference is transported by Hb but there is practically no difference in oxygen saturation for Mb. This is why cooperativity is important in effective oxygen transportation by Hb.

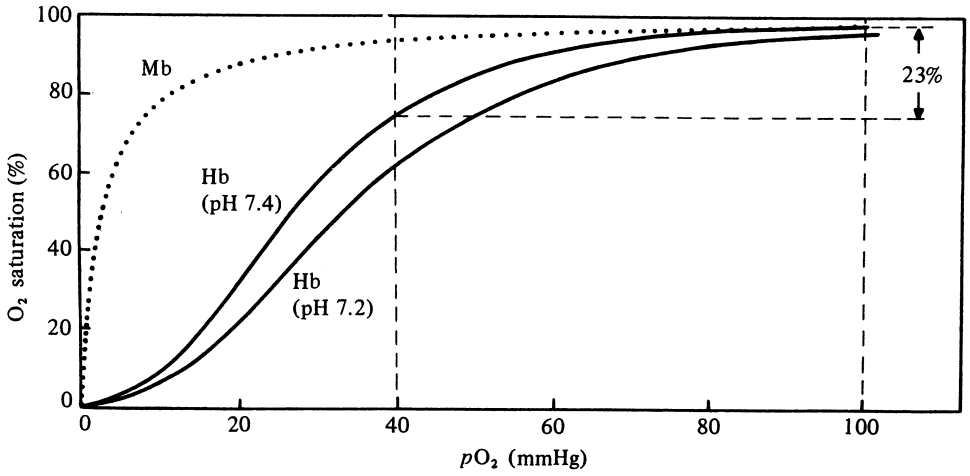

Figure 1.3 Oxygen equilibriun curves of human red cell and sperm whale myoglobin. The curves for the red cells were determined at 37 ^{o}C with fresh human blood which was 150 times diluted with isotonic phosphate buffers (0.15 M KH_2PO_4 + 0.15 M Na_2HPO_4). The curve for myoglobin was determined at 37 ^{o}C with 60 μM myoglobin dissolved in 0.1 M potassium phosphate buffer (pH 7.4). All these curves were determined by the automatic recording method of Imai *et al.* (1970). At pH 7.4, the oxygen saturation of the red cell is 98 % at the arterial blood pO_2 (= 100 mmHg) and 75 % at the mixed venous blood pO_2 (= 40 mmHg) so that oxygen corresponding to 23 % saturation difference is transported by circulating red cells. Data from K. Imai (unpublished).
(ref.1 Imai, K., "Allosteric Effects in Haemoglobin" Cambridge University Press, Cambridge (1982) p.24.)

Cooperativity of Hb has been investigated for a long time since Hb serves as a model of general allosteric proteins (2). Many experimental results show that formation of a tetramer in Hb is essentially important. Therefore, elucidation of a structural mechanism of cooperativity is a major subject of Hb studies. X-ray crystallographic studies have demonstrated the presence of two distinct quaternary structures that correspond to the low-affinity (T or tense) and high-affinity (R or

relaxed) states. Typical structures of the T and R states are seen for the deoxy and ligand-bound forms, respectively (3) (Figure 1.4). The cooperative oxygen binding of Hb has been explained in terms of a reversible transition between the two quaternary states on partial ligation of four hemes (4, 5). The largest structural differences between the T and R structures, revealed by X-ray crystallographic analysis (6), are located in the α1-β2 subunit interface, where resets of hydrogen bonds and salt-bridges take place upon ligation to deoxyHb. The ^{1}H NMR signal of Tyrα42, which forms a hydrogen bond with Aspβ99 in the T state but is free in the R state, has served as a practical diagnostic marker for the quaternary structure (7, 8). However, a single marker is not sufficient to characterize the quaternary state, because Hbs whose structure cannot be described by T or R only are reported (9).

Quaternary structural change of Hb

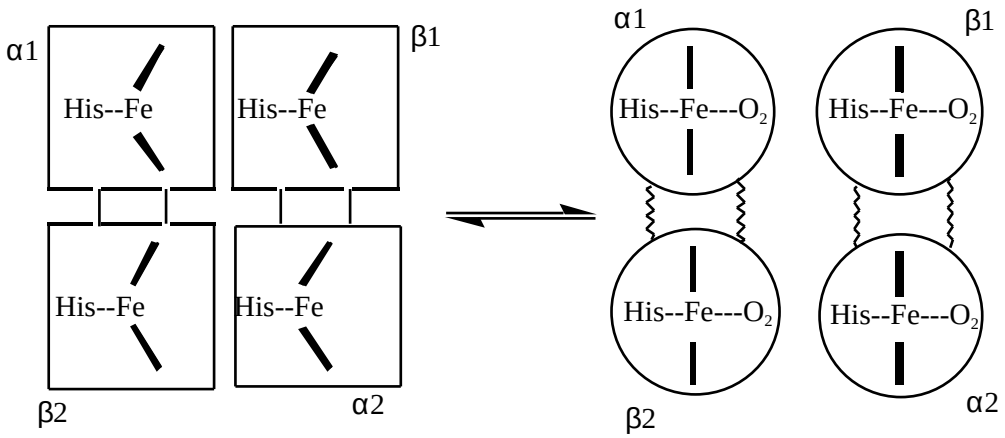

T-structure R-structure

Figure 1.4

The author thinks that the most important problem to be answered for the quaternary structural change of Hb is when and how the quaternary structural change occurs. Therefore, the author searched for samples of Hb in which a partial ligand-bound form can be stabilized in

solution conditions. In normal Hb A most of molecules adopt either no ligand-bound form (DeoxyHb) or fully ligand-bound form (OxyHb or COHb). Accordingly, the population of a partially ligand-bound form is very low. It is reported that Sol-Gel method can stabilize a partially ligand-bound form of Hb (10, 11). However, the author thought it important that Hb should be measured in an intermediate state of solution state near physiological condition. Therefore, the author selected the following samples to investigate an intermediate state of quaternary structural change.

In this thesis, structural change and cooperativity of Hb A are discussed. In Part I, the results from UVRR studies on NOHb, Ni-Fe hybrid Hb, and Hb M Boston will be discussed. Common features of these three samples are to stabilize partially ligand-bound forms. The author aims to elucidate a mechanism of cooperativity using these samples. The three samples are different from one another with regard to the following points.

NOHb has the property that NO binds heme more strongly than CO. As the dissociation rate of NO is different between α-heme and β-heme, it is possible to make a stable intermediate in which NO is bound to α-heme only. In this case, a condition of the Fe-His bond can be controlled by pH or addition of IHP: the heme can be made five- or six-coordinate state. Therefore, we can investigate the Fe-His effect of α-heme on the quaternary structural change of tetramer (Figure 1.5).

Ni-Fe hybrid Hb has the property that CO does not bind to the Ni-heme. In this case, we can investigate quaternary structure of a partially ligand-bound form (Figure 1.6).

Hb M Boston has the property that CO does not bind to ferric α-abnormal chain (Figure 1.7). Hb M Boston is not exactly the same as HbA owing to the difference of distal residue in α-heme. Recently it is reported that Hb M Boston also has cooperativity at high pH (pH = 9).

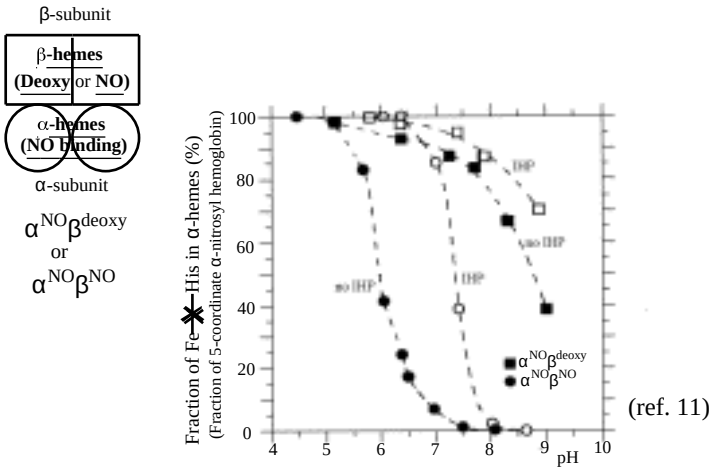

(ref. 11)

Figure 1.5 IHP and pH dependence of $\alpha^{NO}\beta^{deoxy}$ and $\alpha^{NO}\beta^{NO}$

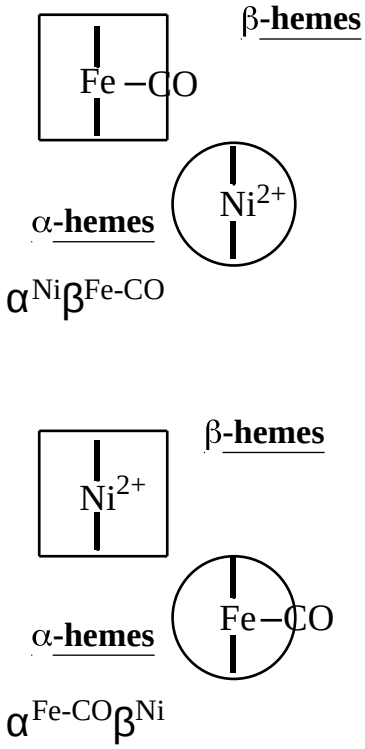

Figure 1.6 Ni-Fe Hybrid Hb
CO cannot bind to Ni^{2+}.

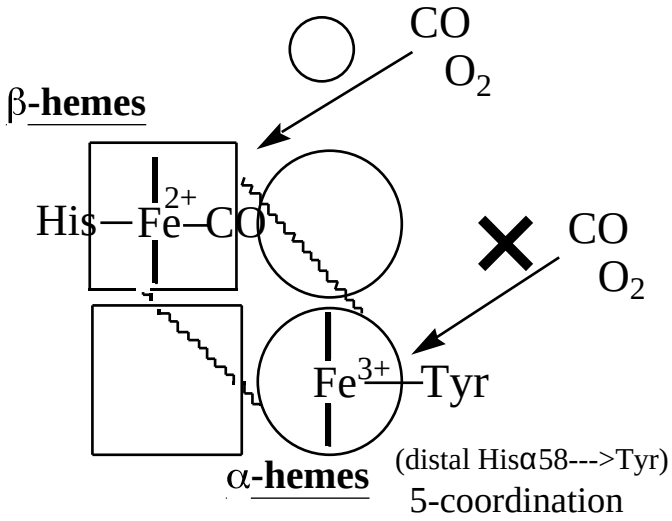

Figure 1.7 Hb M Boston ($\alpha^{Mmet}\beta^{deoxy}$)
CO binds to β-heme only.

This suggests that Hb M Boston may induce a quaternary structural change. The quaternary structure of Hb M Boston in a partially ligand bound form can be studied.

In Part II, the author has examined a relation between the function and structure of Hb which has very low affinity and apparently no cooperativity. This type of Hb can be prepared under low pH in the presence of strong allosteric effector such as bezafibrate (BZF). Generally it has been considered that binding of ligands to Hb causes a quaternary structural change. However it is reported for this type of Hb that ligand binding of Hb occurs with no cooperativity but the quaternary structural change takes place, judging from the ^{1}H NMR signal (12). Therefore the author examined this type of Hb with resonance Raman spectroscopy.

1.2 Resonance Raman Experiment

1.2.1 Theory

Since 1928 when C.V. Raman has first found Raman scattering in liquid, Raman spectroscopy has been widely used as a method for analysis of molecular structure. However, in the case of protein, the number of atoms is too many to characterize vibrational bands in non-resonance Raman spectroscopy. In resonance Raman spectroscopy, it is possible to select some bands related to a real electronic transition.

Figure 1.8 shows a relation between absorption spectra and excitation wavelength in Raman spectroscopy. The Raman spectra excited at the wavelength of λ_a, of λ_b and of λ_c are called non-resonance, pre-resonance and rigorous resonance Raman spectra. In Figure 1.8 the incident light with frequency ν_0 loses energy (ν: vibrational frequency) and the light with the frequency of $\nu_0 - \nu$ is emitted. The scattering in which incident light (ν_0) loses energy is called Stokes scattering. In contrast, the scattering in which incident light (ν_0) gains the vibrational energy is called anti-Stokes scattering. As Raman scattering intensity (I_{if}) can be represented by equation (a), the content of

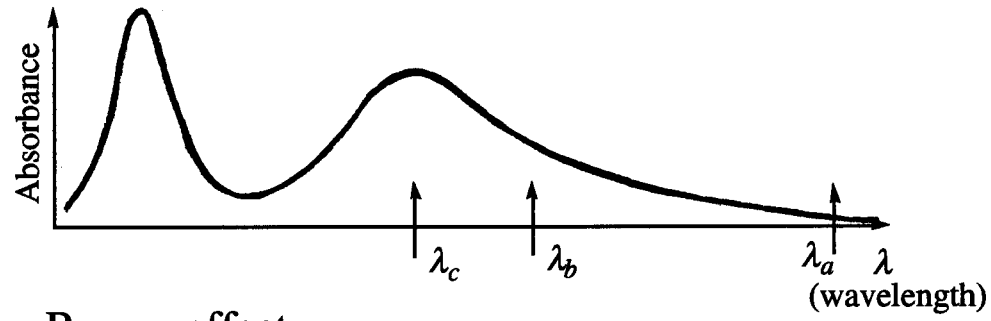

Raman effect

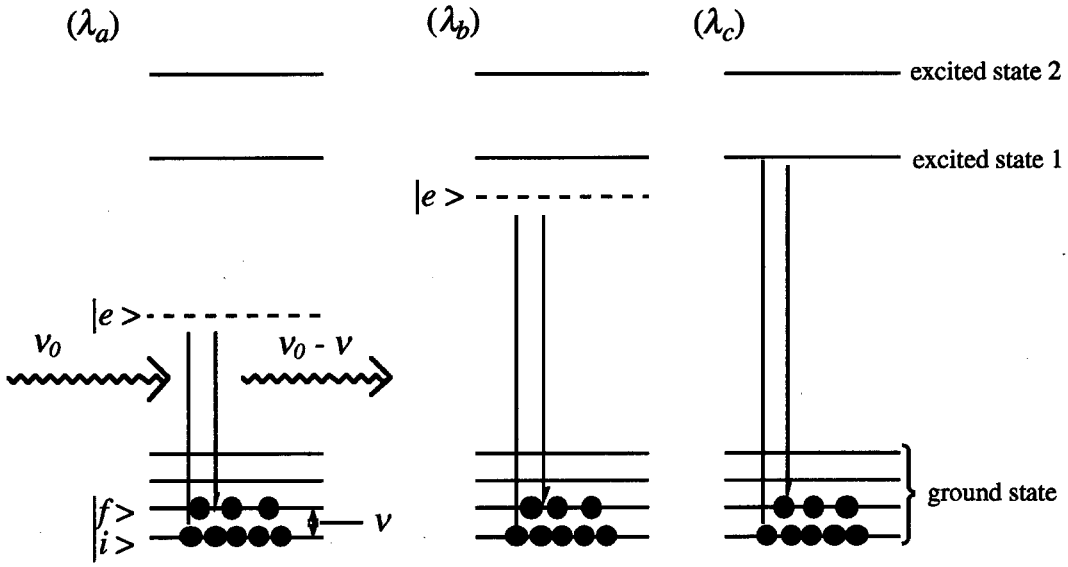

$$I_{if} = \alpha I_0 \nu_0 (\nu_0 - \nu)^3 \sum_{\rho,\sigma} |(a_{\rho\sigma})|^2 \text{ ----- (a)}$$

$$(a_{\rho\sigma}) = \sum_e \left[\frac{\langle i|\mu_\sigma|e\rangle\langle e|\mu_\rho|f\rangle}{E_e - E_i - h\nu_0 - \Gamma_e} + \frac{\langle i|\mu_\rho|e\rangle\langle e|\mu_\sigma|f\rangle}{E_e - E_f + h\nu_0 - \Gamma_e} \right] \text{ ----- (b)}$$

$E_e - E_i \sim h\nu_0$

I_0 : incident light intensity I_{if} : Raman scattering intensity

$(a_{\rho\sigma})$: $\rho\sigma$ component of Raman scattering tensor

μ_ρ , μ_σ : ρ, σ component of dipole moment

Γ_e : damping constant

Figure 1.8

Raman scattering tensor ($a_{\rho\sigma}$) is important. $a_{\rho\sigma}$ is derived from the dispersion formula of Kramers-Heisenberg-Dirac (b) (13). The first term of formula (b) is focused. When the difference energy (E_e – E_i) between initial ground state (E_i) and real excited state (E_e) approaches the energy of incident light ($h\nu_0$), the first term of formula (b) becomes much larger than the second term, because a denominator of the first term approaches zero. This is the reason why resonance Raman scattering intensity becomes much larger than non-resonance Raman scattering intensity. The intensity increase is about 10^4 times. Thus we can obtain the spectra of selected bands only. Owing to this strong intensity enhancement, resonance Raman spectroscopy has made it possible to measure a spectrum of a protein sample with very low concentration (~μM order). Thus by selecting a suitable laser line some marker bands can be distinguished from other bands. As the globin part of Hb consists of non-colored amino acid residues, vibrational bands of amino acid residues can be selectively observed by using ultraviolet laser line. Accordingly, upon excitation around 230 - 240 nm, for instance, vibrations of aromatic amino acids such as Trp, Tyr and Phe are observed. The absorption spectra of some aromatic amino acids are displayed in Figure 1.9. They have absorptions in 200 - 240 nm region. Upon shorter wavelength excitation, the vibrations of not only aromatic amino residues but also amide modes would appear in resonance with the π-π* electronic absorption.

In the case of colored proteins such as heme proteins, the vibrational bands related to a chromopher can be detected upon excitation by visible laser lines.

1.3 Apparatus

The UVRR method has been widely used since 1990's. In the first stage, the production of ultraviolet laser light was mainly from a pulsed laser. Recently, however, many kinds of UV lasers including pulsed and continuous wave (cw) radiation are used. The Excimer laser-pumped dye

laser system can be used not only for static measurement but also for time resolved measurements. In this system an arbitrary laser wavelength can be generated by combining it with a dye laser, but owing to pulsed laser a photon density in the laser beam is very high. As a cw UV laser source, emission lines at 257, 244, 229 and 206nm can be generated by an intracavity SHG crystal in an Ar or a Kr laser.

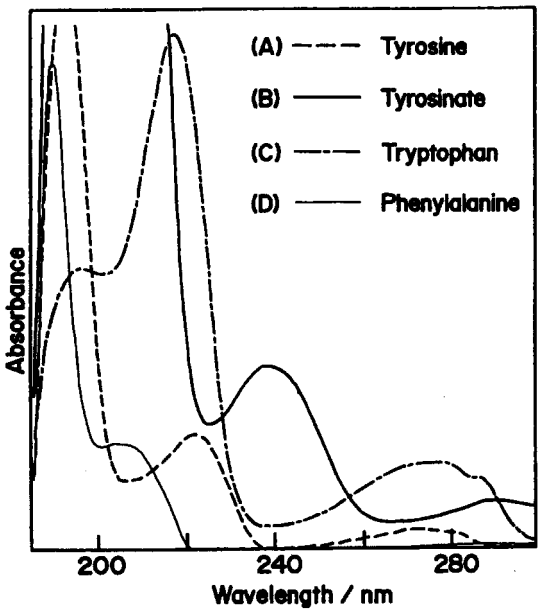

Figure 1.9 Electronic absorption spectra of aromatic amino acids; Tyrosine, Tyrosinate (Tyr^-), Tryptophan and Phenylalanine

It has been demonstrated in this decade that resonance Raman (RR) spectra excited in the UV region around 220-240 nm can explore the environmental and hydrogen-bonding changes of Tyr and Trp residues of proteins (see Refs. 20 and 21 for a review). In fact, there are several papers reported about the quaternary structure dependent features for Tyr and Trp residues in the $\alpha 1$-$\beta 2$ interface of Hb using 230- and 235-nm excited UVRR spectra (14-25).

To study quaternary structure of Hb, the author measured ultraviolet resonance Raman spectra of Hb samples mainly. Therefore, the apparatus used is described in this section. Overview of the apparatus is shown in Figure 1.10. UVRR spectra were excited by a XeCl excimer laser-pumped dye laser (EMG103MSC/LPX105 and FL2002/SCANMATE, Lambda Physik). The 308-

nm line from a XeCl excimer laser (operated at 100 Hz) served as a pump to excite coumarin 480, and the 470-nm output from the dye laser was frequency-doubled with a β-BaB_2O_4 crystal to generate 235-nm pulses. The Raman excitation light (15 μJ/pulse) with the cross section of 0.2 × 3 mm^2 was introduced to a sample cell from the lower front side as illustrated in Figure 1.11 (27). The sample illuminating point was moved vertically by 1mm for every one measurement to avoid repeated illumination of UV laser light to the same position of the sample solution. Scattered light at the scattering angle of 135° was collected with a Cassegrainian mirror optics, dispersed with an asymmetric double monochromator (Spex 1404) in which the gratings in the first and second dispersion steps are 2400 grooves/mm (holographic) and 1200 grooves/mm (machine-ruled, 500 nm blazed), respectively, and detected by an intensified photodiode array (PC-IMD/C5222-0110G) (26).

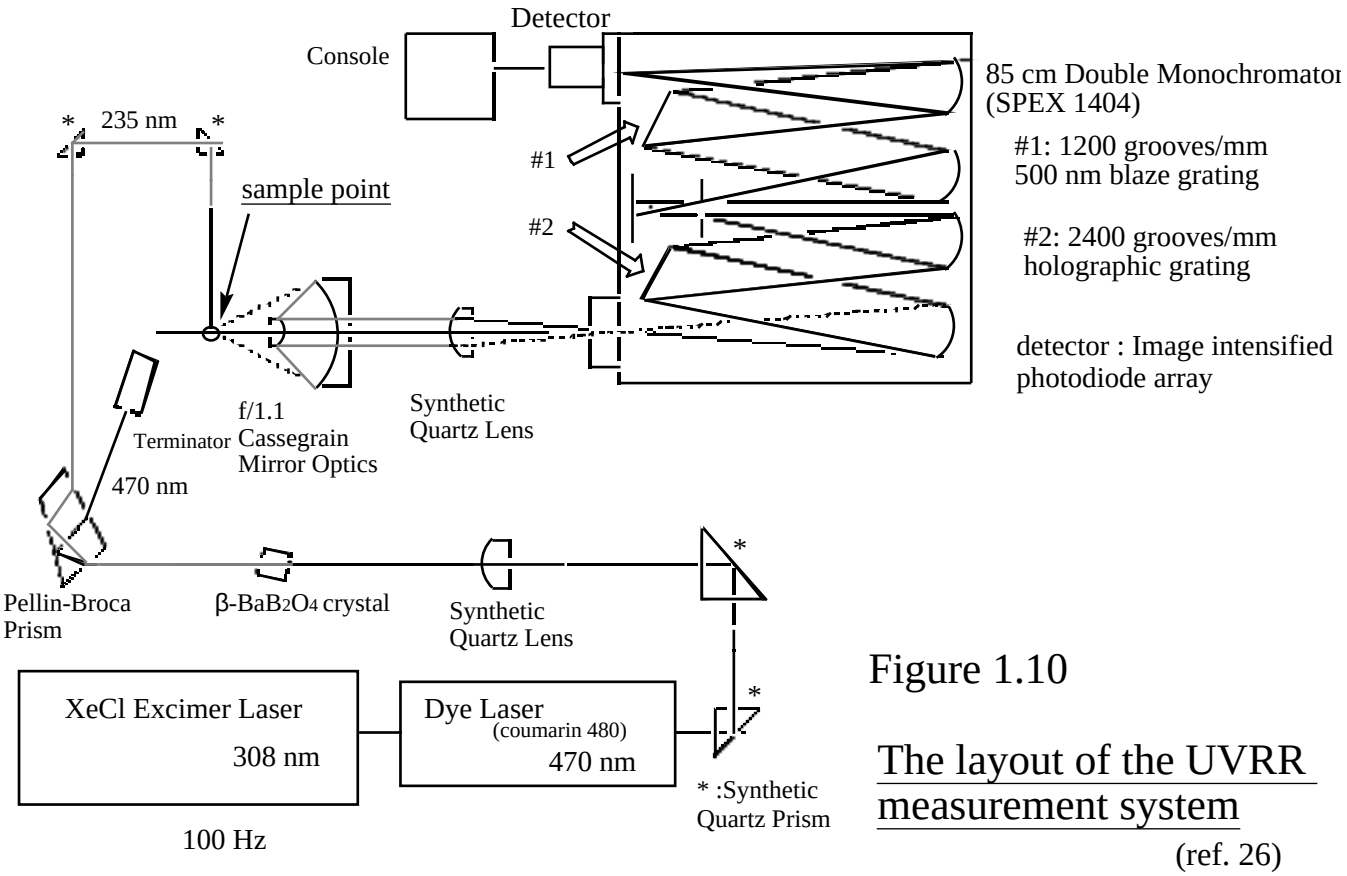

Figure 1.10

The layout of the UVRR measurement system

(ref. 26)

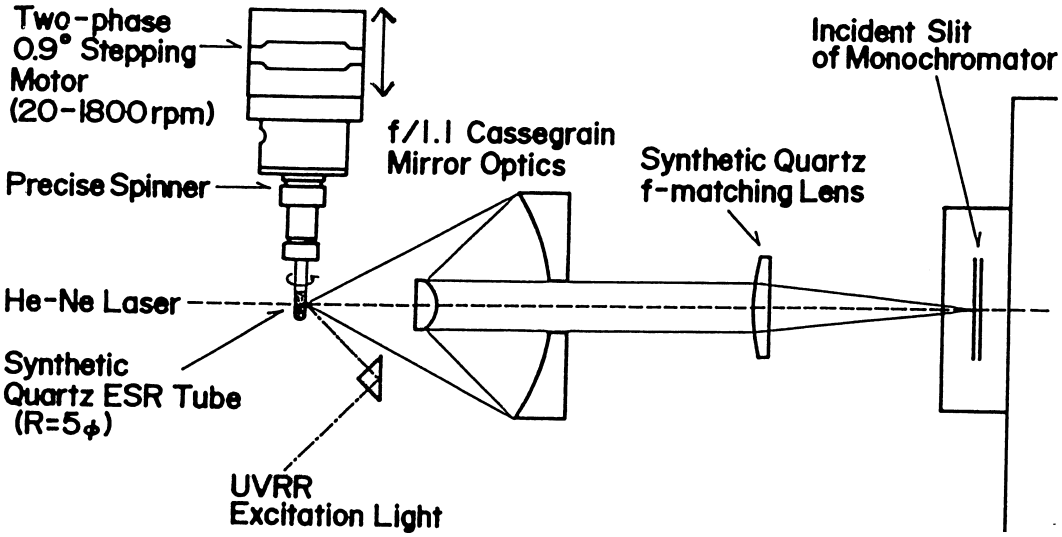

Figure 1.11 Sample illuminating device used in this study. A spinning cell with a synthetic quartz ESR tube and Cassegranian optics with *f*/1.1 are used. Excitation light of Raman scattering is introduced with a square prism from the forward bottom side. (ref. 27)

1.4 An Estimation Method of Subunit Contacts of Hb from UVRR spectra

Figure 1.12 shows the 235 nm excited UVRR spectra for deoxyHb (A), COHb (B), and their difference (C = A - B) at pH 6.7 in the frequency region from 1700 to 700 cm^{-1}. Although a strong broad band due to a synthetic quartz cell appeared between 800 and 900 cm^{-1}, its contribution was subtracted from the spectra shown here. The 982 cm^{-1} band of SO_4^{2-} ions was used to normalize the intensity of the spectra (28). In the spectrum of deoxyHb, RR bands for tyrosine (Tyr) are seen at 1619 (Y8a), 1208 (Y7a), 1178 (Y9a) and 855 cm^{-1} (Y1), and those of Trp are seen at 1557 (W3), 1360-1341 (W7; tryptophan doublet), 1012 (W16), 879 (W17), and 758 cm^{-1} (W18). The assignments are based on Harada and coworkers (20, 29, 30).

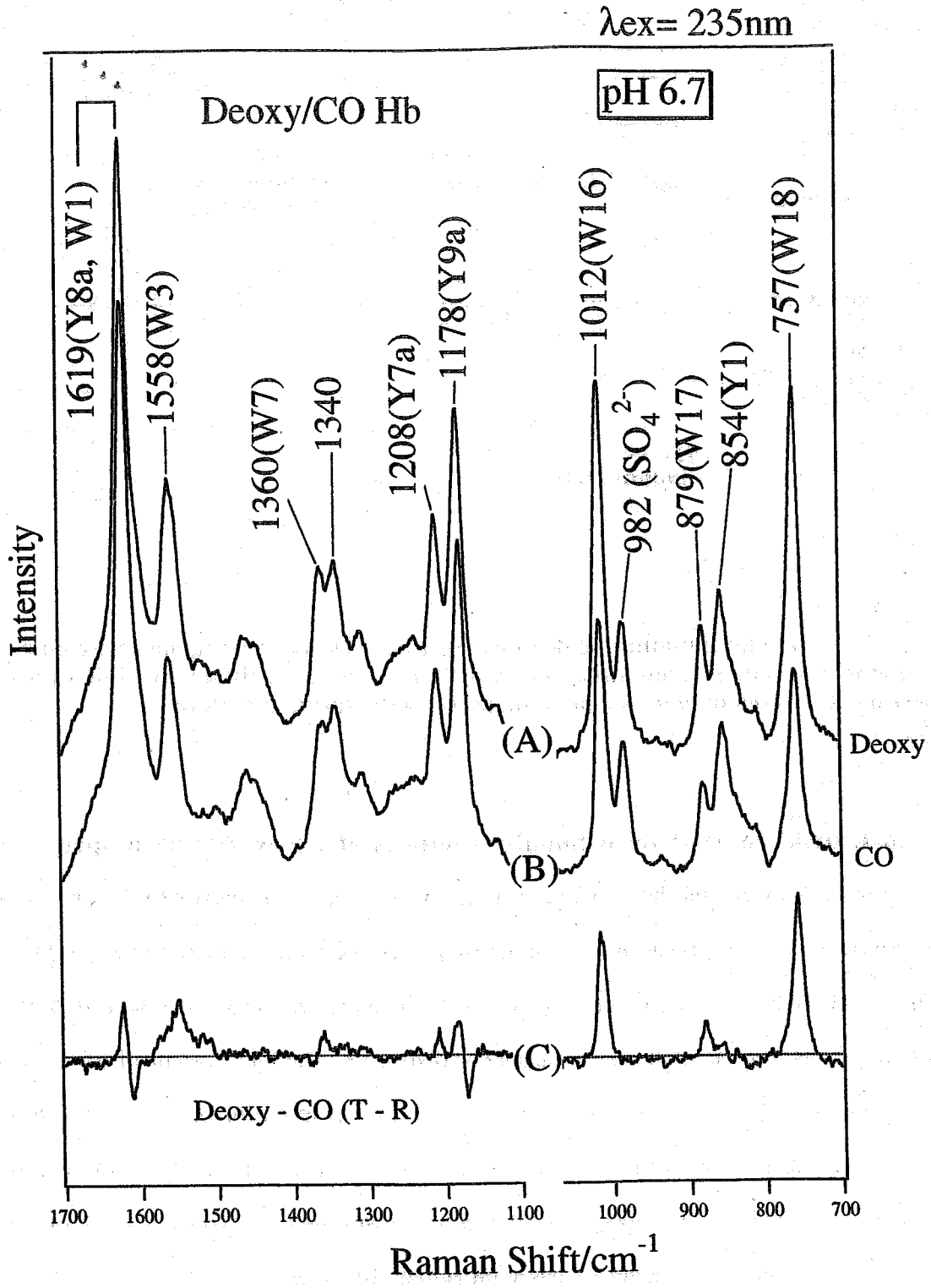

Figure 1.12 235-nm excited UVRR spectra of deoxy Hb (A), COHb (B), and their difference spectra (C) (= deoxy Hb - COHb). Hb samples are equilibrated with 0.05 M phosphate buffer, pH 6.7, containing 0.2 M Na_2SO_4. Hb concentration was 400 μM in heme.

The difference spectrum between deoxyHbA and COHbA indicates that the intensities of the W3, W16, W17, and W18 bands of Trp are much weaker for COHbA than for deoxyHbA, while the peak positions remain unaltered, and that the frequencies of the Y8a and Y9a bands of Tyr are lower for COHbA than for deoxyHbA. These differences arise from some differences in hydrogen bonding states and surrounding hydrophobicity of Trp and Tyr residues between the two states (31) and have been ascribed to a consequence of changes in subunit contacts (14-25). Hereafter spectrum (C) will be referred as the standard for the T minus R difference spectrum, reflecting the typical changes at $\alpha 1$-$\beta 2$ subunit interface upon quaternary structure change ("T-like" and "R-like" will be used to represent that the local structure surrounding a particular residue in question is similar to that in the ordinary T and R subunit contact, but does not always mean that the tertiary structure is T and R, respectively).

The "T structure" in this paper means that the bands of Tyr and Trp are close to those of deoxyHb and the "R structure" means that the bands of Tyr and Trp are close to those of COHb. A quaternary structural change of partially ligated Hb will be estimated on the basis of the typical T – minus – typical R difference spectrum.

References

1. Imai, K., “Allosteric Effects in Haemoglobin” Cambridge University Press, Cambridge (1982).

2. Monod, J., Wyman, J., and Changeux, J. P. (1965) *J. Mol. Biol. 12,* 88-118.

3. Perutz, M. F. (1970) *Nature 228,* 726-739.

4. Perutz, M. F. (1979) *Annu. Rev. Biochem. 48,* 327-386.

5. Perutz, M. F., Fermi, G., Luisi, B., Shaanan, B., and Liddington, R. C. (1987) *Acc. Chem. Res. 20,* 309-321.

6. Baldwin, J., and Chothia, C. (1979) *J. Mol. Biol. 129,* 175-220.

7. Fung, L. W.-M., and Ho, C. (1975) *Biochemistry 14,* 2526-2535.

8. Ho, C. (1992) *Adv. Protein Chem. 43,* 152-312.

9. Miyazaki, G., Morimoto, H., Yun, K.-M., Park, S.-Y., Nakagawa, A., Minagawa, H., and Shibayama, N. (1999) *J. Mol. Biol. 292,* 1121-1136.

10. Shibayama, N., and Saigo, S. (1999) *J. Am. Chem. Soc. 121,* 444-445.

11.Das, T. K., Khan, I., Rousseau, D. L., and Friedman, J. M. (1999) *Biospectroscopy 5*, S64-S70.

12. Yonetani, T., Park, S. I., Tsuneshige, A., Imai, K., and Kanaori, K. (2002) *J. Biol. Chem., 277,* 34508-34520.

13. Kramers, H. A., and Heisenberg, W. (1925) *Z. Phys. 31*, 681

14. Rodgers, K. R., Su, C., Subramaniam, S., and Spiro, T. G. (1992) *J. Am. Chem. Soc. 114*, 3697-3709.

15. Rodgers, K. R., and Spiro, T. G. (1992) *Science 265,* 1697-1699.

16. Nagai, M., Kaminaka, S, Ohba, Y., Nagai, Y, Mizutani, Y., and Kitagawa, T. (1995) *J. Biol. Chem. 270,* 1636-1642.

17. Nagai, M., Imai, K., Kaminaka, S, Mizutani, Y., and Kitagawa, T. (1996) *J. Mol. Struct. 379,* 65-75.

18. Nagai, M, Wajcman, H., Lahary, A, Nakatsukasa, T., Nagatomo, S. and Kitagawa, T. (1999) *Biochemistry, 38*, 1243-1251.

19. Huang, S., Peterson, E. S., Ho, C., and Friedman, J. M. (1997) *Biochemistry 36,* 6197-6206.

20. Harada, I., Miura, T., and Takeuchi, H. (1986) *Spectrochim.Acta 42A,* 307-312.

21. Kitagawa, T. (1992) *Prog. Biophys. Mol. Biol. 58,* 1-18.

22. Huang, J., Juszczak, L., Peterson, E. S., Shannon, C.F., Yang, M., Huang, S., Vidugiris, G. V. A., and Friedman, J. M. (1999) *Biochemistry 38,* 4514-4525.

23. Hu, X., and Spiro, T. G. (1997) *Biochemistry 36,* 15701-15712.

24. Hu, X., Rodgers, K. R., Mukerji, I., and Spiro, T. G. (1999) *Biochemistry 38,* 3462-3467.

25. Peterson, E. S. and Friedman, J. M. (1998) *Biochemistry 37,* 4346-4357.

26. Kaminaka, S., and Kitagawa, T. (1992) *Appl. Spectrosc. 46,* 1804-1808.

27. Kaminaka, S., and Kitagawa, T. (1995) *Appl. Spectrosc. 49,* 685-687.

28. Dudik, J. M., Johnson, C. R., and Asher, S. A. (1985) *J. Chem. Phys. 82,* 1732-1740.

29. Miura, T., Takeuchi, H., and Harada, I. (1988) *Biochemistry 27,* 88-94.

30. Miura, T., Takeuchi, H., and Harada, I. (1989) *J. Raman Spectrosc. 20,* 667-671.

31. Matsuno, M., and Takeuchi, H. (1998) *Bull. Chem. Soc. Jpn. 71,* 851-857.

Part I

CHAPTER 2

UV Resonance Raman Studies of α-Nitrosyl Hemoglobin Derivatives: Relation between the α_1-β_2 Subunit Interface Interactions and the Fe-Histidine Bonding of α heme

Published by *Biochemistry 38,* 9659-9666 (1999)

S. Nagatomo, M. Nagai, A. Tsuneshige, T. Yonetani, and T. Kitagawa

2.1 Abstract

Human α-nitrosyl β-deoxy hemoglobin A, $\alpha^{NO}\beta^{deoxy}$, is considered to have a T (tense) structure with the low O_2 affinity extreme and the Fe-histidine (His87) (Fe-His) bond of α heme cleaved. The Fe-His bonding of α heme and the intersubunit interactions at the α1-β2 contact of α^{NO}-Hbs have been examined under various conditions with EPR and UV resonance Raman (UVRR) spectra excited at 235 nm, respectively. NOHb at pH 6.7 gave the UVRR spectrum of the R structure, but in the presence of inositol-hexakis-phosphate (IHP) for which the Fe-His bond of the α heme is broken, UVRR bands of Trp residues behaved half-T-like while Tyr bands remained R-like. The half-ligated nitrosylHb, $\alpha^{NO}\beta^{deoxy}$, in the presence of IHP at pH 5.6, gave T-like UVRR spectra for both Tyr and Trp, but binding of CO to its β heme ($\alpha^{NO}\beta^{CO}$) changed the UVRR spectrum to half-T-like. Binding of NO to its β heme (NOHb) changed the UVRR spectrum to 70 % T-type for Trp but almost R-type for Tyr. When the pH was raised to 8.2 in the presence of IHP, the UVRR spectrum of NOHb was the same as that of COHb. EPR spectra of these Hbs indicated that the Fe-His bond of α^{NO} heme is partially cleaved. On the other hand, the UVRR spectra of $\alpha^{NO}\beta^{deoxy}$ in the absence of IHP at pH 8.8 showed the T-like UVRR spectrum, but the EPR spectrum indicated that 40~50 % of the Fe-His bond of α hemes was intact. Therefore, it became evident that there is a qualitative correlation between the cleavage of the Fe-His bond of α heme and T-like contact of Trp-β37. We note that the behaviors of Tyr and Trp residues at the α1-β2 interface are not synchronous. It is likely that the behaviors of Tyr residues are controlled by the ligation of β heme through His-β92(F8) → Val-β98(FG5) → Asp-β99(G1) → Tyr-α42(C7) or Tyr-β145(HC2).

2.2 Introduction

Nitric oxide (NO), which binds to deoxyHb similar to CO and O_2 but with much higher affinity (> 1000 times) than CO and O_2 (1) and forms NO adduct (NOHb), is an unusual ligand. Addition of an effector, inositol-hexakis-phosphate (IHP), to NOHb changes its UV absorption and CD spectra, sulfhydryl reactivities, and exchangeable ^{1}H NMR signals sensitive to the R → T transition, although carbonmonoxyHb (COHb) and oxyHb exhibit no such changes. NO binds preferentially to the α subunit (affinity is 10 times higher to the α subunit than to the β subunit) in the presence of IHP (2), causing the transformation of Hb to a low-affinity extreme. Since there is no Bohr effect and no cooperativity in this state, it is conveniently called the 'T-(low affinity extreme)' state in this paper, which has been explicitly defined in ref 3. Indeed, NO has been successfully applied as clinical treatment of newborns with persistent pulmonary hypertension with no apparent acute adverse effect. The half-ligated α-nitrosyl β-deoxy hemoglobin, $\alpha^{NO}\beta^{deoxy}$, is stable and binds O_2 without cooperativity. When O_2 is bound to the β subunit of $\alpha^{NO}\beta^{deoxy}$, EPR study indicated its conversion to the high-affinity state under ordinary conditions but it remained in the low-affinity state in the presence of IHP at pH 4.8 (3).

NOHb normally contains the six-coordinate hemes, but, in the presence of IHP, the visible absorption (4), EPR (5-7), and resonance Raman studies (8) indicated cleavage of the Fe-His bond of α-NO hemes (α^{NO}) with no change for the β-NO hemes (β^{NO}). This change of the α^{NO} heme seems to generate the T-(low affinity extreme) state in the β^{deoxy} hemes. It is known that the Fe-His bond strength, reflected by the Fe-His stretching frequency, sensitively reflects the quaternary structure of Hb (9) and the Fe-His bond strength is weaker in the α than β subunit in the T state while they are similar in the R state (10). These facts may suggest that the intersubunit interactions at the α1-β2 interface have close correlation with the Fe-His bonding of the α subunit, while details remain to be clarified.

It has been demonstrated recently that resonance Raman (RR) spectra excited in the UV region around 220-240 nm can explore the environmental and hydrogen-bonding changes of Trp and Tyr residues of proteins (see refs 11 and 12 for a review). In fact, Rodgers et al. (13, 14), Nagai, M., et al. (15, 16), Huang et al. (17, 18), Hu et al. (19, 20), and Peterson and Friedman (21) reported the quaternary structure dependent features for Tyr and Trp residues in the α1-β2 interface of Hb from 230- and 235-nm excited UVRR spectra. In this paper, we present 235-nm excited UVRR spectra for normal NOHb, the half-ligated $\alpha^{NO}\beta^{deoxy}$, and the mix-ligated $\alpha^{NO}\beta^{CO}$ in the presence and absence of IHP at several pH values, discussing possible correlation between the Fe-His bonding of α hemes and intersubunit interactions at the α1-β2 interface for the quaternary structure change.

2.3 Experimental Procedures

Sample Preparation

Hemoglobin A was purified from fresh human blood by a preparative isoelectric focusing electrophoresis (22). Approximately 150 μL of the Hb solution (400 μM in heme) was put into a spinning cell made of a synthetic quartz ESR tube (diameter = 5 mm) (23). DeoxyHb and COHb were prepared by adding sodium dithionite (1 mg/mL) to oxyHb after replacement of the inside air of the sample tube with N_2 and CO, respectively. NOHb was obtained by addition of NO, which had been in advance passed through 1 M NaOH solution, to deoxyHb. The NO/O_2-mixed-ligated Hb, $\alpha^{NO}\beta^{O_2}$, was prepared by mixing equal amounts of isolated α-NO and β-O_2 chains, while a method for the preparation of the isolated α-NO chain was described elsewhere (3). The half-ligated Hb, $\alpha^{NO}\beta^{deoxy}$, was obtained through addition of a small amount of sodium dithionite to $\alpha^{NO}\beta^{O_2}$. The NO/CO-mixed-ligated Hb, $\alpha^{NO}\beta^{CO}$, was prepared by adding CO to $\alpha^{NO}\beta^{deoxy}$.

Just before the measurements of UVRR spectra, Na_2SO_4 was added to the samples at a final concentration of 0.2 M as an internal intensity standard of Raman spectra. It was confirmed that the

addition of sulfate did not cause any apparent Raman spectral change for the states examined in this study, since its use in Raman experiments was warned against due to possible tertiary structure change (24). IHP was added to the samples at a final concentration of 5 mM just before the Raman measurement. We used sodium acetate buffer under pH 6, phosphate buffer for the pH region from pH 6.5 to 7.5, and Tris buffer or borate buffer over pH 8.

Ultraviolet Resonance Raman Measurements

UVRR spectra were excited by a XeCl excimer laser-pumped dye laser system (EMG103MSC/LPX120 and FL2002/SCANMATE, Lambda Physik) as shown in Figure 1.10 of CHAPTER 1.3 Apparatus (25). The spinning cell was moved vertically by 1 mm for every spectrum (every 5 min) to shift the laser illumination spot on the sample (23). The temperature of the sample solution was kept at 10 ˚C by flashing with cooled N_2 gas against the cell. The scattered light was collected with Cassegrainian optics with f/1.1. One spectrum is composed of the sum of 400 exposures, each exposure accumulating the data for 0.8 sec. The Raman spectra shown in the figures are averages of 8-25 spectra. Raman shifts were calibrated with cyclohexane. Denaturation of the samples due to exposure to the ultraviolet laser light was carefully checked by inspecting a possible change in the visible absorption spectrum before and after the measurements of UVRR spectra. If some spectral changes were recognized, the Raman spectrum was discarded. Visible absorption measurements were carried out with a Hitachi 220S spectrophotometer.

EPR Measurements

EPR spectra were measured with a Varian X-band EPR spectrometer, Model E109 (Varian Associates, CA), integrated with a data acquisition system (Scientific Software Services, IL). EPR samples (300 μL of 500 μM heme) in quartz EPR tubes (3-mm precision bore) were frozen by immersion into liquid nitrogen and measured at liquid nitrogen temperature. The spectrometer was

operated at a microwave frequency of 9.11 GHz, microwave power of 20 mW, modulation frequency of 100 kHz, modulation amplitude of 2.0 G, magnetic field scan rate of 125 G/min, and time constant of 0.2 s. Recorded EPR data were manipulated with EPR software (Scientific Software Services) for quantitative analyses.

2.4 Results

Figure 2.1 shows the 235 nm excited UVRR spectra for deoxyHb (A), COHb (B), and their difference (C = A - B) at pH 6.7 in the frequency region from 1700 to 700 cm^{-1}. Although a strong broad band due to a synthetic quartz cell appeared between 800 and 900 cm^{-1}, its contribution was subtracted from the spectra shown here. The band at 982 cm^{-1} arises from SO_4^{2-} ions and was used to normalize the intensity of the spectra. (26). In the spectrum of deoxyHb, RR bands of tyrosine (Tyr) are seen at 1619 (Y8a), 1208 (Y7a), 1178 (Y9a) and 854 cm^{-1} (Y1), and those of tryptophan (Trp) are seen at 1558 (W3), 1360-1340 (W7; tryptophan doublet), 1012 (W16), 879 (W17), and 757 cm^{-1} (W18). The assignments are based on Harada and co-workers (11, 27, 28). The UVRR spectra of deoxyHbA and COHbA in the 1700-850 cm^{-1} region are in agreement with those reported by Rodgers et al. (13) and Nagai, M., et al. (15), while the spectra between 850 and 700 cm^{-1} are newly added. It was confirmed that the spectra of deoxyHb and COHb exhibited negligible changes upon addition of IHP (not shown).

The difference spectrum between deoxyHbA and COHbA (C) indicates that the intensities of the W3, W16, W17, and W18 bands of Trp are much weaker for COHbA than for deoxyHb, while the peak positions remain unaltered, and that the frequencies of the Y8a and Y9a bands of Tyr are lower for COHb than for deoxyHb. These differences arise from some differences in hydrogen bonding states and surrounding hydrophobicity of Trp and Tyr residues between the two states (29) and have been ascribed to a consequence of changes in subunit contacts (13-21, 30).

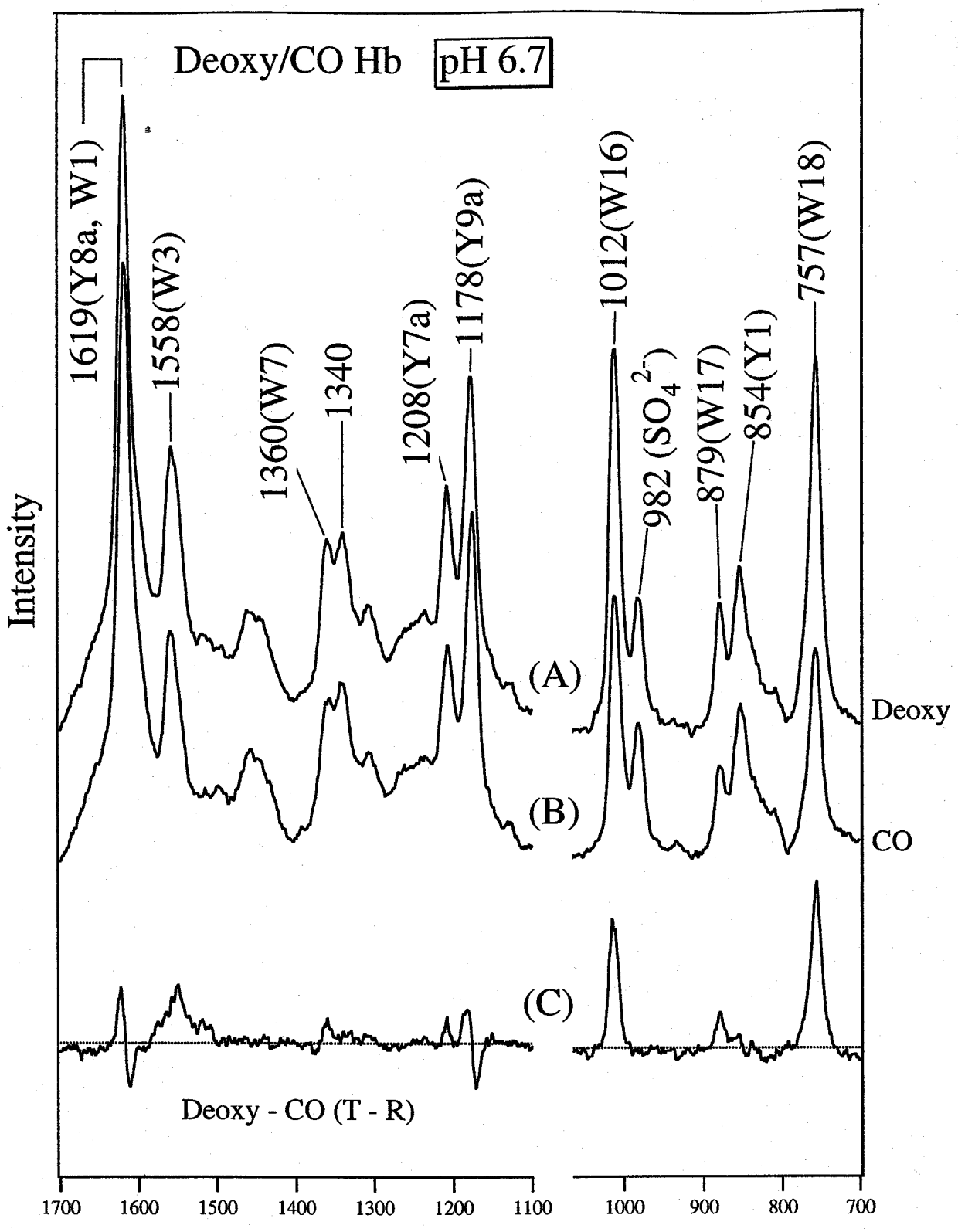

Figure 2.1

235-nm excited UVRR spectra of deoxy Hb (A), COHb (B), and their difference spectra (C) (= deoxy Hb - COHb).

Hereafter spectrum (C) is referred to as the standard for the T minus R difference spectrum, reflecting the typical changes at the α1-β2 subunit interface upon quaternary structure transition ("T-like" and "R-like" will be used to represent that the local structure surrounding a particular residue in question is similar to that in the ordinary T and R subunit contact, but does not always mean that the tertiary structure is T and R, respectively).

Figure 2.2 shows the UVRR spectra of NOHb in the presence (A) and absence (B) of IHP at pH 6.7 and their difference (D) in addition to the difference (C) between deoxyHb and NOHb in the absence of IHP. A relatively strong band appeared around ~1340 cm^{-1} in the raw spectrum of NOHb. This band is due to NO_2^- ions produced from NO in water. The UVRR spectrum of NO_2^- ions in water was measured separately and subtracted from the spectrum of NOHb prior to the difference calculations. As shown by spectrum (C), the difference spectrum between deoxyHb and NOHb is almost the same as spectrum Figure 2.1(C), suggesting that NOHb in the absence of IHP has an R-like α1-β2 contact similar to COHb. Addition of IHP, however, causes distinct spectral changes especially on Trp bands; the intensities of the W3, W16, and W18 bands increased. The magnitude of the intensity increase of Trp bands is nearly half of those seen in the standard T minus R difference spectrum (Figure 2.1(C)), when the intensity of the SO_4^{2-} band is referred. It is noted that the peak positions of Tyr bands are not shifted upon addition of IHP. Therefore, Tyr residues of NOHb in the presence of IHP adopt the same structure as that in the R structure, while Trp residues are half-T-like structure (half may mean either the number of residues involved or all residues with half strength). Thus, the behaviors of Trp and Tyr residues are not always synchronous with the change of subunit contacts.

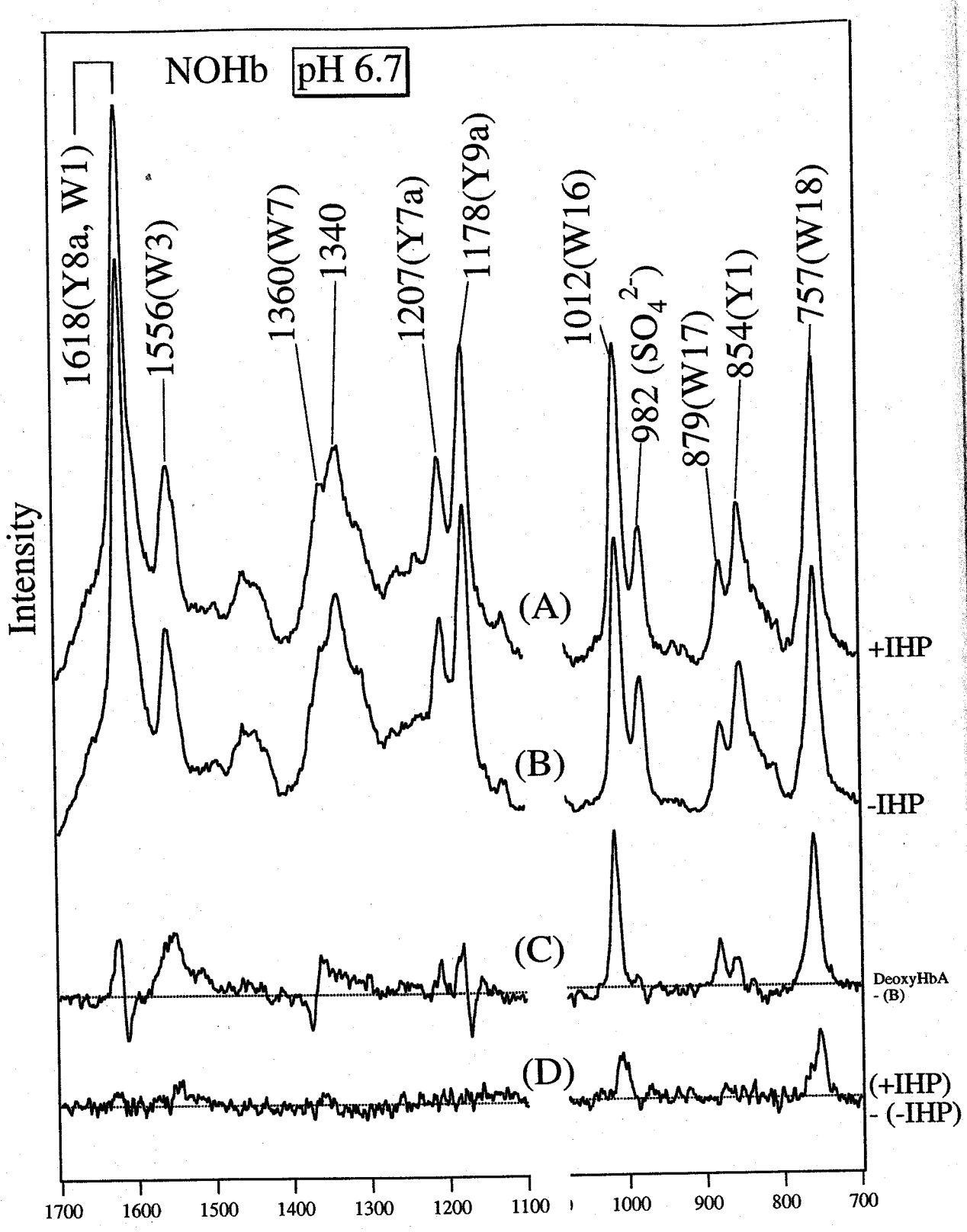

Figure 2.2

UVRR spectra of NOHb at pH 6.7 in the presence of IHP (A) and in its absence (B), the difference spectrum deoxyHb minus NOHb(-IHP) (C), and the difference spectrum NOHb(+IHP) - NOHb(-IHP) (D).

Figure 2.3 shows the UVRR spectra of NOHb in the presence (A) and absence (B) of IHP at pH 5.2 in the frequency region from 1700 to 700 cm^{-1}. There has been no difference between spectra of deoxyHb at pH 6.7 and 5.2. The difference spectra between deoxyHb and NOHb in the absence (C) and presence (D) of IHP at pH 5.2 are somewhat dissimilar to each other, and both are appreciably different from the standard T - R difference spectrum [reproduced by (E)]. In the absence of IHP, the difference spectrum (C) is apparently the same as that between deoxyHb and COHb (E), while detailed analysis has clarified the presence of an intensity difference in Trp bands, especially W16 and w18 [weaker in (C)]. This means that the structure of Trp in NOHb(-IHP) is somewhat different from that in COHb. The intensity patterns of Tyr in spectra (C) and (E) are alike. In the presence of IHP (D), the intensities of Trp bands are weaker, indicating that the structures of Trp residues become closer to those of deoxyHb, while Tyr bands are slightly affected by IHP. The difference spectrum of NOHb between the presence and absence of IHP (F) shows weak but definite changes for Tyr bands in addition to those of Trp bands. It is evident from the comparison of Figure 2.3(F) with Figure 2.2(D) that the effect of IHP was recognized only for Trp bands at pH 6.7 but for both Tyr and Trp bands at pH 5.2.

Figure 2.4 shows the UVRR spectrum of NOHb in the presence of IHP at pH 8.2. The spectrum remained unchanged between the presence and absence of IHP. Its difference spectra with regard to deoxyHb and COHb are depicted by spectra (B) and (C), respectively. Spectrum (B) is almost the same as Figure 2.1(C), and there are no clear difference peaks in spectrum (C), meaning that the subunit interface structures of NOHb in the presence of IHP at pH 8.2 resemble those of COHb, and effects of IHP as an allosteric effector are small.

Figure 2.5 shows the UVRR spectra of the half-ligated Hb, $\alpha^{NO}\beta^{deoxy}$, in the presence of IHP at pH 5.6 (A) and in its absence at pH 8.8 (B) in the frequency region from 1700 to 700 cm^{-1}. It was confirmed by EPR that there was no detectable migration of NO from the α^{NO} to β^{deoxy} heme in $\alpha^{NO}\beta^{deoxy}$ during the measurement time under these experimental conditions (3).

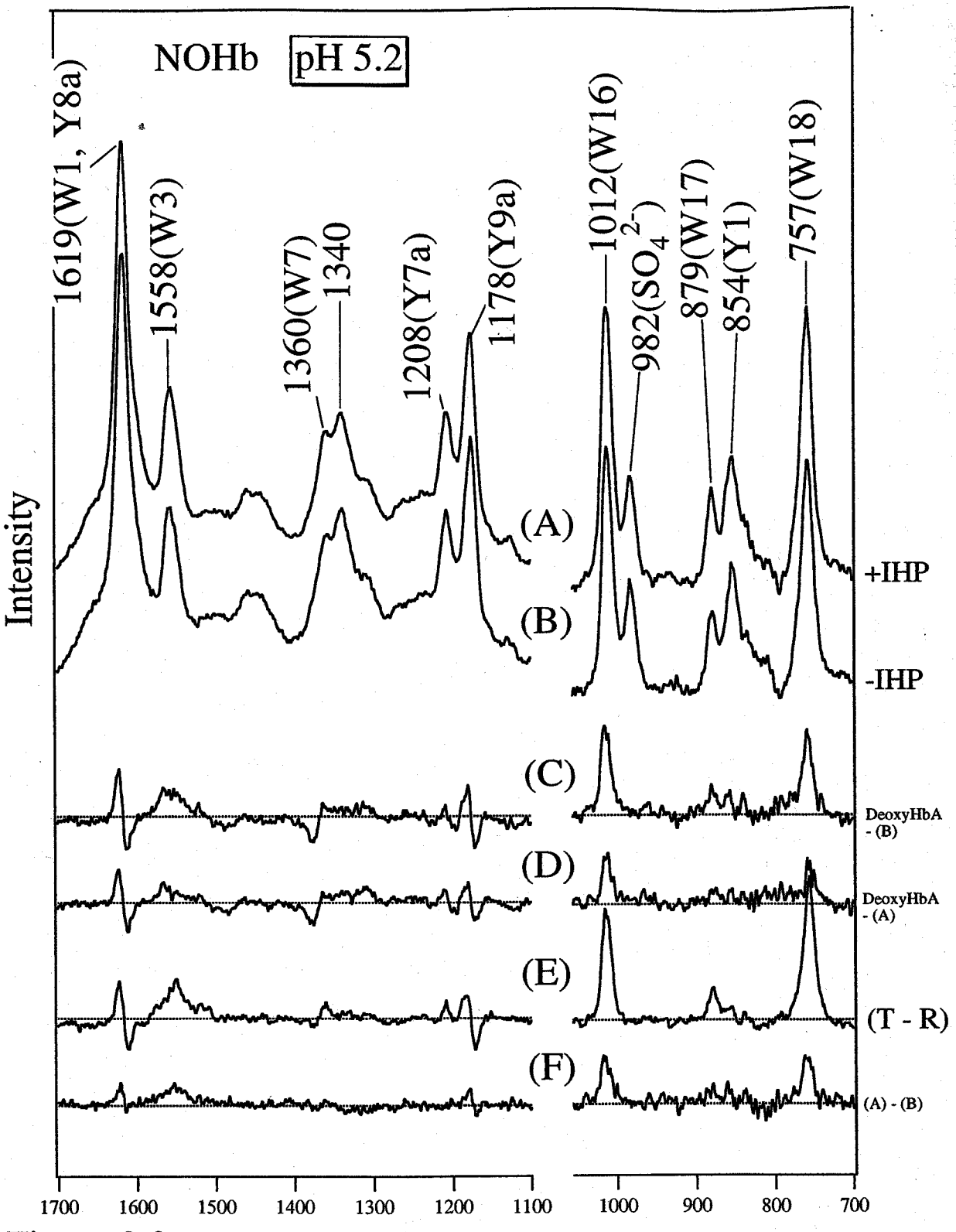

Figure 2.3

UVRR spectra of NOHb at pH 5.2 in the presence (A) and absence (B) of IHP, and difference spectra: (C) deoxyHb at pH 6.7 - (B); (D) deoxyHb at pH 6.7 - (A); (E) Figure 1(C); and (F) (A) - (B).

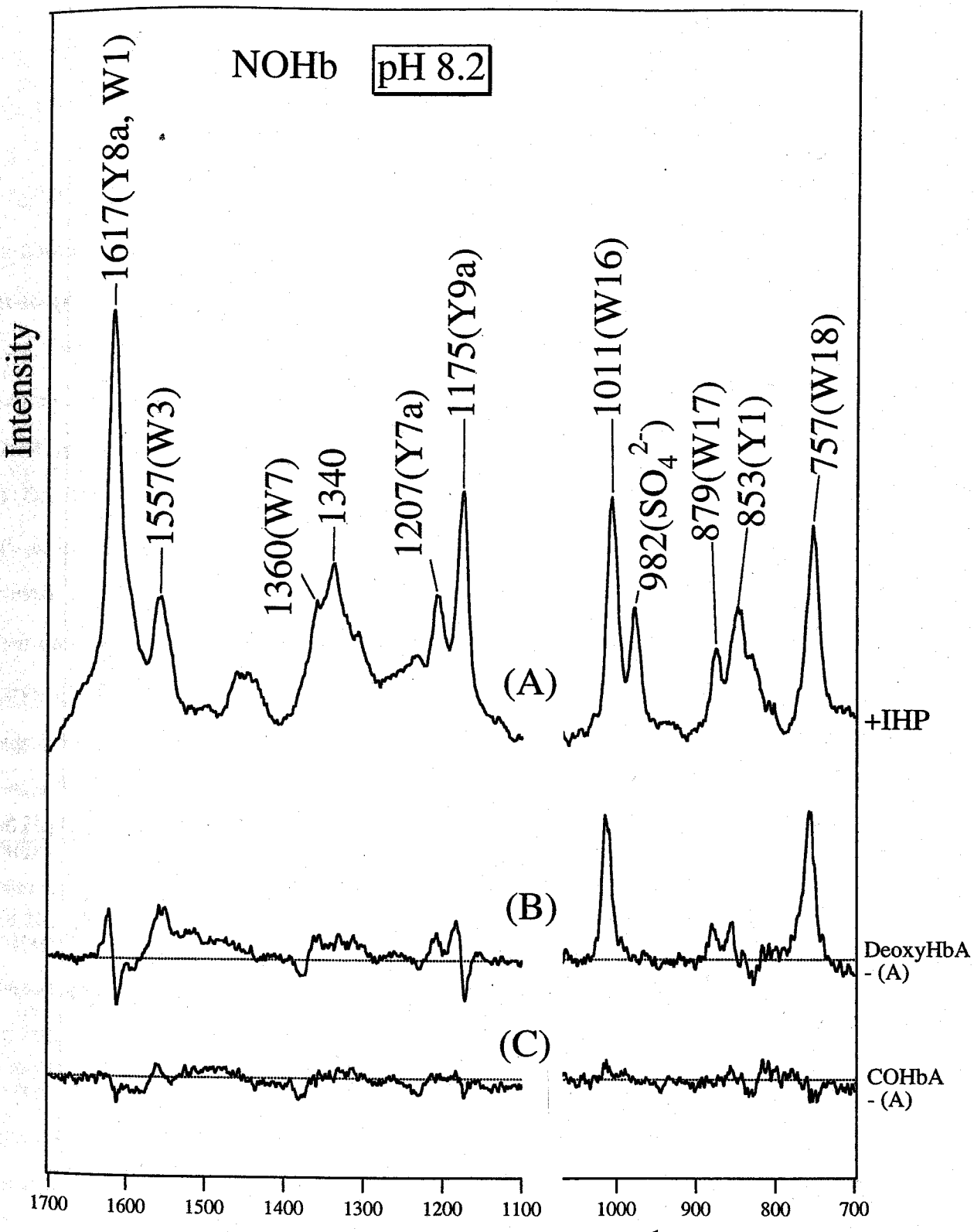

Figure 2.4

UVRR spectrum of NOHb at pH 8.2 in the presence of IHP (A)
nd difference spectra: (B) deoxyHb at pH 6.7 - (A); (C) COHb at pH 6.7 - (A).

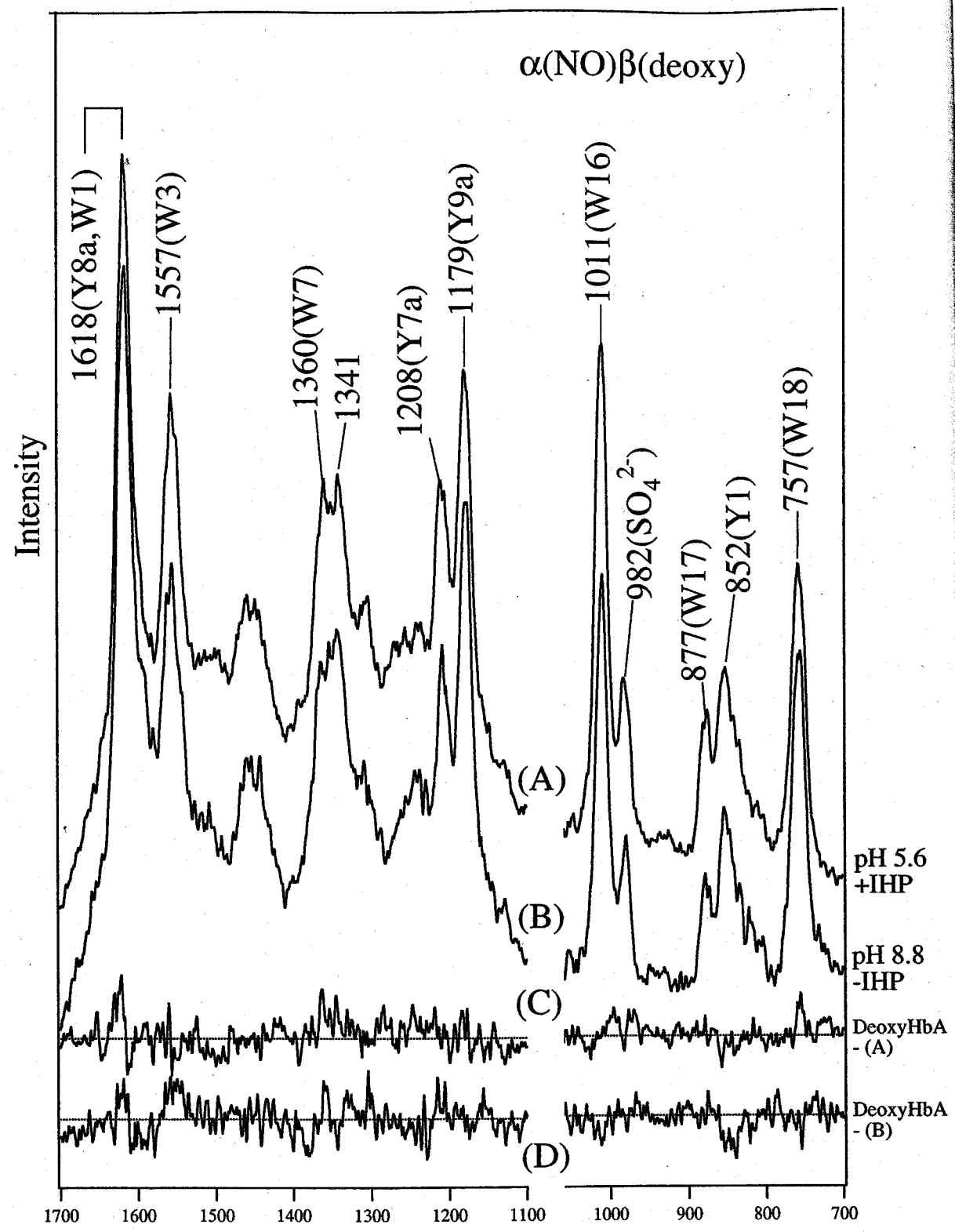

Figure 2.5

UVRR spectra of a(NO)b(deoxy) in the presence of IHP at pH 5.6 (A) and in the absence of IHP at pH 8.8 (B) and difference spectra with regard to deoxyHb: (C) deoxyHb at pH 6.7 - spectrum(A); (D) deoxyHb at pH 8.8 - a(NO)b(deoxy) at pH 8.8 in the absence of IHP.

Since partial deprotonation of Tyr, that would give rise to a more intense Y8a band around 1600 cm^{-1}, may be involved at higher pH, the spectrum of deoxyHb was measured at pH 8.8 (not shown), and used for the difference calculations described below. The difference spectra of $\alpha^{NO}\beta^{deoxy}$ [(A) and (B)] with regard to deoxyHb are depicted by traces (C) and (D), respectively. These difference spectra exhibit no clear peaks, indicating that the half-ligated $\alpha^{NO}\beta^{deoxy}$ at both pHs adopts the T structure, similar to deoxyHb irrespective of the presence or absence of IHP.

Figure 2.6 shows the UVRR spectrum of the mixed-ligated Hb, $\alpha^{NO}\beta^{CO}$, at pH 8.8 in the absence of IHP. Its spectra at pH 5.5 in the presence of IHP (A) and at pH 7.5 in the absence of IHP (B) are also shown in the inset together with their differences against deoxyHb at pH 6.7 [(C) and (D)]. The difference spectrum, deoxyHb at pH 6.7 minus $\alpha^{NO}\beta^{CO}$ at pH 8.8 in the absence of IHP, is depicted by spectrum (F). We confirmed by EPR that no detectable ligand exchange occurred in the mixed-ligand Hb, $\alpha^{NO}\beta^{CO}$, under the present experimental conditions (3). Spectrum (F) is almost the same as Figure 2.1(C), meaning that the mixed-ligated $\alpha^{NO}\beta^{CO}$ in the absence of IHP at pH 8.8 adopts the R structure similar to COHb. However, this situation is changed when the pH is lowered. The intensities of the W16, W17, and W18 bands of Trp are stronger in spectra (A) than (B). The difference spectra for deoxyHb at pH 6.7 - $\alpha^{NO}\beta^{CO}$ at pH 5.5 and 7.5, represented by traces (C) and (D), respectively, exhibit similar patterns, but peak intensities are stronger in trace (D) than trace (C). Accordingly, Trp residues of $\alpha^{NO}\beta^{CO}$ in the presence of IHP at pH 5.5 stay in a more T-like structure.

Figure 2.7 plots the proportions of the five-coordinated α^{NO} heme in NOHb determined with EPR against pH. The proportions of the T-like contact evaluated by UVRR Trp bands under the assumption that deoxyHb and COHb at pH 6.7 adopt the 100% T and R structures, respectively, are also plotted against pH in the same figure. It is clear that the proportion of five-coordinate species decreases at higher pH and the transition pH from the five- to six-coordinate

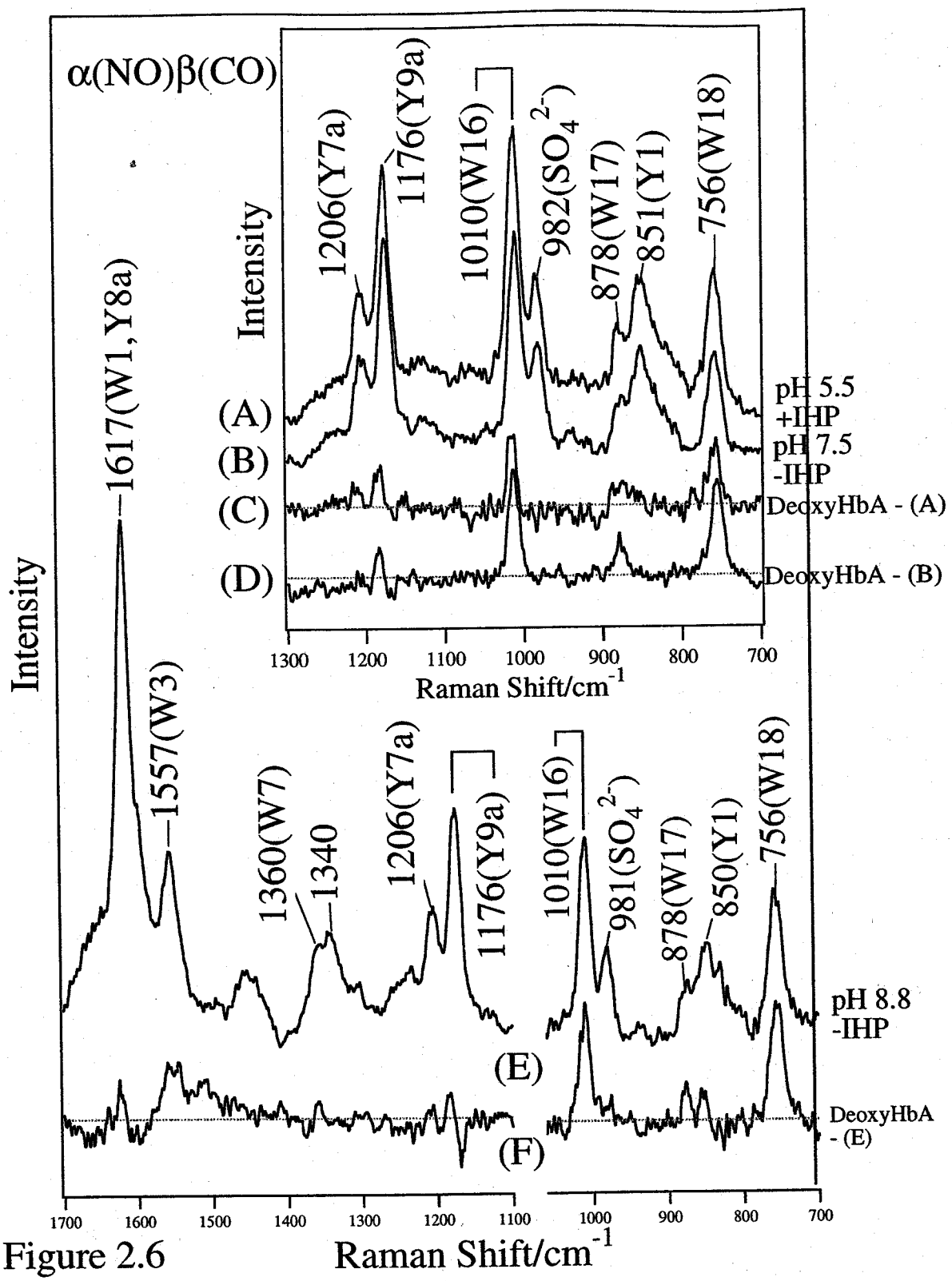

Figure 2.6

UVRR spectra of α(NO)β(CO) at pH 5.5 in the presence of IHP (A) and α(NO)β(CO) at pH 7.5 in the absence of IHP (B) and difference spectra: (C) deoxyHb at pH 6.7 - (A); (D) deoxyHb at pH 6.7 - (B); raw spectrum of α(NO)β(CO) at pH 8.8 in the absence of IHP (E), and its difference spectrum; (F) deoxyHb (pH 6.7) - (E).

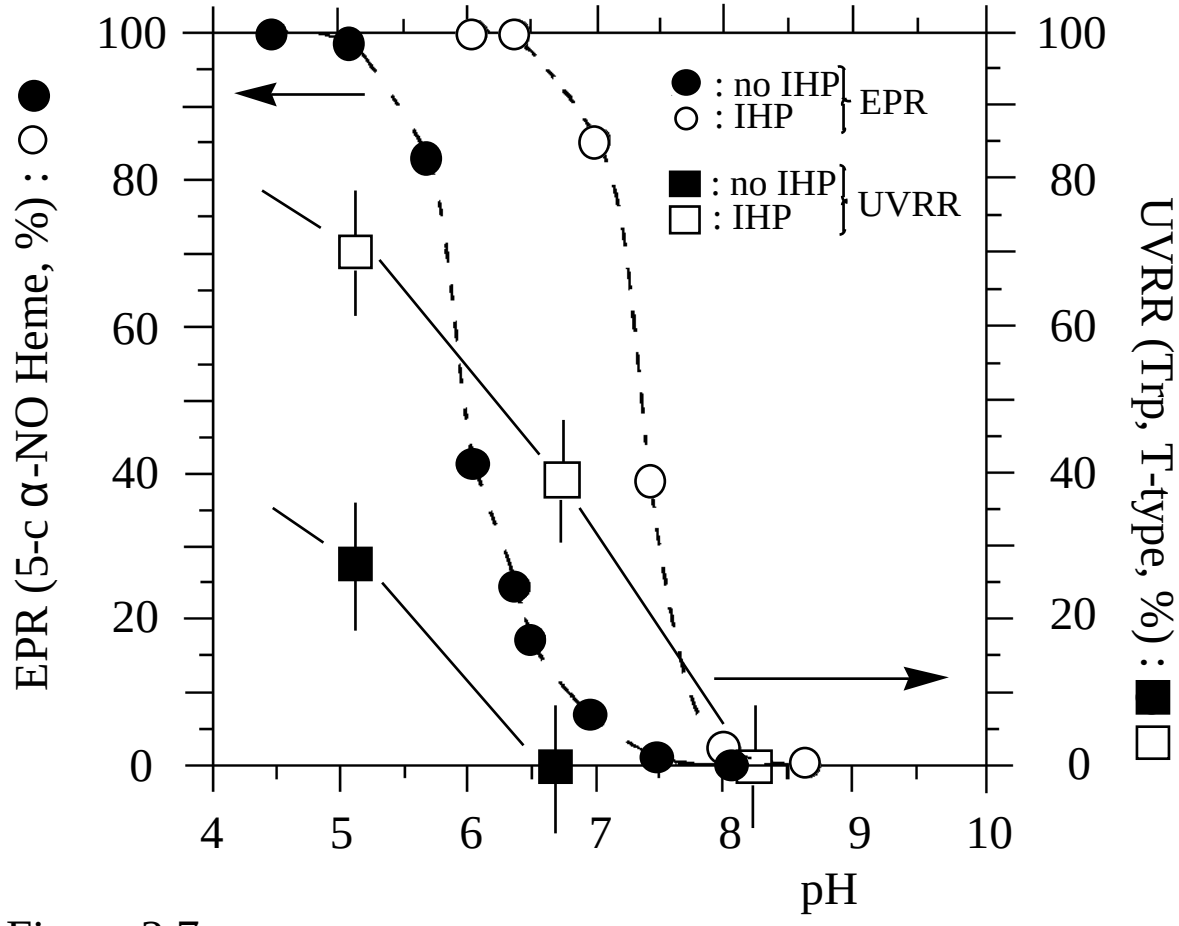

Figure 2.7

Proportion of the cleaved Fe-His bond of α heme in NOHb determined by EPR and proportion of the T-type contact of Trp residues at the subunit interface determined for NOHb by UVRR (see text). Squares are circles denote the UVRR and EPR data, respectively, and closed and open symbols represent the data for the solution in the absence and presence of IHP, respectively.

structure is higher in the presence of IHP. The proportion of the T-like contact deduced from UVRR at room temperature exhibits the same trend, although the percentage values are not in

agreement with the amount of five-coordinate α hemes deduced from EPR at 77K. The difference in the experimental temperature could be a possible origin of the discrepancy, since the stabilities of hydrogen bonds and hence of quaternary structures are temperature dependent. Nevertheless, we emphasize that the behavior of the Trp residue at the α1-β2 interface is qualitatively correlated with the Fe-His bonding of α heme. The presence of such a qualitative correlation between the Fe-His bond and the α1-β2 interface contacts has been pointed out by recent RR studies (20, 21). It is clear that IHP shifts the pK_a of two equilibrium structures toward an alkaline side.

2.5 Discussion

Correlation between the Fe-His Bond of the α heme and the α1-β2 Subunit Interface Structure

NOHb has been extensively studied because it has been demonstrated from EPR (5-7), visible absorption (4), and RR (8) studies that the Fe-His bond of the α heme is cleaved in the presence of IHP. However, the structure of the α1-β2 subunit interface of NOHb has not been clarified so far. UVRR spectroscopy excited at 220-240 nm can sensitivity monitor the structural changes of aromatic residues located in the α1-β2 subunit interface (13, 14, 17-21). Previous studies have demonstrated that the major intensity change of Trp UVRR bands upon the T – R transition arises from Trp-β37 (15) and that the frequency shift of Y8a and Y9a bands of Tyr upon the T - R transition is mainly due to α42- and α140-Tyr residues, while their intensity changes are due to α140- and β145-Tyr residues (16, 31). The results are consistent with the recent UVRR study on subunit-specific isotope labeling of recombinant HbA (19).

NOHb in the absence of IHP exhibited the UVRR spectrum of R structure at pH 6.7, but the spectrum changed upon the addition of IHP (Figure 2.2). The resultant subunit interface contains Tyr residues with R-like contact and Trp residues with R/T-intermediate contact. The proportion of the T-type contact of Trp exhibited qualitative correlation with the cleaved proportion of the Fe-His bond of the α heme (Figure 2.7). However, it should be stressed that the behaviors

of Trp and Tyr bands are not synchronous, meaning that the whole protein structures cannot be represented by simple two concepts, that is, T and R structures, although individual residues may take two alternative structures. A recent UVRR study of Hb Kempsey (20) has also shown that Trp and Tyr signals do not develop in concert. In its time-resolved UVRR, Trp W3 difference develops much faster than the sigmoidal Y8a/Y8b bands of Tyr residues. Accordingly, we use T-like or R-like contact to describe the local structure of a given residue. The Tyr bands of NOHb behaved mostly R-like except for $\alpha^{NO}\beta^{deoxy}$.

The UVRR spectrum of the mixed-ligand $\alpha^{NO}\beta^{CO}$, in the presence of IHP indicated an intermediate state between the T and R structures as shown in the inset of Figure 2.6, similar to NOHb. This suggests that irrespective of the species of the sixth ligand bound to the β heme the subunit interface adopts an intermediate contact for Trp residues and R-like contact for Tyr residues, when NO is bound to the α heme in the presence of IHP. However, the content of the T structure evaluated with Trp bands does not always agree with the population of the α heme with the Fe-His bond cleaved.

In the case of half-NO-ligated Hb, $\alpha^{NO}\beta^{deoxy}$, both Tyr and Trp bands in UVRR spectra exhibited the characteristics of the T-structure similarly at pH 5.6 and 8.8. On the other hand, EPR showed that the population of the α^{NO} heme with the Fe-His bond broken is ~100% at pH 5.5 but 50-60% at pH 8.8 in the presence of dithionite (not shown). Here again, the cleaved proportion of the Fe-His bond of α heme does not agree with the proportion of T-like contact at the α1-β2 interface evaluated from the Trp UVRR bands. The difference in temperature of the two measurements might be a possible origin of the discrepancy. Nonetheless, there is a qualitative trend that the cleavage of the Fe-His bond of the α heme leads to the T-like α1-β2 interface structure, and the addition of IHP promotes both features. The effect of IHP is smaller at higher pH, and one reason is that the Fe-His bond is more stable at higher pH. The lack of complete correspondence between Fe-His bond cleavage and T-like subunit contacts is presumably due to the

fact that ligand binding to the β heme appreciably affects the α1-β2 subunit contact, although it is mainly determined by the Fe-His bond of α heme. In fact, detailed comparison of UVRR spectra of NOHb and $\alpha^{NO}\beta^{deoxy}$ suggests that the Tyr contacts at the α1-β2 interface are more sensitive to ligand binding to β heme than the cleavage of Fe-His bond of α heme.

Communication between the Heme Moiety and Subunit Interface

Figure 2.8 illustrates the main chain arrangements of deoxyHb at the α1-β2 contact region where significant rearrangements of residues occur upon the T → R transition (32). Three likely pathway of communication from the α heme to β heme have been proposed (33). In all of them, a change of the Fe-His bond of α heme is perceived first by Val-α93 (FG5). This residue communicates the change of the Fe-His bond to Tyr-α140 (HC2), which forms a hydrogen bond in T-like contact, and then it is communicated to Trp-β37. There is also another pathway that includes Val-α93 (FG5) → Arg-α92 (FG4) → Arg-β40 (C6) → Tyr-α42 (C7) → Asp-β99 (G1) → Val-β98 (FG5) His-β92 (F8), in which Thr-α41 (C6) instead of Asp-β99 (G1) can also communicate the information to Val-β98 (FG5) through Tyr-β145 (HC2) (33). Other study suggests communication from the α heme to the β heme through a hydrogen bond between Asp-α94 and Trp-β37 which exists in the T-state but not in the R-state (34). In any cases, cleavage of the Fe-His bond in the α heme causes appreciable changes in the environmental conditions of Tyr-α42, Tyr-α140, Tyr-β145, and Trp-β37. Accordingly, it is reasonable that UVRR spectral change of Trp-β37 has qualitative correlation with the cleavage of the Fe-His bond of the α heme. The recent X-ray crystallographic (35) as well as Raman studies (21) of β37 mutants together demonstrated a direct link between changes in the Fe-His bond and those of both Tyr-α140 and Trp-β37. These results are directly relevant to the present UVRR findings.

When NO binds to β hemes, it is thought that Val-β67 (E11) imposes steric hindrance to bound NO. However, the X-ray crystallographic analysis pointed out that movements of Val-β67

(E11) upon ligand binding to the β heme are not large but the change in the proximal side is rather large (36, 37). It means that the proximal His (His-β92) moves upon ligand binding and the

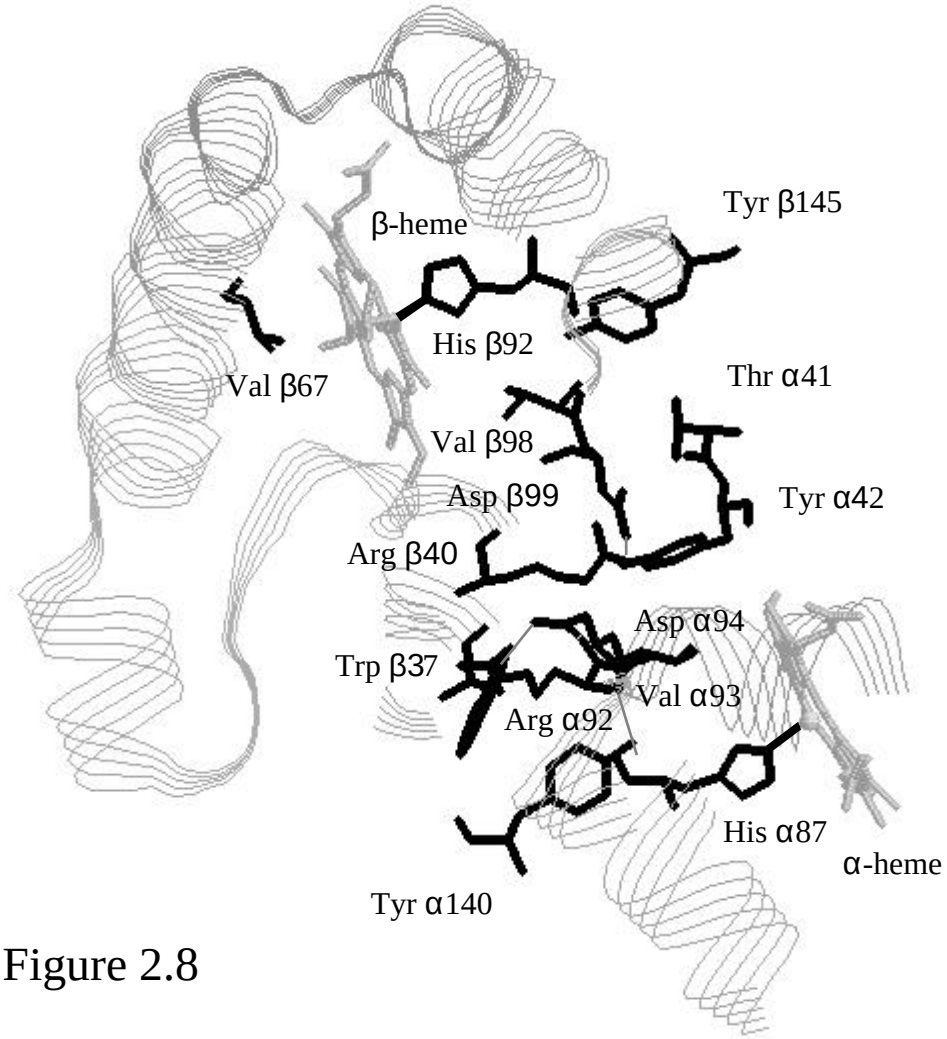

Figure 2.8

Main chain arrangement and orientation of amino acid side chains at α1-β2 contact of deoxyHbA. Tyr-α42, Tyr-α140, and Trp-β37 which are responsible for the UVRR spectral changes are also contained. X-ray crystallographic coordinates are taken from the Protein Data Bank (39). The thick and thin broken lines denote the Fe-His bond and hydrogen bond, respectively.

neighboring Val-β98 (FG5) follows it in a way similar to that in the α subunit. Then, the information can proceed to the opposite direction through the communication pathway which was described above for the transmission of information from the α to the β subunit, and accordingly Tyr-β145 (HC2) and Tyr-α42 (C7) would be more sensitively influenced than Trp-β37. These two tyrosine residues would be sensitive when the β heme is six-coordinate but the α heme is five-coordinate. In fact, both $\alpha^{NO}\beta^{deoxy}$ (Figure 2.5A) and $\alpha^{NO}\beta^{NO}$ (Figure 2.3A) at pH 5.2-5.6 in the presence of IHP have the cleaved Fe-His bond of α heme, but the Tyr bands of the former and latter are T- and R-like, respectively. The Trp-β37 is less T-like in the latter than in the former.

However, we cannot rule out the idea that the role of the Fe-His bond of β heme is functionally different from that of the Fe-His bond of α heme, when the following facts are considered: $\alpha(Fe)_2\beta(porphyrin)_2$ Hb undergoes normal T - R transition upon ligation at the α subunits in the absence of the Fe-His bond of β heme. In the case, Tyr-α42 and Tyr-β145 must be influenced by the passageway originating from the α subunits. On the other hand, $\alpha(porphyrin)_2\beta(Fe)_2$ Hb is regarded as the T-(low affinity extreme) state at low pH regardless of the ligation at the β subunits because of the absence of the Fe-His bond of α heme (38). The UVRR spectrum of $\alpha(porphyrin)_2\beta(Fe)_2$ Hb, which has not yet been obtained, would be close to that of $\alpha^{NO}\beta^{deoxy}$ at pH 5.5 in the presence of IHP observed in this study. Presumably the ligand binding effects of β heme must be smaller in strength (of energetically smaller contribution) than those of α heme but disturb the qualitative correlation between Fe-His bond cleavage of α heme and the population of T-like α1-β2 contact estimated from UVRR.

The result of $\alpha^{NO}\beta^{deoxy}$ in the absence of IHP at pH 8.8 is to be noted. There is no migration of NO from the α to the β subunit during the experiment (3). The UVRR spectrum of $\alpha^{NO}\beta^{deoxy}$ suggests the T-like contact at the α1-β2 interface, but its EPR spectrum indicates that the six-coordinate state holds 50-60% in the α^{NO} heme (not shown). This may suggest that the coordination of an external ligand to the β heme also causes some movement of Trp-β37 and

changes the α1-β2 contact toward the R-type. In fact, ligation of NO or CO to the β heme of $\alpha^{NO}\beta^{deoxy}$ in the absence of IHP changed the α1-β2 contact to yield the complete R structure, and the ligation in the presence of IHP caused the change from T- to half-R-like. This apparently inconsistent observation would also be interpreted by taking the ligand binding effects of the β heme mentioned above into consideration. Consequently, the factor that determines the interface contact is not only the Fe-His bond of the α heme but also the Fe-His bond of the β subunit which is caused by ligation to the β heme, although the strength of the effect of β heme is smaller than that of α heme.

The importance of the coordination of a ligand to the β heme is also noted for the half-ligated normal Hb, $\alpha^{O_2}\beta^{deoxy}$, for which X-ray crystallographic analysis (39, 40) demonstrated a T-structure similar to deoxyHb, although its crystal was grown from poly(ethylene glycol). The fact that $\alpha^{O_2}\beta^{deoxy}$ takes the T-structure means that the sum of free energy resulting from the structural changes of α hemes by ligand binding and from the subunit contacts at the α1-β2 interface is of a magnitude comparable to the lattice energy required to retain the structure of a whole molecule in the initially prepared crystal. A qualitatively similar conclusion is obtained with the α(Fe)β(Ni) metal hybrid Hb, $\alpha^{Fe}\beta^{Ni}$, for which the ^{1}H NMR study (41) demonstrated the presence of T-like contact at the α1-β2 interface even after CO was bound to the α heme in the presence of IHP at pH 7.4. In both $\alpha^{Fe\text{-}CO}\beta^{Ni}$ and $\alpha^{O_2}\beta^{deoxy}$ Hbs, the Fe-His bond of α heme remains intact, but the quaternary structure takes the T structure.

Relation between the Fe-His Bond of α Heme and Quaternary Structure

UVRR results show that $\alpha^{NO}\beta^{CO}$ in the absence of IHP at pH 8.8 (Figure 2.6E) and in the presence of IHP at pH 5.5 (Figure 2.6A) takes R and half-R contact, respectively, with regard to Trp-β37. In contrast, Trp-β37 in $\alpha^{NO}\beta^{deoxy}$ was T-like under both conditions (Figure 2.5). This means that binding of CO to the β^{deoxy} heme causes a shift of the quaternary equilibrium to R but

the structural change is more difficult for the latter than the former conditions. One of the differences between $\alpha^{NO}\beta^{deoxy}$ in the presence of IHP at pH 5.5 and in its absence at pH 8.8 is population of the cleaved Fe-His bond of the α heme. On the basis of the EPR spectra observed (not shown), the Fe-His bond is retained by 50-60% of the α hemes in the absence of IHP at pH 8.8 but no α hemes in the presence of IHP at pH 5.5 (not shown). This suggests that cleavage of the Fe-His bond of α heme stabilizes the T-type contacts at the α1-β2 interface. Liddington et al. (40) pointed out from the structural analysis of $\alpha^{O_2}\beta^{deoxy}$ Hb that the preservation of the six-coordinate planar structure of the α heme within the T structure increases the conformational strain and thus results in unstability of the T structure. For an abnormal Hb, Hb Yakima (Asp-β99 → His), known as a high-affinity Hb (42), the high affinity has been attributed to the lack of a hydrogen bond between Tyr-α42 and Asp-β99 (Figure 2.8) in the α1-β2 interface which normally stabilizes the T structure. Accordingly, the higher oxygen affinity to the β heme of $\alpha^{NO}\beta^{deoxy}$ in the absence of IHP at pH 8.8 than that to ordinary deoxyHb is also consistent with the unstability of the T structure at the α1-β2 interface. In this sense, the Fe-His bond of α hemes seems to influence the quaternary structural transition and oxygen affinity.

In conclusion, the Fe-His bond of α hemes is not the sole origin of the structural changes at α1-β2 interface, because $\alpha^{NO}\beta^{deoxy}$ exhibits T-like UVRR spectra regardless of pH and IHP while the proportion of the cleaved Fe-His bond of α hemes is varied. There are, however, appreciable differences in the stability of the T-like contact of the α1-β2 interface between the absence and presence of the Fe-His bond of α heme. Ligand binding to β hemes also changes the α1-β2 interface contact through the movement of the proximal His (β92, F8) and thus the quaternary structure.

References

1. Gibson, Q. H., and Roughton, F. W. (1957) *Proc. R. Soc. London B 147,* 44-56.

2. Huang, T.-H. (1979) *J.Biol.Chem. 254,* 11467-11474.

3. Yonetani, T., Tsuneshige, A., Zhou, Y., and Chen, X. (1998) *J. Biol. Chem. 273*, 20323-20333.

4. Perutz, M. F., Kilmartin, J. V., Nagai, K., Szabo, A., and Simon, S. R. (1976) *Biochemistry, 15,* 378-387.

5. Salhany, J. M., Ogawa, S., and Shulman, R. G., (1975) *Biochemistry, 14,* 2180-2190.

6. Nagai, K., Hori, H., Yoshida, S., Sakamoto, H., and Morimoto, H. (1978) *Biochim. Biophys. Acta* 532, 17-28

7. Hille, R., Olson, J. S., and Palmer, G. (1979) *J.Biol.Chem. 254,* 12110-12120.

8. Nagai, K., Welborn, C., Dolphin D., and Kitagawa, T. (1980) *Biochemistry 19,* 4755-4761.

9. Nagai, K., Kitagawa, T., and Morimoto, H. (1980) *J. Mol. Biol. 136,* 271-289.

10. Nagai, K., and Kitagawa, T. (1980) *Proc. Natl. Acad. Sci. USA 77,* 2033-2037.

11. Harada, I., Miura, T., and Takeuchi, H. (1986) *Spectrochim.Acta 42A,* 307-312.

12. Kitagawa, T. (1992) *Prog. Biophys. Mol. Biol. 58,* 1-18.

13. Rodgers, K. R., Su, C., Subramaniam, S., and Spiro, T. G. (1992) *J. Am. Chem. Soc. 114,* 3697-3709.

14. Rodgers, K. R., and Spiro, T. G. (1992) *Science, 265,* 1697-1699.

15. Nagai, M., Kaminaka, S, Ohba, Y, Nagai, Y, Mizutani, Y., and Kitagawa, T. (1995) *J.Biol.Chem. 270,* 1636-1642.

16. Nagai, M., Imai, K., Kaminaka, S, Mizutani, Y., and Kitagawa, T. (1996) *J. Mol. Struct., 379,* 65-75.

17. Huang, S., Peterson, E. S., Ho, C., and Friedman, J. M. (1997) *Biochemistry 36,* 6197-6206.

18. Huang, J., Juszczak, L., Peterson, E. S., Shannon, C.F., Yang, M., Huang, S., Vidugiris, G. V. A., and Friedman, J. M. (1999) *Biochemistry 38,* 4514-4525.

19. Hu, X., and Spiro, T. G. (1997) *Biochemistry 36,* 15701-15712.

20. Hu, X., Rodgers, K. R., Mukerji, I., and Spiro, T. G. (1999) *Biochemistry 38,* 3462-3467.

21. Peterson, E. S., and Friedman, J. M. (1998) *Biochemistry 37,* 4346-4357.

22. Nagai, M., Nishibu, M., Sugita, Y., Yoneyama, Y., Jones, R. T., and Gordon, S. (1975) *J. Biol. Chem. 250,* 3169-3173.

23. Kaminaka, S., and Kitagawa, T. (1995) *Appl. Spectrosc. 49,* 685-687.

24. Song, S., and Asher, S. A. (1991) *Biochemistry 30,* 1199-1205.

25. Kaminaka, S., and Kitagawa, T. (1992) *Appl. Spectrosc. 46,* 1804-1808

26. Dudik, J. M., Johnson, C. R., and Asher, S. A. (1985) *J .Chem. Phys. 82,* 1732-1740.

27. Miura, T., Takeuchi, H., and Harada, I. (1988) *Biochemistry 27,* 88-94.

28. Miura, T., Takeuchi, H., and Harada, I. (1989) *J. Ranan Spectrosc. 20,* 667-671.

29. Harada, I., and Takeuchi, H. (1986) *Adv. Spectrosc.13,* 113-175.

30. Kaminaka, S., and Kitagawa, T. (1992) *J. Am. Chem. Soc. 114,* 3256-3260.

31. Nagai, M., Wajcman, H., Lahary, A., Nakatsukasa, T., Nagatomo, S., and Kitagawa, T. (1999) *Biochemistry 38,* 1243-1251.

32. Fermi, G., Perutz, M. F., Shaanan, B., Fourme, R. (1984) *J. Mol. Biol. 175,* 159-174.

33. Ho, C. (1992) *Adv. Protein Chem. 43,* 152-312.

34. Ishimori, K., Imai, K., Miyazaki, G., Kitagawa, T., Wada, Y., Morimoto, H., and Morishima, I. (1992) *Biochemistry, 31,* 3256-3264.

35. Kavanaugh, J. S., Weydert, J. A., Rogers, P. H., and Arnone, A. (1998) *Biochemistry 37,* 4358-4373.

36. Perutz, M. F., Fermi, G., Luisi, B., Shaanan, B., and Liddington, R. C. (1987) *Acc. Chem. Res. 20,* 309-321.

37. Baldwin, J., and Chothia, C. (1979) *J. Mol. Biol. 129,* 175-220.

38. Fujii, M., Hori, H., Miyazaki, G., Morimoto, H., and Yonetani, T. (1993) *J. Biol. Chem. 268,* 15386-15393.

39. Brzozowski, A., Derewenda, Z., Dodson, E., Dodson, G., Grabowski, M., Liddington, R., Skarzynski, T., and Vallely, D. (1984) *Nature (London) 307,* 74-76.

40. Liddington, R., Derewenda, Z., Dodson, G., Harris, D. (1988) *Nature (London) 331,* 725-728.

41. Shibayama, N., Inubushi, T., Morimoto, H., and Yonetani, T. (1987) *Biochemistry 26,* 2194-2201.

42. Novy, M. J., Edwards, M. J., and Metcalfe, J. (1967) *J. Clin. Invest. 46,* 1848-1854.

CHAPTER 3

Differences in Changes of the α1-β2 Subunit Contacts between Ligand Binding to the α and β Subunits of Hemoglobin A: UV Resonance Raman Analysis Using Ni-Fe Hybrid Hemoglobin

Published by *Biochemistry 41*, 10010 –10020 (2002).

Shigenori Nagatomo, Masako Nagai, Naoya Shibayama, and Teizo Kitagawa

3.1 Abstract

The α1-β2 subunit contacts in the half-ligated hemoglobin A (Hb A) have been explored with ultraviolet resonance Raman (UVRR) spectroscopy using the Ni-Fe hybrid Hb under various solution conditions. Our previous studies demonstrated that Trpβ37, Tyrα42 and Tyrα140 are mainly responsible for UVRR spectral differences between the complete T (deoxyHb A) and R (COHb A) structures [Nagai, M, Wajcman, H., Lahary, A, Nakatsukasa, T., Nagatomo, S. and Kitagawa, T. (1999), *Biochemistry, 38,* 1243-1251]. On the basis of it, the UVRR spectra observed for the half-ligated $\alpha^{Ni}\beta^{CO}$ and $\alpha^{CO}\beta^{Ni}$ at pH 6.7 in the presence of IHP indicated the adoption of the complete T structure similar to $\alpha^{Ni}\beta^{deoxy}$ and $\alpha^{deoxy}\beta^{Ni}$. The extent of the quaternary structural changes upon ligand binding depends on pH and IHP, but their characters are qualitatively the same. For $\alpha^{Ni}\beta^{Fe}$, it is not until pH 8.7 in the absence of IHP that the Tyr bands are changed by ligand binding. The change of Tyr residues is induced by binding of CO, but not of NO, to the α heme, while it was similarly induced by binding of CO and NO to the β-heme. The Trp bands are changed toward R-like similarly for $\alpha^{Ni}\beta^{CO}$ and $\alpha^{CO}\beta^{Ni}$, indicating that the structural changes of Trp residues are scarcely different between CO binding to either the α or β heme. The

---

Footnotes

Abbreviations used are; Hb A, hemoglobin A; COHb A, carbonmonoxy Hb A; IHP, inositol-hexa(kis)phosphate; RR, resonance Raman; UVRR, ultraviolet resonance Raman; $\alpha^{Ni}\beta^{deoxy}$, α(Ni)β(Fe-deoxy)Hb A; $\alpha^{Ni}\beta^{CO}$, α(Ni)β(Fe-CO)Hb A; $\alpha^{deoxy}\beta^{Ni}$, α(Fe-deoxy)β(Ni)Hb A; $\alpha^{CO}\beta^{Ni}$, α(Fe-CO)β(Ni)Hb A; $\alpha^{Ni}\beta^{O2}$, α(Ni)β(Fe-O_2)Hb A; $\alpha^{O2}\beta^{Ni}$ Hb A, α(Fe-O_2)β(Ni)Hb A; Ni-PPDME; Ni-protoporphyrin IX dimethylester; $\alpha^{NO}\beta^{deoxy}$, α(Fe-NO)β(Fe-deoxy)Hb A; $\alpha^{NO}\beta^{CO}$, α(Fe-NO)β(Fe-CO)Hb A; NOHb A, nitrosyl Hb A; NOMb, nitrosyl myoglobin; THF, tetrahydrofuran; TPP, tetraphenyl-porphyrin

ligand induced quaternary structural changes of Tyr and Trp residues did not take place in a concerted way and were different between $\alpha^{Ni}\beta^{CO}$ and $\alpha^{CO}\beta^{Ni}$. These observations directly indicate that the phenomenon occurring at the $\alpha 1$-$\beta 2$ interface is different between the ligand binding to the α and β hemes and is greatly influenced by IHP. A plausible mechanism of the intersubunit communication upon binding of a ligand to the α or β subunit to the other subunit and its difference between NO and CO as a ligand are discussed.

3.2 Introduction

If the two-state model of MWC theory (1) is correct, all residues at the $\alpha 1$-$\beta 2$ interface should change in a concerted way at the crossover point of the T and R states. To investigate protein structures in intermediate states of ligand binding to Hb A, a variety of metal substituted Hbs including their hybrid has been prepared with Ni, Co, Cu, Cr, Zn, Mn, Mg, and so on (2-12). The Co substituted Hb can bind O_2 with lower affinity than Hb A by a factor of 10, but cannot bind CO (4). The subunit substituted with other metal species cannot bind even O_2. Accordingly, hybrid Hbs with Fe and another metal can generate the half-liganded intermediate with two ligands on the Fe subunits. A quaternary structure of the half liganded Hb depends on the metal species hybridized. Physicochemical properties of Ni-Fe hybrid Hb changes with whether Ni is incorporated into the α ($\alpha^{Ni}\beta^{Fe}$) or β ($\alpha^{Fe}\beta^{Ni}$) subunit (2, 3, 10-12). X-ray crystallographic analysis demonstrated that both $\alpha^{Ni}\beta^{CO}$ (10) and $\alpha^{O2}\beta^{Ni}$ (11) maintain the T structure at pH 6.8 even in the ligand-bound state. The ^{1}H NMR measurements on the Ni-Fe hybrid Hb revealed appreciable pH dependence. At pH 7.4 in the presence of IHP both $\alpha^{Ni}\beta^{CO}$ and $\alpha^{CO}\beta^{Ni}$ gave the ^{1}H signals of Tyrα42 and Trpβ37, which mean the presence of the T-type $\alpha 1$-$\beta 2$ contact. As pH was raised, intensities of these signals became weaker, and the extent of weakening was definitely different between Tyrα42 and Trpβ37 for $\alpha^{Ni}\beta^{CO}$ but not always so for $\alpha^{CO}\beta^{Ni}$. This suggests that the structural changes of Tyrα42 and Trpβ37 are not synchronous in $\alpha^{Ni}\beta^{CO}$ (3). The absorption

spectra of $\alpha^{Ni}\beta^{CO}$ suggested a pH-dependent change for a coordination number of Ni; four at pH 6.5 and five at pH 8.5. Presumably, proximal Hisα87 is coordinated to Ni at pH 8.5 but is dissociated at pH 6.5, while His (proximal histidine) is always coordinated to Ni in the β-heme (2). The great difference between the α and β subunits is also incompatible to the two-state model. Previously (in Chapter 2) we examined UV resonance Raman (UVRR) spectra of α-nitrosyl β-deoxy Hb A ($\alpha^{NO}\beta^{deoxy}$) and pointed out its structural change upon ligation to the deoxyFe subunit (13). In an extension of the investigation of the α1-β2 contacts in partially liganded Hb, which can be different between α- or β-ligation, we treated Ni-Fe hybrid Hb in this study.

It has been demonstrated in this decade that resonance Raman (RR) spectra excited in the UV region around 220-240 nm can explore the environmental and hydrogen-bonding changes of Tyr and Trp residues of proteins (see refs 13 and 14 for a review). In fact, Rodgers et al. (16, 17), Nagai, M., et al. (18-20), Huang et al. (21, 22), Hu et al. (23, 24), and Peterson and Friedman (25) reported the quaternary structure dependent features for Tyr and Trp residues in the α1-β2 interface of Hb using 230- and 235-nm excited UVRR spectra. The quaternary structure dependent UVRR bands have been assigned to Trpβ37, Tyrα42 and Tyrα140 (18-20). Here we present 235-nm excited UVRR spectra for $\alpha^{Ni}\beta^{deoxy}$, $\alpha^{Ni}\beta^{CO}$, $\alpha^{deoxy}\beta^{Ni}$, and $\alpha^{CO}\beta^{Ni}$ in the presence and absence of IHP at various pH values, discussing differences in a communication route between the α to β subunits and the β to α subunits, and also possible correlation between the Fe-His bonding of α hemes and intersubunit interactions at the α1-β2 interface in the quaternary structure change.

3.3 Experimental Procedures

Sample Preparation

Hb A was purified from fresh human blood by a preparative isoelectric focusing electrophoresis (26). Approximately 150 μL of the 200 μM (in terms of heme) Hb A solution was put into a spinning cell made of a synthetic quartz ESR tube (diameter = 5 mm) (27). DeoxyHb and

COHb were prepared by adding sodium dithionite (1 mg/ml) to oxyHb after replacement of the inside air of the sample tube with N_2 and CO, respectively.

Ni-Fe hybrid Hb was prepared as described previously (1). The $\alpha^{Ni}\beta^{deoxy}$ and $\alpha^{deoxy}\beta^{Ni}$ were generated from $\alpha^{Ni}\beta^{CO}$ and $\alpha^{CO}\beta^{Ni}$, respectively, by photodissociation of CO under flowing of O_2, followed by addition of sodium dithionite (1 mg/ml) under N_2 atmosphere. The $\alpha^{Ni}\beta^{CO}$ and $\alpha^{CO}\beta^{Ni}$ used for UVRR measurements were obtained by addition of CO to the $\alpha^{Ni}\beta^{deoxy}$ and $\alpha^{deoxy}\beta^{Ni}$ thus generated. Solvents used were phosphate buffer for the pH range from pH 6.7 to 7.4, Tris buffer at pH 8.1, and borate buffer at pH 8.7. IHP was added to the samples, when necessary, with the final concentration of 5 mM. Ni-PPDME was a kind gift of Prof. H. Ogoshi (28).

Just before the measurement of UVRR spectra, Na_2SO_4 was added to the samples with the final concentration of 0.1 M as an internal intensity standard for Raman spectra. It was confirmed that the addition of sulfate did not cause any apparent Raman spectral change for the states examined in this study, although its use in Raman experiments was warned against due to a possible tertiary structure change (29).

Ultraviolet Resonance Raman Measurements

UVRR spectra were excited by a XeCl excimer laser-pumped dye laser (EMG103MSC/LPX105 and FL2002/SCANMATE, Lambda Physik) as shown in CHAPTER 1.3 Apparatus (30). The spinning cell was moved vertically by 1 mm for every spectrum (every 5 min) to shift the laser illumination spot on the sample (27). The temperature of the sample solution was kept at 10 ˚C by flushing with cooled N_2 gas against the cell. The scattered light was collected with Cassegrainian optics with f/1.1. One spectrum is composed of the sum of 400 exposures, each exposure accumulating the data for 0.8 sec. The Raman spectra shown in the figure are averages of 10 or 15 spectra. Raman shifts were calibrated with cyclohexane. Raman intensity was

standardized with the band intensity of sulfate ions at 982 cm^{-1}. Denaturation of the samples due to exposure to UV laser light was carefully checked by inspecting a possible change in the visible absorption spectra before and after the measurements of UVRR spectrum. If some spectral changes were noticed, the Raman spectrum was discarded. Visible absorption measurements were carried out with a Hitachi 220S spectrophotometer.

*Visible Resonance Raman Measurement*s

The 441.6 nm line from a He/Cd laser (Model CD4805R, Kimmon Electrics Corp.) was used as an excitation source. Visible resonance Raman scattering was detected with a liquid nitrogen-cooled CCD detector (Model CCD3200, Astromed) attached to a 100-cm single polychromator (Model MC-100DG, Ritsu Oyo Kogaku). The slit width and slit height were set to be 200 μm and 20 mm, respectively. The corresponding spectral slit width is 8 cm^{-1}. The wavenumber width per one channel of the detector was 0.7 cm^{-1}. The laser power used was 5.4 mW at the sample point. All measurements were carried out at room temperature with a spinning cell (1000 rpm). Raman shifts were calibrated with indene and accuracy of peak positions of Raman bands was ±1 cm^{-1}.

3.4 Results

UVRR Spectra of the Isolated α *and* β *Chains and* $\alpha_2\beta_2$ *Tetramer*

Figure 3.1 shows the 235-nm excited UVRR spectra of the isolated β chain in the deoxy (A) and CO-bound (B), and the isolated α chain in the deoxy (C) and CO-bound (D) states at pH 6.7 in the frequency region from 1700 to 700 cm^{-1} and the deoxy-minus-CO difference spectra for

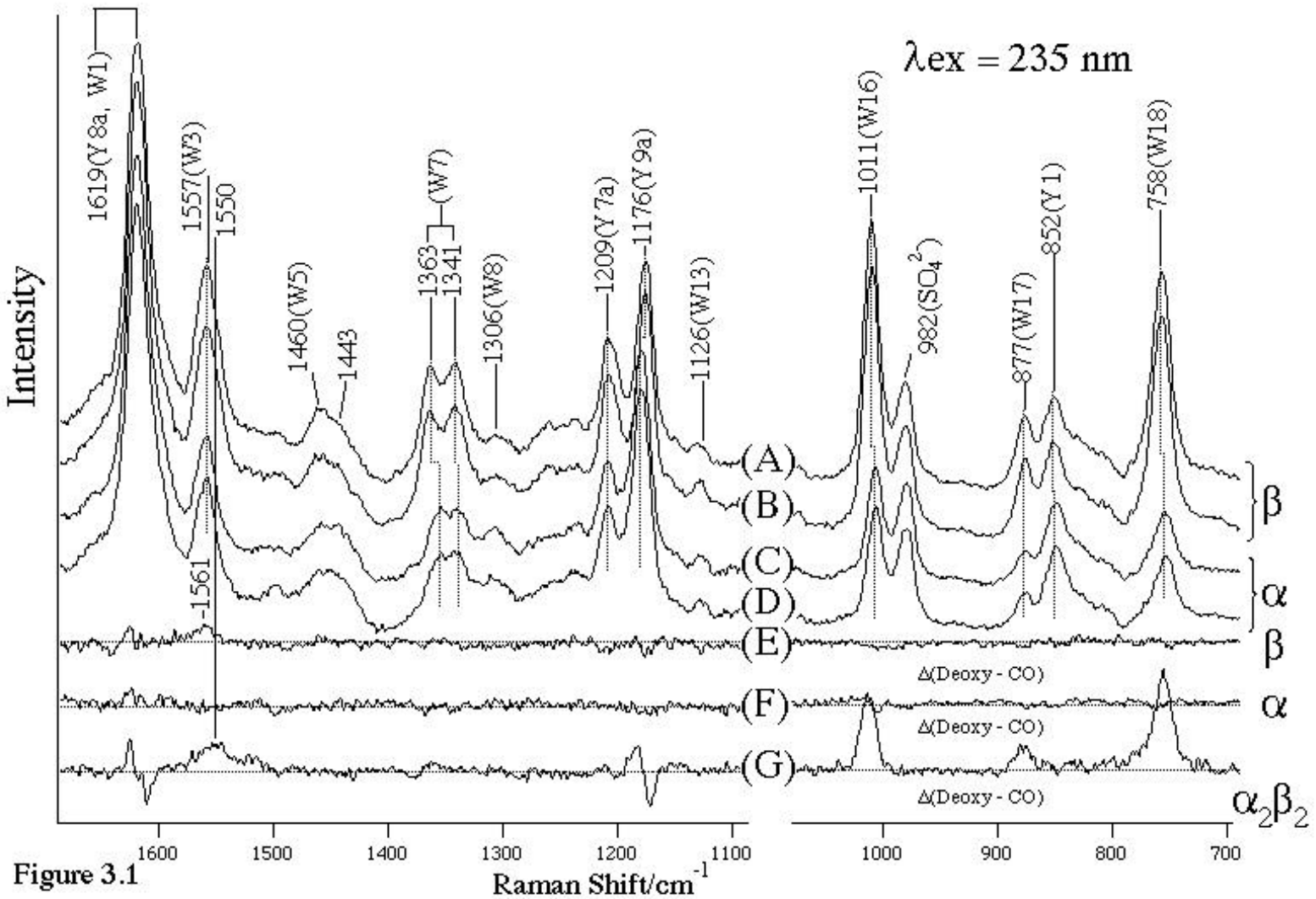

Figure 3.1

The 235-nm excited UVRR spectra of the isolated β-chain in the deoxy (A) and CO-bound (B) forms, the isolated α-chain in the deoxy (C) and CO-bound (D) forms and the deoxy-minus-CO difference spectra for the isolated β (E) (= A - B) and α chains (F) (= C - D), and native Hb A (G).

the isolated β (E) and α (F) chains and native Hb A (G). Although a strong broad band due to a synthetic quartz cell appeared between 800 and 900 cm^{-1}, its contribution was subtracted from the spectra shown here. The 982 cm^{-1} band of SO_4^{2-} ions was used to normalize the intensity of the spectra, as their presence did not affect the observed spectra (31). In the spectrum of the β-deoxy chain (A), RR bands of tyrosine (Tyr) are seen at 1619 (Y8a), 1209 (Y7a), 1176 (Y9a) and 852 cm^{-1} (Y1), and those of tryptophan (Trp) are seen at 1619 (W1, overlapped), 1557 (W3), 1363-1341 (W7; tryptophan doublet), 1011 (W16), 877 (W17), and 758 cm^{-1} (W18). The assignments are based on Harada and coworkers (14, 32, 33). The UVRR spectra of deoxyHb A and COHb A in the 1700-850 cm^{-1} (not shown) are in agreement with those reported by Rodgers et al. (16) and Nagai et al. (18, 20). It was confirmed that the spectra of deoxyHb A and COHb A exhibited negligible changes upon addition of IHP (spectra not shown).

The Raman scattering from Trp residues is stronger for the β-deoxy chain than for the α-deoxy chain due to the number of residues (two in the β-chain and one in the α-chain). The peak frequencies of the W7, W16, and W18 bands are slightly different between the isolated α- and β-chains. Digital sum of the UVRR spectra of the α-CO and the β-CO chains almost coincides with the spectrum observed for native COHb A, but the corresponding digital sum of the α-deoxy and the β-deoxy chains is slightly but definitely different from the spectrum observed for native deoxyHb A. The difference lies mainly in intensity of Trp bands, suggesting that the surroundings of Trp residues are unique in the T-structure tetramer but not so in the R-structure tetramer. The intensity increase of Trp bands in the 235 nm-excited UVRR spectrum is generally ascribed to a shift of the B_b absorption maximum to a longer wavelength and thus to the increase of hydrophobicity around the indole ring (34) or the formation of a hydrogen bond at the indole NH site in hydrophobic environments (35). Such differences of Trp residue between the α (or β) oligomers and the $\alpha_2\beta_2$ tetramer would occur more easily to a Trp residue on the contact surfaces of subunits than that in the interior of individual subunits. Consequently, it is quite reasonable that the

Trp residue responsible for the difference peak in the deoxy-minus-CO difference spectrum is mainly Trpβ37 rather than Trpβ15 and Trpα14.

The Tyr spectrum of the isolated β chain also differs from that of the isolated α chain. The frequency of the Y9a band of the β-deoxy chain is lower than that of the α-deoxy chain by as much as 4 cm^{-1}, although the frequencies are unaltered by CO binding within the α (or β) oligomers. This means that the surroundings of Tyr in the α-deoxy chain are more hydrophilic than that in the β-deoxy chain. This spectral difference may be related with the status difference between the α and β chains, that is, dimer for the α and tetramer for the β chains.

The deoxy-minus-CO difference spectrum of the isolated α chain (F) exhibits no peak, indicating that the surroundings around Tyr and Trp are scarcely altered by the tertiary structure change induced by the ligand binding. The corresponding difference spectrum of the isolated β chain (E) also exhibits no peak except for a small peak due to the Trp W3 band at 1561 cm^{-1}. Note that these reflect the extent of contributions to the UVRR spectral changes from the tertiary structure change in oligomers of isolated chains upon the ligand binding. It is known that the W3 frequency reflects the torsion angle around the C_2-C_3-C_β-C_α linkage of Trp (24,33).

The difference spectrum between deoxyHb A and COHb A (G) indicates that the intensities of the W3, W16, W17, and W18 bands of Trp are much weaker for COHb A than for deoxyHb A, while the peak positions remain unaltered except for the W3 band, and that the frequencies of Y8a and Y9a bands of Tyr are lower for COHb A than for deoxyHb A. These differences arise from some differences in hydrogen bonding states and surrounding hydrophobicity of mainly Trpβ37, Tyrα42 and Tyrα140 residues between the two states (20, 36) and have been ascribed to a consequence of changes in subunit contacts (16-25, 37). It was pointed out previously by Rodgers (16) and Hu and Spiro (23) that the C_2-C_3-C_β-C_α torsion angle of Trpβ37 is smaller than those of Trpα14 and Trpβ15 for Hb A and accordingly, its W3 frequency is lower than others. Therefore,

the difference peak at 1550 cm^{-1} is ascribed to Trpβ37. The absence of this peak in the spectra for the isolated chains may mean that the smaller torsion angle is specific to the $\alpha_2\beta_2$ tetramer.

It is evident that the spectral sum of the deoxy-minus-CO differences of the isolated α and β chains does not yield the deoxy-minus-CO difference spectrum of the $\alpha_2\beta_2$ tetramer having a special contact at the α1-β2 subunit interface. This demonstrates that the UVRR spectral differences shown by trace (G) reflect mostly the quaternary structure change, but not the tertiary one. Hereafter, spectrum (G) will be referred as the standard for the T-minus-R difference spectrum, reflecting 100% changes at the α1-β2 subunit interface due to the quaternary structure transition ("T-like" and "R-like" will be used to represent that the local structure around a particular residue in question is closer to that in the ordinary T and R subunit contact, respectively, but does not always mean that the whole tetramer structure is close to the T and R, respectively).

Figure 3.2 compares the spectra of Ni-Fe hybrid Hb (B and C) with those of Hb A (A) in the deoxy state. The spectrum of $\alpha^{Ni}\beta^{deoxy}$ (B) is different from that of deoxyHb A (A), although the spectrum of $\alpha^{deoxy}\beta^{Ni}$ (C) is not so. The difference spectrum for the α subunit (E), $\alpha^{Ni}\beta^{deoxy}$ – deoxyHb A, yields positive peaks at 1624(ν_{10}), 1382(ν_4), 1130(ν_{22}) and 753(ν_{16}) cm^{-1} while the difference spectrum for the β subunit (F), $\alpha^{deoxy}\beta^{Ni}$ – deoxyHb A, yielded no peaks. These peaks are not present in spectrum (A) and are ascribed to porphyrin vibrations, because the peak positions are the same as those of four-coordinated Ni-protoporphyrin, whose spectrum excited at 235 nm is delineated by spectrum (D). The mode numbers of porphyrin vibrations (38, 39) are specified in parentheses. The absence of the corresponding peaks in trace (F) means that the Ni-porphyrin in the β subunit adopts the five-coordinate structure, yielding no prominent Raman bands upon excitation at 235 nm.

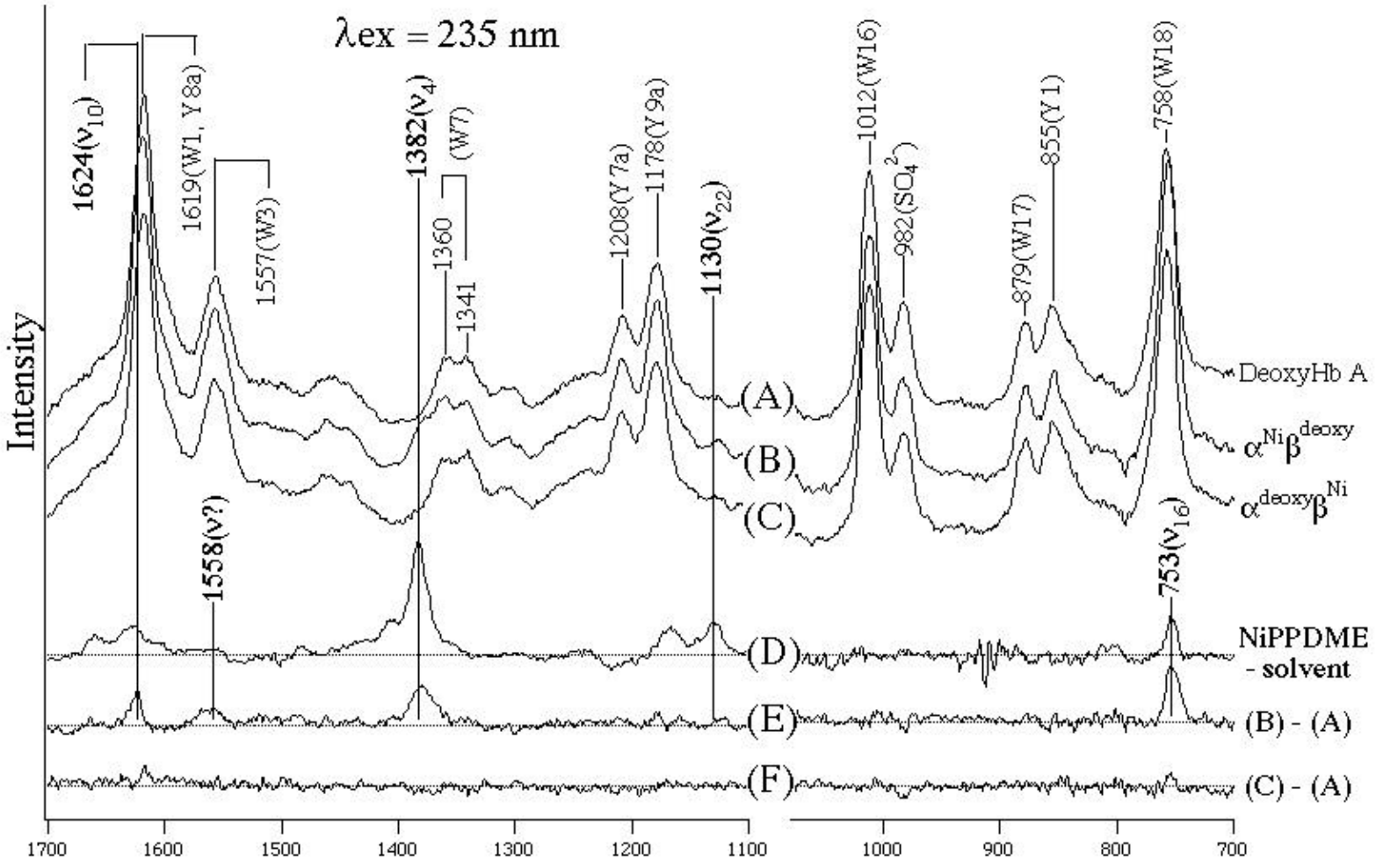

Figure 3.2

The 235-nm excited UVRR spectra of deoxyHbA (A), $\alpha^{Ni}\beta^{deoxy}$(+IHP) (B), $\alpha^{deoxy}\beta^{Ni}$(+IHP) (C) and Ni-PPDME (D), and their difference spectra of $\alpha^{Ni}\beta^{deoxy}$(+IHP) - deoxyHbA (E), and of $\alpha^{deoxy}\beta^{Ni}$(+IHP) - deoxyHbA (F).

Figure 3.3 shows the visible-excited RR spectra of four-coordinated Ni-PPDME (A) in $CHCl_3$ (1750-950 cm^{-1}) or THF (950-600 cm^{-1}) and six-coordinated Ni-PPDME (B) in piperidine. The ν_{16} band at 752 cm^{-1} is very weak for six-coordinated Ni-PPDME (B) compared with that for four-coordinated one (A). Accordingly, the 753 cm^{-1} band in Fig. 3.2(E) is assigned to the ν_{16} mode of the four-coordinated α(Ni) heme. Similarly, the 1382 cm^{-1} band in Fig. 3.2(E) corresponds to the ν_4 (1379 cm^{-1}) band in Fig. 3.3(A), whose frequency depends on the coordination number, and is ascribed to the four-coordinated α(Ni) heme. Thus, some caution is necessary to distinguish between the UVRR bands of Ni-porphyrin and of globin, particularly for $\alpha^{Ni}\beta^{deoxy}$.

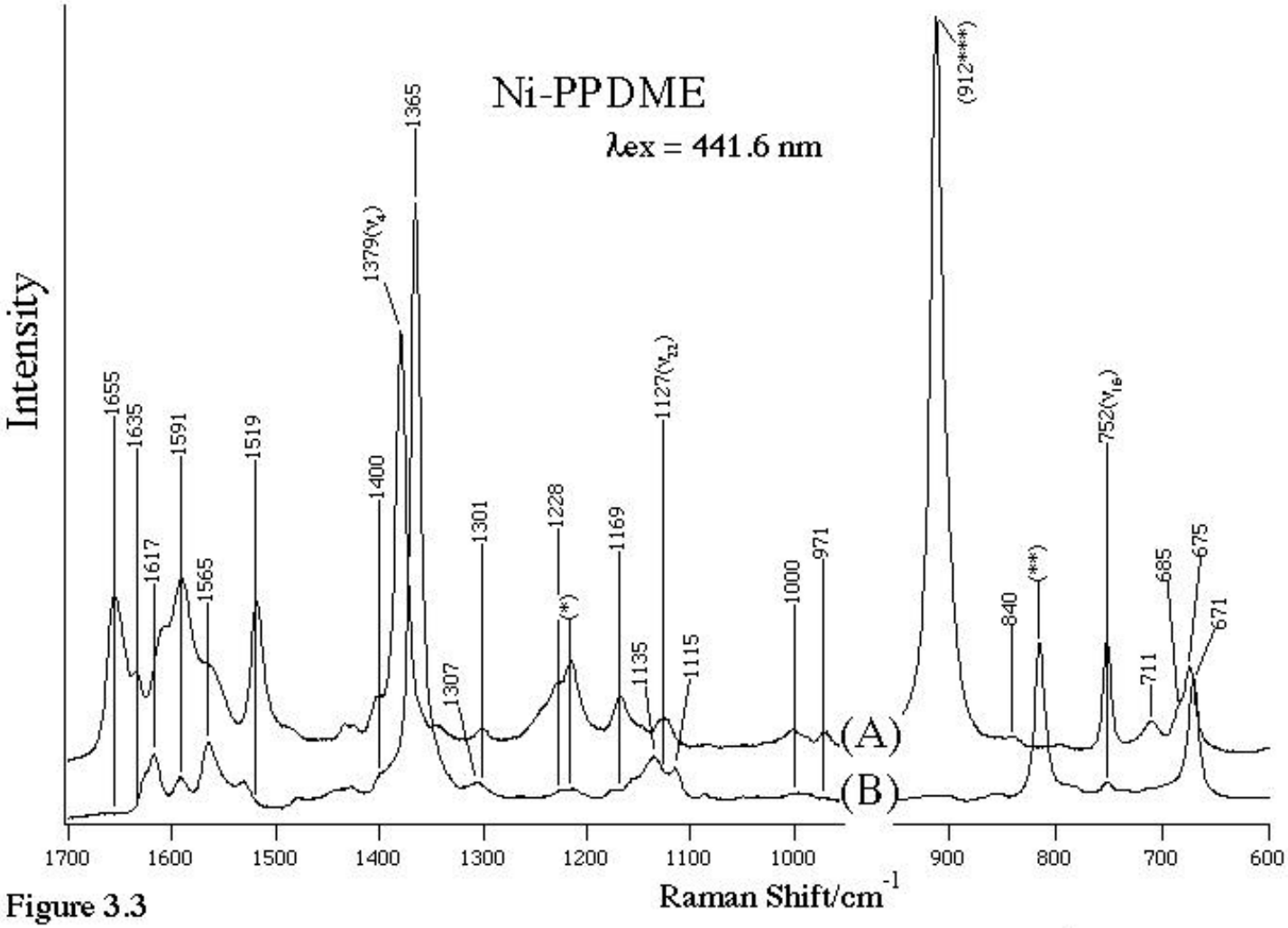

Figure 3.3

The 441.6-nm excited RR spectra of Ni-PPDME in CHCl3 (1700 - 950 cm^{-1}) or THF (950 - 600 cm^{-1}) (A), and in piperidine (B). Ni-PPDME concentration was 100 μM (in $CHCl_3$ or THF) and 150 μM (in piperidine). The bands marked by *, **, and *** mean bands of CHCl3, piperidine, and THF, respectively.

UVRR Spectra of $\alpha^{Ni}\beta^{CO}$ *Hybrid Hb*

Figure 3.4 shows the raw UVRR spectrum of $\alpha^{Ni}\beta^{CO}$ (A) at pH 6.7 in the presence of IHP and the difference spectra between $\alpha^{Ni}\beta^{deoxy}$ and $\alpha^{Ni}\beta^{CO}$ at various pH values in the presence or absence of IHP in the frequency region from 1700 to 700 cm^{-1}. The general trend of these difference spectra for $\alpha^{Ni}\beta^{Fe}$ is that peak intensities in the difference spectra increase as proceeding from spectra (B) to (H), that is, more R-like contacts are promoted in the ligand bound form of the β subunit at higher pH. Detailed analysis, however, clarifies that the Tyr and Trp bands do not change in a concerted way. The first change to the R-type occurs only on the Trp bands in spectrum (C) at pH 6.7 in the absence of IHP, although there is no difference in its presence (B). It is stressed that the change to the R-type is not observed at all for Tyr bands even at pH 7.1 in the presence of IHP (D), which is almost the same as spectrum (C). At pH 8.1 in the presence of IHP (F), small changes of Tyr bands to R-like are recognized, while the changes of Trp bands to the R-type proceed. It is not until pH 8.7 in the absence of IHP (G) that the changes of Tyr bands to the R-type become evident, although it is still smaller than that of normal Hb A, which is depicted by spectrum (H) for comparison.

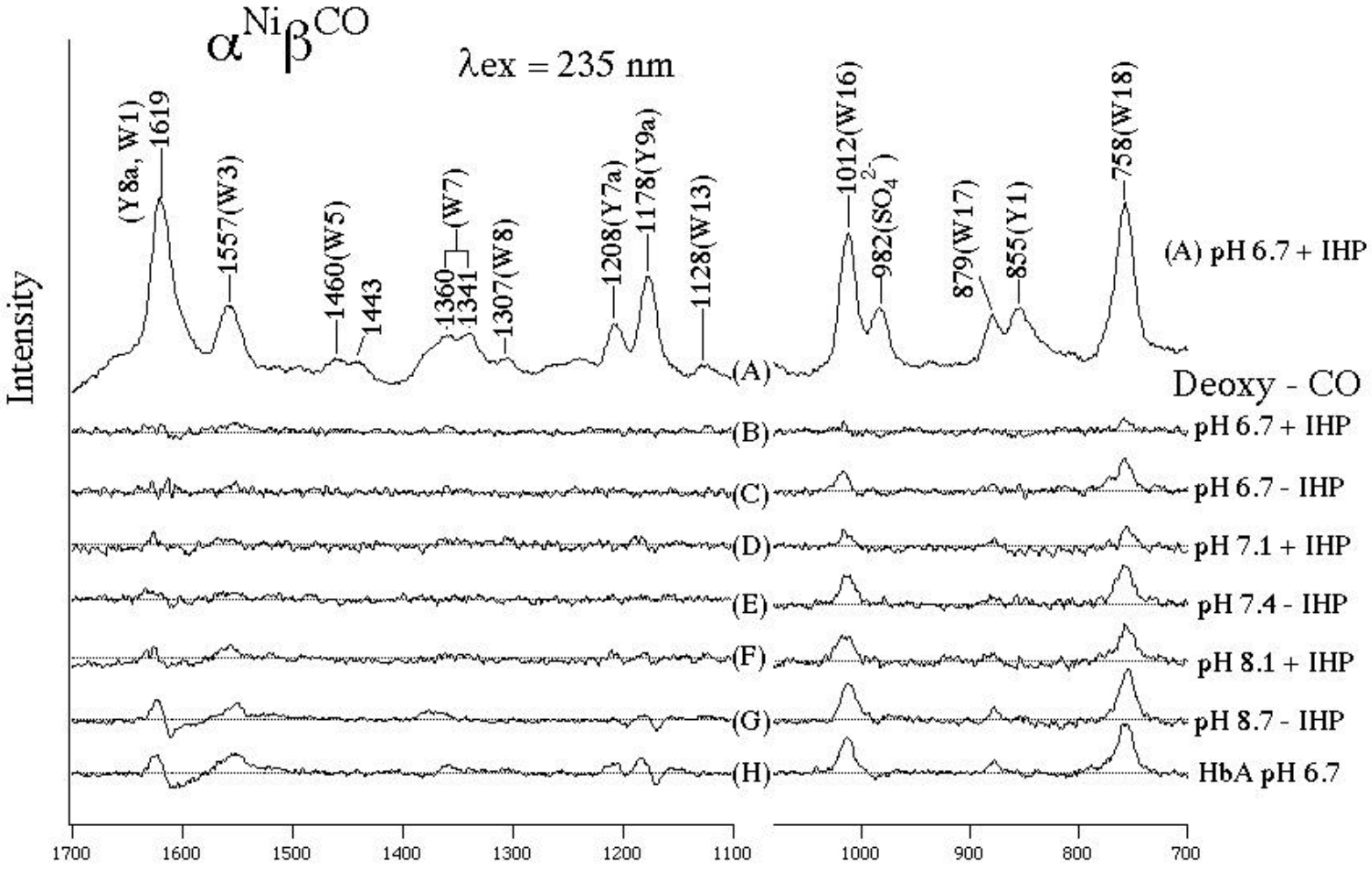

Figure 3.4

UVRR spectrum of $\alpha^{Ni}\beta^{CO}$ at pH 6.7 (+IHP) (A) and the difference spectra of $\alpha^{Ni}\beta^{deoxy}$ - $\alpha^{Ni}\beta^{CO}$ at pH 6.7 (+IHP) (B), pH 6.7 (-IHP) (C), pH 7.1 (+IHP) (D), pH 7.4 (-IHP) (E), pH 8.1 (+IHP) (F), and pH 8.7 (-IHP) (G) and deoxyHbA - COHbA at pH 6.7 (H).

UVRR Spectra of $\alpha^{CO}\beta^{Ni}$ Hybrid Hb

Figure 3.5 shows the raw UVRR spectrum of $\alpha^{CO}\beta^{Ni}$ (A) in the frequency region from 1700 to 700 cm^{-1} and the difference spectra between $\alpha^{deoxy}\beta^{Ni}$ and $\alpha^{CO}\beta^{Ni}$ at various pH values in the presence and absence of IHP. The R-like contacts at the subunit interface due to ligand binding to the α subunit are promoted by raising pH, and thus difference peaks are intensified. In this context general trend of the difference spectra for $\alpha^{CO}\beta^{Ni}$ Hb are similar to those of $\alpha^{Ni}\beta^{CO}$, although in delicate points the behaviors of $\alpha^{CO}\beta^{Ni}$ and $\alpha^{Ni}\beta^{CO}$ are different from each other. A large difference between them is that changes of Tyr bands toward the R-type occur in the earlier stage: it is already seen in the spectrum at pH 6.7 in the absence of IHP (C). At the same pH, however, the Tyr bands are not discernible in the presence of IHP (B). The size of change of Tyr bands is nearly full at pH 6.7 in the absence of IHP (C), while the spectral changes of Trp bands toward the R-type are still on going. In the presence of IHP, the change of Tyr bands are not so clear even at pH 7.2 (D), where the change of Trp bands proceeds to the level of 40-50% R-like, similar to the case of pH 6.7 in the absence of IHP (C). Thus, it is evident that *IHP has a propensity to keep Tyr in the T-like contact but not so for Trp*. The difference spectrum at pH 8.7 in the absence of IHP (F) exhibits the same spectrum as that for normal Hb A, which is delineated by spectrum (G) for comparison. The changes of Tyr and Trp to R-like upon CO binding to the deoxy-heme of $\alpha^{deoxy}\beta^{Ni}$ were observed in a manner different from the case for $\alpha^{Ni}\beta^{deoxy}$. Moreover, a size of the T to R spectral change for Trp seems to be somewhat smaller in $\alpha^{CO}\beta^{Ni}$ than that in $\alpha^{Ni}\beta^{CO}$ under the same conditions.

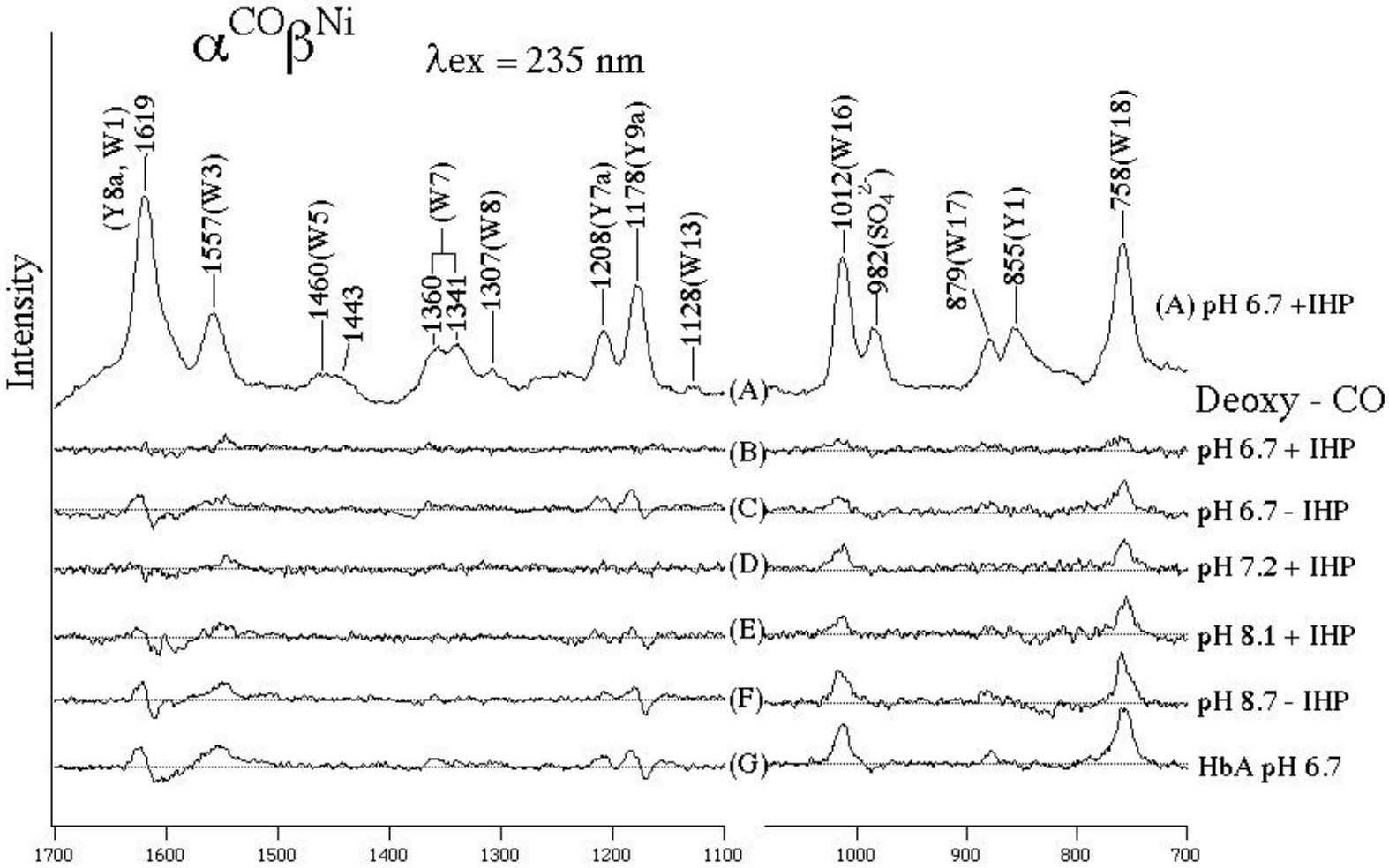

Figure 3.5

UVRR spectrum of $\alpha^{C}\beta^{Ni}$ at pH 6.7 (+IHP) (A), and the difference spectra of $\alpha^{deoxy}\beta^{Ni}$ - $\alpha^{CO}\beta^{Ni}$ at pH 6.7 (+IHP) (B), pH 6.7 (-IHP) (C), pH 7.2 (+IHP) (D), pH 8.1 (+IHP) (E), and pH 8.7 (-IHP) (F), and of deoxyHbA - COHbA at pH 6.7 (G).

3.5 Discussion

Differences in Structural Changes between Ligand Binding to the α and β Subunits

The CO-bound forms of Ni-Fe hybrid Hb serve as a good model for studying a structure of half-liganded Hb which is not stable in the normal Hb A, because Ni-porphyrins cannot bind O_2 and CO. The function and structure of the Ni-Fe hybrid Hb have been extensively studied (2, 3, 10-12), and in the present experiments we have detected conformational changes of the protein moiety of the Ni-Fe hybrid Hb with 235-nm excited UVRR spectroscopy, which provides strong enhancement of Raman intensity for vibrational modes associated with Tyr and Trp residues. DeoxyHb A gives a typical UVRR spectrum of the T-structure which is distinct from the spectrum of COHb A with the R-structure. These two spectra will be referred as the standard in the analysis below. When the ligand binding to the deoxy-Fe heme caused to shift the α1-β2 contact toward more R-like, peak intensity in the deoxy-minus-CO difference spectrum approaches more to that in the deoxyHb A-minus-COHb A difference spectrum.

It was demonstrated in Figure 3.1 that Tyr and Trp residues in the isolated α or β chains exhibited almost no changes in their structure and environments between the deoxy- and CO-forms unless the particular contact at the α1-β2 interface was attained in the $\alpha_2\beta_2$ tetramer. The Ni-Fe hybrid Hb at pH 6.7 in the presence of IHP gave the T-like spectrum regardless of CO binding to the Fe subunit, being consistent with ^{1}H NMR studies (10). The fact that the UVRR spectra of $\alpha^{Ni}\beta^{CO}$ and $\alpha^{CO}\beta^{Ni}$ are hardly different from those of $\alpha^{Ni}\beta^{deoxy}$ (Fig. 3.4B) and $\alpha^{deoxy}\beta^{Ni}$ (Fig. 3.5B), respectively, means that Tyr and Trp residues do not undergo any changes by CO binding in the presence of IHP at pH 6.7. These residues exhibit appreciable changes upon CO binding to the Fe subunit at higher pH. The most interesting point in the results of the Ni-Fe hybrid Hb is that a pattern of quaternary structural change is different between the CO binding to the α- and β-hemes. It means that the communication route from the α to β subunit is different from the corresponding route from the β to α subunit.

Binding of CO to $\alpha^{Ni}\beta^{deoxy}$, which is expected to reveal the route from the β to the α1-β2 interface, mainly induced the subunit contact change of Trp residues toward R-like, that is summarized as follows. As pH is raised, the population of R-like contacts of Trp becomes more dominant. IHP has an effect to maintain the T-like contacts at lower pH (<pH 6.7), but no effect at higher pH (>pH 8.1). It is not until pH 8.7 in the absence of IHP (Figure 3.4G) that the spectral change of Tyr to R-like occurs. The change of Tyr in $\alpha^{Ni}\beta^{Fe}$ is smaller than that in the normal Hb A. This might mean that the ligand binding only to the β heme is not sufficient to induce the complete quaternary structure change.

The behaviors of Tyr and Trp residues at the α1-β2 interface are not synchronous in $\alpha^{Ni}\beta^{Fe}$. This is illustrated in Figure 3.6 where the peak intensities in the deoxy-minus-CO difference spectra (Figs. 3.4 and 3.5) of the Y9a bands of Tyr (denoted by Y) and the W18 bands of Trp (denoted by W) are plotted against pH. The right and left panels represent the results for $\alpha^{Ni}\beta^{Fe}$ and $\alpha^{Fe}\beta^{Ni}$, respectively, and the closed and open characters represent the results obtained in the presence and absence of IHP, respectively. The peak intensities increase generally at higher pH, meaning that the protein of the CO-bound form adopts a more R-like structure at higher pH, but the detailed behaviors of Tyr and Trp bands are dissimilar for $\alpha^{Ni}\beta^{Fe}$. In contrast, the behaviors of the Tyr and Trp bands for $\alpha^{deoxy}\beta^{Ni}$ are somewhat alike. Even in this case, however, the spectral changes of Trp and Tyr are not synchronous.

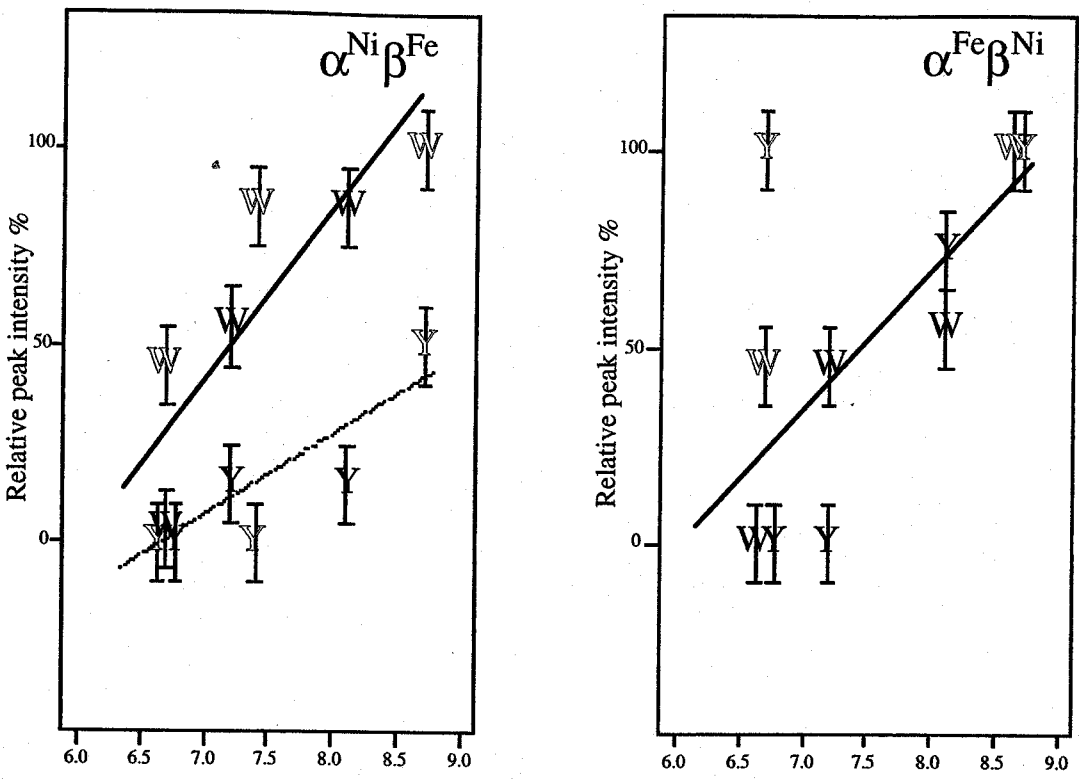

Figure 3.6

The pH dependence of the peak intensities in the deoxy-minus-CO difference spectra shown in Figures 4 and 5 relative to the corresponding one in the deoxyHb A-minus-COHb A difference spectra. The left and right panels show the results from $\alpha^{Ni}\beta^{Fe}$ (Fig. 4) and $\alpha^{Fe}\beta^{Ni}$ (Fig. 5), respectively, and the filled and open markers indicate the values obtained in the presence and absence of IHP, respectively. "W" and "Y" denote the W18 band of Trp and the Y9a band of Tyr, respectively.

The result from $\alpha^{Ni}\beta^{Fe}$ shows that binding of CO to the β-heme promotes the change of Trp to the R-type, but not of Tyr until pH becomes basic. This means that the change of Trpβ37 to R-like is not always accompanied by the changes of Tyrα42 and Tyrα140, which are known to be quaternary structure sensitive. In other words, the communication route from the β-heme to Trpβ37 does not involve Tyrα42 and Tyrα140. In contrast, the result of $\alpha^{Fe}\beta^{Ni}$ shows that binding of CO to the α-heme causes almost equally the changes of Tyr and Trp residues. Thus, the information might be communicated to Trpβ37 through Tyrα42 and Tyrα140, supporting Perutz's hypothesis (40-42) and Ho's communication route (43,44). In this case the movement of the Fe-

His bond in the α-heme is substantial to the quaternary structure transition. Anyway, the communication routes upon the CO binding to the α and β hemes are different from each other.

Relation between Overall Oxygen Affinity and Extent of T → R Quaternary Structural Change at the Half-Ligated State

Oxygen affinity of the Ni-Fe hybrid Hb has been investigated by Shibayama, et al. (2) who noted that the affinity is sensitive to pH and IHP similar to the case of Hb A. The UVRR spectra of $\alpha^{Ni}\beta^{deoxy}$ and $\alpha^{deoxy}\beta^{Ni}$ at pH 6.7 in the presence of IHP and at pH 8.7 in the absence of IHP are analogous to those of deoxyHb A at pH 6.7 and pH 8.7, respectively. In other words, their quaternary structures in the absence of a ligand are alike and adopt the T structure regardless of pH and IHP. However, oxygen affinities under the corresponding conditions are largely different. Here we discuss a possible relation of the oxygen affinity with the structural probe at the α1-β2 interface.

P_{50} is used as the parameter representing the oxygen affinity, although it may not be correct in the case of $\alpha^{deoxy}\beta^{Ni}$, because of an asymmetrical feature in its oxygen binding curve at higher pH. The UVRR spectroscopic T % is defined for each of Tyr and Trp residues as the ratio of peak intensities in the deoxy-minus-CO difference spectrum to that in the deoxyHb A-minus-COHb A difference spectrum at pH 6.7 in the absence of IHP. This reflects the structural T-like character in the half-ligated state. The results for $\alpha^{Ni}\beta^{Fe}$ and $\alpha^{Fe}\beta^{Ni}$ are plotted against pH in the left and right panels in Figure 3.7, respectively, where oxygen affinities in the presence and absence of IHP at various pHs reported in Ref. (2) are designated by the filled and open markers, respectively, with the ordinate scale at the left side. The UVRR spectroscopic T % estimated with the W3, W16 and W18 bands of Trp are denoted by characters of ‘3’, ‘16’, and ‘18’ using the ordinate scale at the right side, and the filled and open characters mean the values obtained in the presence and absence of IHP, respectively. The characters are located at the center of individual error bars.

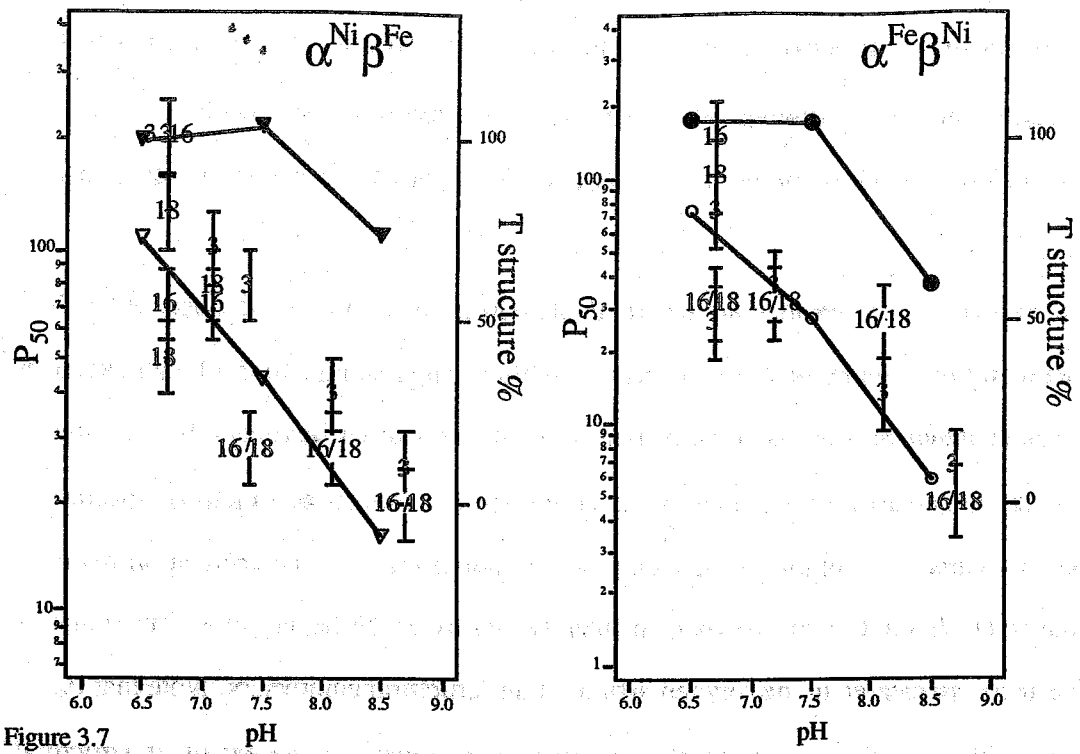

Figure 3.7

The relation between oxygen affinity (P_{50}) and the Raman T-like nature of tryptophan. P_{50} of $\alpha^{Ni}\beta^{Fe}$ (—) and $\alpha^{Fe}\beta^{Ni}$ (O) reported (Ref. 8) are plotted with the ordinate scale of the left side. The percentage values of T-like nature in the half-liganded form are plotted with the ordinate scale at the right side, in which the values obtained from the W3, W16, and W18 bands of Trp are represented simply with '3', '16', and '18', respectively. The position of the marker denotes the center of individual error bars. The filled and open letters (or symbols) indicate the values obtained in the presence and absence of IHP, respectively.

One may argue that the behavior of the W3 band differs from those of the W16 and W18 bands and that the Raman intensities do not correctly reflect the structure. In fact, the behaviors of the W16 and W18 bands are nearly the same but are slightly different from that of W3. The UVRR spectroscopic T% value for $\alpha^{Ni}\beta^{Fe}$ in the absence of IHP is higher with the W3 band than that with the W16 and W18 bands at pH 6.7 and 7.2 but such differences disappear at pH 8.7. Contrary to this, the UVRR spectroscopic T% values for $\alpha^{Fe}\beta^{Ni}$ in the presence of IHP are lower with the W3 band than those with the W16 and W18 bands at pH 6.7 and 8.1, while such a difference is absent at pH 7.4. One of the reasons for such discrepancy lies in the character of sensitivity. For the W3

band a frequency is sensitive to the $\chi^{2,1}$ angle, but for W16 and W18 bands Raman intensity is sensitive to hydrophobicity around the residue. Thus, the inclusion of the contribution from Trpα14 and Trpβ15 is different between the W3 and W16 (or W18) bands. The other reason is rather technical, that is, incorrect drawing of a base line. Considering these uncertainties, we can conclude that the overall behaviors of both the W3 and W16 (or W18) bands are qualitatively similar.

The plots in Figure 3.7 mean that the trend of Raman markers in the absence of IHP appears to parallel with that of open markers of oxygen affinity, suggesting that the T-like character of Trpβ37 in the half-liganded state is directly related with the overall oxygen affinity. In the presence of IHP, the oxygen affinity is generally lower and the T % values from Raman spectra are higher than those in its absence, although the behaviors are complicated. The correlation between the structural parameter (UVRR) and the oxygen affinity seems to be better for $\alpha^{Ni}\beta^{Fe}$ than for $\alpha^{Fe}\beta^{Ni}$, and IHP effects are clearer in the oxygen affinity than structural parameters. Note that P_{50} is an average character of K_1 and K_2, but the Raman parameters represent the extent of structural change at the half-liganded stage and thus are related to K_3. Similar plots for Tyr bands (not shown) were more complicated, but it is understood from the fact that the behaviors of Tyr and Trp are not concerted.

Correlation between Fe-His Bond and the α1-β2 Interface Contacts

In the previous RR study on NOHb, we proposed that although the movement of the proximal His due to the out-of-plane displacement of Fe in the α subunit is substantial to the quaternary structure change, it is not a sole origin, and that the movement of the proximal His in the β subunit also contributes to it (13). In the case of $\alpha^{NO}\beta^{deoxy}$, binding of CO or NO to the β-heme affects Tyr and Trp residues. For $\alpha^{Ni}\beta^{deoxy}$, however, the change of Trp occurs in a manner similar to that in $\alpha^{NO}\beta^{deoxy}$, but the change of Tyr is much smaller. The two proteins are common with

regard to that the Fe-His or Ni-His bond is cleaved in the α subunit. Binding of CO to the α-heme in $\alpha^{deoxy}\beta^{Ni}$ affects Tyr and Trp residues, but binding of NO to the α-heme in $\alpha^{deoxy}\beta^{deoxy}$ (deoxyHb A) affects neither Tyr nor Trp residues. Their behaviors in the Ni-Fe hybrid Hb are different from those in NOHb regarding the difference in the R-like shifts of Tyr between $\alpha^{NO}\beta^{deoxy}$ and $\alpha^{CO}\beta^{Ni}$ and also that between NOHb ($\alpha^{NO}\beta^{NO}$) and $\alpha^{Ni}\beta^{CO}$. These differences are discussed below.

It is well-known that the physicochemical effects of ligand binding are significantly different between CO and NO as a ligand. Six coordination is more favorable than five coordination with CO, but it is opposite with NO (45-48). The Fe-His bond in the α subunit of $\alpha^{NO}\beta^{deoxy}$ is cleaved at lower pH, but it recovers at higher pH where six coordination is attained (49-54). This situation of $\alpha^{NO}\beta^{deoxy}$ at higher pH is apparently similar to that in $\alpha^{CO}\beta^{Ni}$ at pH 6.7 in the absence of IHP in the sense that the α heme adopts six coordination. Nevertheless, in $\alpha^{NO}\beta^{deoxy}$ at pH 8.8, both Tyr and Trp residues remain in the T structure, while in $\alpha^{CO}\beta^{Ni}$ at pH 6.7 in the absence of IHP, Tyr is of R type and Trp is of half R-type. We attribute this to the difference in the metal-His bonding (13). The metal-His distance in the four-coordinated α subunit of $\alpha^{Ni}\beta^{CO}$ is sufficiently long (320 pm) (10). Table 1 summarizes the Fe-ligand and Fe-His bond lengths and the Fe-Ct distances determined by X-ray crystallographic analysis (55-64). The Fe-His distance in the α subunit is 216 pm or longer for the T state whereas it is shorter (194 pm) for the R state, meaning that the Fe atom draws the proximal His toward the heme less in the T than R state.

Figure 3.8 schematically illustrates an empirical relation between the positions of the proximal His in the α subunit and the quaternary structures of the tetramer. The X-ray crystallographic analysis determined that the Fe-His distances of oxyT and oxyR Hbs are *ca.* 218 (59, Fig. 3.8D) and 194 pm (64, Fig. 3.8E), respectively. The former is close to that in deoxyHb A (58, Fig. 3.8A). Scheidt and coworkers (56, 57, 60) noted that the Fe-NO distance is hardly

different between the five- and six-coordinated ferrous NO porphyrins (172 and 174 pm, respectively). Since the local structure around the α-heme of horse Hb (61) is similar to that of

Table 3.1: Structural Parameters of the Heme Proximity for NO-bound Heme Proteins and Related Model Compounds Determined by X-ray Crystallographic Analysis

		Fe-NO(O_2) [a]		Fe-His [b]		Fe---Ct [c),d)]		reference
		α	β	α	β	α	β	
5-coordinate	Fe(TPP)(NO)	171.7		———		-21.1 [d)]		55
	Fe(OEP)(NO)	172.2		———		-29 [d)]		56
	Fe(TpivP)(NO)	172		———		-26.0 [c)]		57
	DeoxyHbA	———		216	209	40 [c)]	36 [c)]	58
6-coordinate	T(α-oxy)Hb	180	200	α_1 218 α_2 232	217	18 [c)]	43 [c)]	59
	Fe(TPP)(NO)(N-MeIm)	174.3		218		7 [c)]		60
	SNO-NOHb	174	175	228	228			61
	NOLb	172		220		2 [c)]		62
	NOMb(SW)	189		218		0 [d)]		63
	OxyHbA	166	187	194	207	-12 [c)]	11 [c)]	64

a) Fe-N(NO) or Fe-O(O_2) distance in pm unit.
b) Fe-N(histidine) distance in pm unit.
c) Ct is a center of porphyrin in the plane of four pyrrole nitrogen atoms. The out-of-plane displacement of Fe is represented in pm unit. "-" is the direction toward distal histidine.
d) Same as (c) except that Ct is a center of mean plane of porphyrin.

Fe(TPP)(NO)(N-MeIm) (60), the Fe-His distance in the six-coordinated Hb would be close to the Fe-(N-MeIm) distance (218 pm) of Fe(TPP)(NO)(N-MeIm), which is depicted by Fig. 3.8C. This distance is similar to that of the oxyT Hb structure (Fig. 3.8D) rather than that of oxyR Hb (Fig. 3.8E). It means that the proximal His is located at the position of T quaternary structure. Therefore, even if the Fe-His distance becomes further longer due to the out-of-plane movement of Fe toward the opposite direction as illustrated in Fig. 3.8B, the position of proximal His would remain unaltered (stay at the position of T).

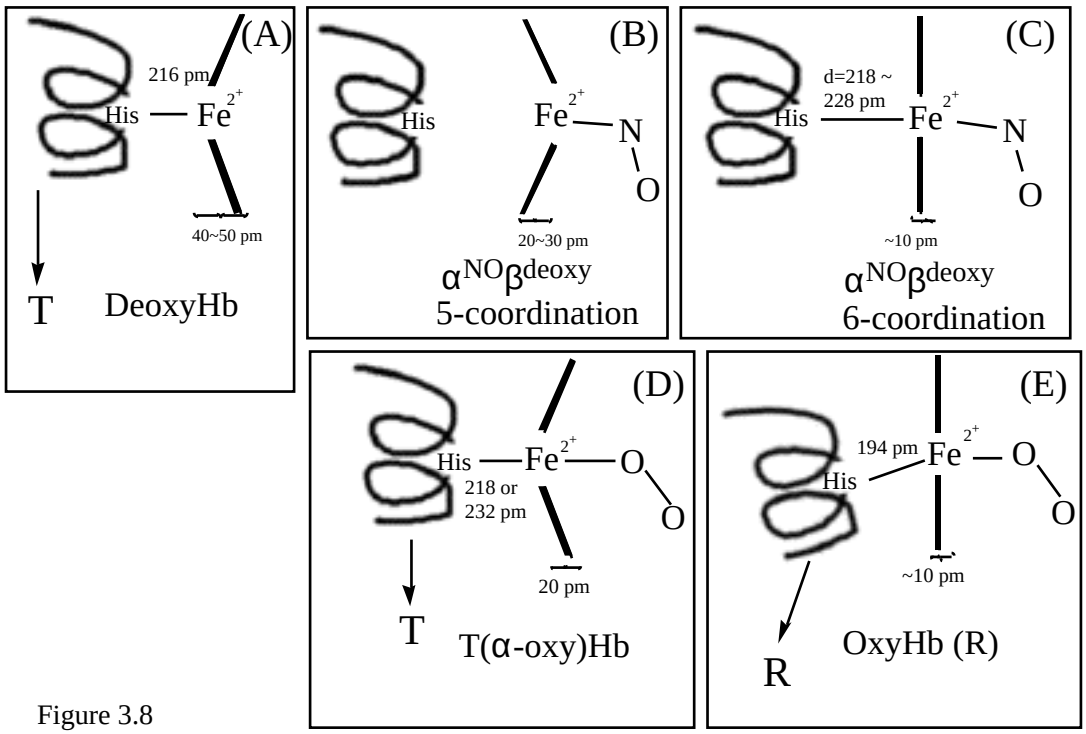

Figure 3.8

Schematic illustration of the position of the proximal histidine in the α subunit for various forms. The Fe-His distance is transferred from each X-ray crystallographic analysis quoted. A) deoxyHb A (Ref. 58), B) $\alpha^{NO}\beta^{deoxy}$ at pH 5.6, +IHP, C) $\alpha^{NO}\beta^{deoxy}$ at pH 8.8 in the absence of IHP, D) α-oxy form in the T structure Hb (Ref. 59), E) oxyHb A in the normal R structure (Ref. 64).

Communication Route of Ligand Binding between the α and β Subunits

The aforementioned second problem is the difference in the spectral changes of Tyr bands between NOHb ($\alpha^{NO}\beta^{NO}$) and $\alpha^{Ni}\beta^{CO}$. The change of Tyr bands toward R-like was not observed for $\alpha^{Ni}\beta^{CO}$ at neutral pH, while it was almost fully changed to R-like in $\alpha^{NO}\beta^{NO}$ even at lower pH (pH 5.5) in the presence of IHP (13). Their structural features before the ligand binding to the β-heme are alike, that is, the Fe-His bond is cleaved in the α subunit for both $\alpha^{Ni}\beta^{deoxy}$ at pH 6.7 in the absence of IHP and $\alpha^{NO}\beta^{deoxy}$ at pH 5.5 in the presence of IHP (2, 45-48, 52-54). The clearly

different point between $\alpha^{NO}\beta^{deoxy}$ and $\alpha^{Ni}\beta^{deoxy}$ is whether a ligand (NO) is present or absent in the heme pocket of the α subunit. It is well-known that the heme-bound NO forms a hydrogen bond with Hisα58 of E-helix (65). Tomita et al. (66) also confirmed it with mutant NOMbs by observing the ν_{NO} frequency which is sensitive to the hydrogen bonding from the protein moiety to NO. This suggests the existence of a hydrogen bonding network from Fe-NO---Hisα58 to the subunit interface, and a similar network will be present in the O_2-bound form of Hb A. There is no such a network between the α heme and the α1-β2 subunit interface in $\alpha^{Ni}\beta^{CO}$.

In the previous study we assumed the communication route of quaternary structure change from the β-heme to the subunit interface as follows (13); 1) Hisβ92 (F8) → Valβ98 (FG5) → Aspβ99 (G1) → Tyrα42 (C7) → Argβ40 (C6) → Argα92 (FG4) → Valα93 (FG5) → Tyrα140 (HC2) → Trpβ37 (C3), and 2) Hisβ92 (F8) → Valβ98 (FG5) → Tyrβ145 (HC2). Roughly speaking, these are the reversed course of the communication route from the α heme to the β heme proposed by Ho (44). These routes assumed that Tyrβ145 and Tyrα42 would be more sensitively influenced by ligand binding than Trpβ37, and that therefore the ligand binding to the β heme promotes the change of Tyr toward R-like. However, the result on $\alpha^{Ni}\beta^{CO}$ at pH 6.7 in the absence of IHP means that Tyr residues remain in the T structure after binding of a ligand to the β heme (Fig. 4C). Therefore, although the behavior of Trp upon ligand binding to the β-heme is almost the same between $\alpha^{NO}\beta^{NO}$ and $\alpha^{Ni}\beta^{CO}$, that of Tyr is different. In this regard, we supplement our previous conclusion on NOHb by noting that the Tyr routes mentioned above are contributing but its relative importance may depend on the existence of the ligand-protein hydrogen bonding network such as the Fe-NO---Hisα58.

In conclusion, UVRR spectroscopic studies on the Ni-Fe hybrid Hb demonstrated the differences in structural changes at the α1-β2 subunit interface between ligand binding to the α- and β-hemes. Ligation to the α-heme affects both Tyr and Trp residues, but ligation to the β-heme affects only Trp residues. The differences in behaviors between Trp and Tyr residues as well as

between the α and β subunits are stressed. Comparison of the results on $\alpha^{Ni}\beta^{CO}$ with the results from our previous study on $\alpha^{NO}\beta^{CO}$ and $\alpha^{NO}\beta^{NO}$ suggests that the structure of interface Tyr residues is related to a structure of distal His (Hisα58) in the α subunit, which depends on the presence or absence of a hydrogen bond network between the bound ligand and the distal His. In $\alpha^{Ni}\beta^{CO}$, the T to R change of Trp residues proceeds smoothly as pH is raised but that of Tyr does not. In $\alpha^{CO}\beta^{Ni}$, on the other hand, the T to R changes of Trp and Tyr residues take place to a similar extent as pH is raised. IHP retards the T to R change of Tyr, particularly at lower pH. Finally it is noted that $\alpha^{Ni}\beta^{CO}$ and $\alpha^{CO}\beta^{Ni}$ at pH 6.7 in the presence of IHP stays in the complete T quaternary structure, indicating its unusual stability of the T structure.

References

1. Monod, J., Wyman, J., and Changeux, J. P. (1965) *J. Mol. Biol. 12,* 88-118.

2. Shibayama, N., Morimoto, H., and Miyazaki, G. (1986) *J. Mol. Biol. 192,* 323-329.

3. Shibayama, N., Inubushi, T., Morimoto, H., and Yonetani, T. (1987) *Biochemistry 26,* 2194-2201.

4. Inubushi, T., Ikeda-Saito, M., and Yonetani, T. (1987) *Biochemistry 22,* 2904-2907.

5. Venkatesh, B. Hori, H., Miyazaki, G., Nagatomo, S. Kitagawa, T., and Morimoto, H. (2002) *J. Inorg. Biochem. 88,* 310-315.

6. Miyazaki, G., Morimoto, H., Yun, K.-M., Park, S.-Y., Nakagawa, A., Minagawa, H., and Shibayama, N. (1999) *J. Mol. Biol. 292,* 1121-1136.

7. Park, S.-Y., Nakagawa, A., and Morimoto, H. (1996) *J. Mol. Biol. 255,* 726-734.

8. Arnone, A., Rogers, P., Blough, N. V., McGourty, J. L., and Hoffman, B. M. (1986) *J. Mol. Biol. 188,* 693-706.

9. Unzai, S., Eich, R., Shibayama, N., Olson, J. S., and Morimoto, H. (1998) *J. Biol. Chem. 273,* 23150-23159.

10. Luisi, B., Liddington, B., Fermi., G., and Shibayama, N. (1990) *J. Mol. Biol. 214,* 7-14.

11. Luisi, B., and Shibayama, N. (1989) *J. Mol. Biol. 206,* 723-736.

12. Shibayama, N., Yonetani, T., Regan, R. M., and Gibson, Q. H. (1995) *Biochemistry 34,* 14658-14667.

13. Nagatomo, S., Nagai, M., Tsuneshige, A., Yonetani, T., and Kitagawa, T. (1999) *Biochemistry 38,* 9659-9666.

14. Harada, I., Miura, T., and Takeuchi, H. (1986) *Spectrochim. Acta 42A,* 307-312.

15. Kitagawa, T. (1992) *Prog. Biophys. Mol. Biol. 58,* 1-18.

16. Rodgers, K. R., Su, C., Subramaniam, S., and Spiro, T. G. (1992) *J. Am. Chem. Soc. 114,* 3697-3709.

17. Rodgers, K. R., and Spiro, T. G. (1992) *Science 265,* 1697-1699.

18. Nagai, M., Kaminaka, S, Ohba, Y, Nagai, Y, Mizutani, Y., and Kitagawa, T. (1995) *J. Biol. Chem. 270,* 1636-1642.

19. Nagai, M., Imai, K., Kaminaka, S, Mizutani, Y., and Kitagawa, T. (1996) *J. Mol. Struct. 379,* 65-75.

20. Nagai, M, Wajcman, H., Lahary, A, Nakatsukasa, T., Nagatomo, S. and Kitagawa, T. (1999) *Biochemistry, 38*, 1243-1251.

21. Huang, S., Peterson, E. S., Ho, C., and Friedman, J. M. (1997) *Biochemistry 36,* 6197-6206.

22. Huang, J., Juszczak, L., Peterson, E. S., Shannon, C.F., Yang, M., Huang, S., Vidugiris, G. V. A., and Friedman, J. M. (1999) *Biochemistry 38,* 4514-4525.

23. Hu, X., and Spiro, T. G. (1997) *Biochemistry 36,* 15701-15712.

24. Hu, X., Rodgers, K. R., Mukerji, I., and Spiro, T. G. (1999) *Biochemistry 38,* 3462-3467.

25. Peterson, E. S. and Friedman, J. M. (1998) *Biochemistry 37,* 4346-4357.

26. Nagai, M., Nishibu, M., Sugita, Y., Yoneyama, Y., Jones, R. T., and Gordon, S. (1975) *J. Biol. Chem. 250,* 3169-3173.

27. Kaminaka, S., and Kitagawa, T. (1995) *Appl. Spectrosc. 49,* 685-687.

28. Ogoshi, H., Watanabe, E., Yoshida, Z., Kincaid, J., and Nakamoto, K. (1973) *J. Am. Chem. Soc. 95*, 2845

29. Song, S., and Asher, S. A. (1991) *Biochemistry 30,* 1199-1205.

30. Kaminaka, S., and Kitagawa, T. (1992) *Appl. Spectrosc. 46,* 1804-1808

31. Dudik, J. M., Johnson, C. R., and Asher, S. A. (1985) *J. Chem. Phys. 82,* 1732-1740.

32. Miura, T., Takeuchi, H., and Harada, I. (1988) *Biochemistry 27,* 88-94.

33. Miura, T., Takeuchi, H., and Harada, I. (1989) *J. Ranan Spectrosc. 20,* 667-671.

34. Chi, Z, and Asher, S., A. (1998) *J. Phys. Chem. B. 102,* 9595-9602.

35. Matsuno, M., and Takeuchi, H. (1998) *Bull. Chem. Soc. Jpn. 71,* 851-857.

36. Harada, I., and Takeuchi, H. (1986) *Adv. Spectrosc. 13,* 113-175.

37. Kaminaka, S., and Kitagawa, T. (1992) *J. Am. Chem. Soc. 114,* 3256-3260.

38. Kitagawa, T., Abe, M., and Ogoshi, H. (1978) *J. Phys. Chem. 69,* 4516-4525.

39. Abe, M., Kitagawa, T., and Kyogoku, Y. (1978) *J. Phys. Chem. 69,* 4526-4534.

40. Perutz, M. F. (1970) *Nature 228,* 726-739.

41. Perutz, M. F. (1979) *Annu. Rev. Biochem. 48,* 327-386.

42. Perutz, M. F., Fermi, G., and Luisi, B., Shaanan, B., and Liddington, R. C. (1987) *Acc.Chem.Res. 20,* 309-321.

43. Fung, L. W.-M., and Ho, C. (1975) *Biochemistry 14,* 2526-2535.

44. Ho, C. (1992) *Adv. Protein Chem. 43,* 152-312.

45. Rougee, M., and Brault, D. (1975) *Biochemistry 14,* 4100-4106.

46. Rose, E. J., and Hoffman, B. M. (1983) *J. Am. Chem. Soc. 105,* 2866-2873.

47. Gibson, Q. H., and Roughton, F. J. W. (1957) *J. Physiol. 136,* 507-526.

48. Antonini, E., and Brunori, M. (1971) "Hemoglobin and Myoglobin in their Reactions with Ligands", North-Holland, Amsterdam.

49. Yonetani, T., Tsuneshige, A., Zhou, Y., and Chen, X. (1998) *J. Biol. Chem. 273,* 20323-20333.

50. Perutz, M. F., Kilmartin, J. V., Nagai, K., Szabo, A., and Simon, S. R. (1976) *Biochemistry 15,* 378-387.

51. Salhany, J. M., Ogawa, S., and Shulman, R. G., (1975) *Biochemistry 14,* 2180-2190.

52. Nagai, K., Hori, H., Yoshida, S., Sakamoto, H., and Morimoto, H. (1978) *Biochim. Biophys. Acta 532,* 17-28

53. Hille, R., Olson, J. S., and Palmer, G. (1979) *J. Biol. Chem. 254,* 12110-12120.

54. Nagai, K., Welborn, C., Dolphin D., and Kitagawa, T. (1980) *Biochemistry 19,* 4755-4761.

55. Scheidt, W. R., and Frisse, M. E. (1975) *J. Am. Chem. Soc. 97,* 17-21.

56. Ellison, M. K., and Scheidt, W. R. (1975) *J. Am. Chem. Soc. 119,* 7404-7405.

57. Nasri, H., Haller, K. J., Wang, Y., Huynh, B. H., and Scheidt, W. R. (1992) *Inorg. Chem. 31,* 3459-3467.

58. Fermi, G., Perutz, M. F., Shaanan, B., and Fourme, R. (1984) *J. Mol. Biol. 175*, 159-174.

59. Liddington, R., Derewenda, Z., Dodson, E., Hubbard, R., and Dodson, G. (1992) *J. Mol. Biol. 228,* 551-579.

60. Scheidt, W. R., and Piciulo, L. (1976) *J. Am. Chem. Soc. 98,* 1913-1919.

61. Chan, N-L., Rogers, P. H., and Arnone, A. (1998) *Biochemistry 37,* 16459-16464.

62. Harutyunyan, E. H., Safonova, T. N., Kuranova, I. P., Popov, A. N., Teplyakov, A. V., Obmolova, G. V., Vainshtein, B. K., Dodson, G. G., and Wilson, J. C. (1996) *J. Mol. Biol. 264,* 152-161.

63. Brucker, E. A., Olson, J. S., Ikeda-Saito, M., and Phillips, G. N., Jr. (1998) *Proteins 30,* 352-356.

64. Shaanan, B. (1983) *J. Mol. Biol. 171,* 31-59.

65. Olson, J. S., and Phillips, G. N. Jr. (1997) *J. Bio. Inorg. Chem. 2,* 544-552.

66. Tomita, T, Hirota, S, Ogura, T, Olson, J. S., and Kitagawa, T. (1999*) J. Phys. Chem. B 103,* 7044-7054.

CHAPTER 4

Changes in the Abnormal α-Subunit upon CO-Binding to the Normal β-Subunit of Hb M Boston: Resonance Raman, EPR, and CD Study

Published by *Biophysical Chemistry 98*, 217-232 (2002).

Shigenori Nagatomo, Yayoi Jin, Masako Nagai, Hiroshi Hori, and Teizo Kitagawa

4.1 Abstract

Heme-heme interaction in Hb M Boston (Hisα58 → Tyr) was investigated with visible and UV resonance Raman (RR), EPR, and CD spectroscopies. Although Hb M Boston has been believed to be frozen in the T quaternary state, oxygen binding exhibited appreciable cooperativity (n = 1.4) and the near-UV CD spectrum indicated weakening of the T marker at pH 9.0. Binding of CO to the normal β subunit gave no change in the EPR and visible Raman spectra of the abnormal α subunit at pH 7.5, but it caused an increase of EPR rhombicity and significant changes in the Raman coordination markers as well as the Fe(III)-tyrosine related bands of the α subunit at pH 9.0. The UVRR spectra indicated appreciable changes of Trp but not of Tyr upon CO binding to the β subunit at pH 9.0. Therefore, we conclude that the ligand binding to the β heme induces quaternary structure change at pH 9.0 and is communicated to the α heme presumably through Hisβ92 → Trpβ37 → Hisα87.

Footnotes

[1)] Abbreviations used are; Hb A, hemoglobin A; COHb A, carbonmonoxy Hb A; IHP, inositolhexakisphosphate; RR, resonance Raman; UVRR, ultraviolet resonance Raman; $\alpha_2^{Co}\beta^{deoxy}$, α-Co-β-Fe-deoxy hybrid Hb; $\alpha_2^{Mmet}\beta_2^{deoxy}$, α-Fe(III)-β-Fe(II)-deoxy Hb M Boston; $\alpha_2^{Mmet}\beta_2^{CO}$, α-Fe(III)-β-Fe(II)-CO Hb M Boston; $\alpha_2^{Ni}\beta_2^{deoxy}$, α-Ni-β-Fe-deoxy Hb; $\alpha_2^{deoxy}\beta_2^{Ni}$, α-Fe-deoxy-β-Ni Hb; 5c-hs, five-coordinate high-spin; 6c-hs, six-coordinate high-spin; 6c-ls, six-coordinate low-spin; PPIXDBE, protoporphyrin-IX dibenzylester.

4.2 Introduction

Hemoglobins (Hb) M have an abnormal chain in either α or β subunit of $\alpha_2\beta_2$ tetramer, yielding a natural valency-hybrid Hb under physiological conditions, that is, a ferric heme in the abnormal subunit and a ferrous heme in the normal subunit. There are four kinds of Hb Ms in which either the proximal or the distal histidine is replaced by tyrosine in the α or β subunit. They are named Hb M Iwate (Hisα87 → Tyr), Hb M Boston (Hisα58 → Tyr), Hb M Hyde Park (Hisβ92 → Tyr), and Hb M Saskatoon (Hisβ63 → Tyr). Hb Ms have properties different from those of normal Hb A as the replaced tyrosine is coordinated to the abnormal heme. Hb M Iwate and Hb M Boston, whose α-chains are abnormal, have very low oxygen affinity and show neither cooperativity nor Bohr effect at neutral pH (1,2). Hb M Hyde Park and Hb M Saskatoon, whose β-chains are abnormal, have normal oxygen affinity and decreased but significant cooperativity (3,4). Although the residues constituting the subunit interfaces are the same between Hb Ms and Hb A, the apparent heme-heme interaction is distinct between whether the replacement is present in the vicinity of heme of the α or β subunit.

The cooperative oxygen binding of Hb A has been explained in terms of reversible transition between the two quaternary structures (5), called T (tense) with low oxygen affinity and R (relaxed) states with high oxygen affinity (6, 7). The largest structural differences between the T and R structures, revealed by X-ray crystallographic analysis (8), are located in the α1-β2 subunit interface, where resets of hydrogen bonds and salt-bridges take place upon ligand binding or dissociation. The appearance of a heme-heme interaction is different when a ligand is bound to the α or β subunit, but such feature cannot be clarified with normal Hb, because the α and β hemes cannot be distinguished from each other. A method to investigate a more detailed mechanism of the heme-heme interaction is to use a Hb which allows ligand binding only to the α- or β-heme. Hb Ms are suitable to this purpose. Although Hb M Iwate and Hb M Boston, having an abnormal α chain, hardly show cooperativity in oxygen binding, it does not always mean depletion of the α1-

β2 intersubunit interactions. Presumably, binding of two ligands to normal β subunits at pH 7 is not sufficient to change a quaternary structure from T to R. However, for Co-Fe hybrid Hb, the subunit communication is present and observed upon binding of two ligands. For instance, CO cannot bind to the α subunit in the $\alpha_2^{Co}\beta_2^{deoxy}$ hybrid deoxyHb similar to Hb M Iwate and Hb M Boston, but binding of CO to its β heme causes a low field shift of ^{1}H NMR of proximal Hisα87 (9), indicating that the ligand binding in the β subunit is communicated to the proximal His of the α subunit and to have made the Co-His bond-length shorter.

The Fe(III) heme in the α subunit of Hb M Boston allows us to measure EPR signals and thus to monitor a change in an electronic state of the Fe(III) heme in the α subunit upon binding of a ligand to the ferrous heme of the partner β subunit. So far it is known that anisotropy of g values changes upon oxygenation to the normal α heme of Hb M Hyde Park at pH 7 (10). Proton NMR studies of Hb M Milwaukee, in which Valβ67 is replaced by Glu and therefore the β heme always remains in the ferric state, have shown that the CO and O_2 binding to the normal α subunit can affect the hyperfine-shifted ^{1}H resonances of the abnormal β subunit (11,12). These data indicate the presence of the communication from the α to β subunit during the ligation process of these Hbs, although direct electrostatic interaction between the two hemes is unlikely as their distance is approximately 250 pm. To answer a question, how the effect of O_2-binding to one heme is communicated to the other heme, we investigated, in this study, the communication from the β to α subunit upon ligand binding to the β subunit by monitoring the EPR and visible RR spectra of the α heme together with the measurement of UVRR and CD spectra reflecting the α1-β2 subunit contacts.

4.3 Experimental Procedures

Sample Preparations

Hb A was purified from fresh human blood by a preparative isoelectric focusing electrophoresis (13). Hb M Boston was separated from Hb A on Amberlite CG-50 column pre-equilibrated with 0.05 M phosphate buffer pH 7.0. After Hb A was washed out of the column with the same buffer, Hb M Boston remaining on the column was eluted with 0.2 M phosphate buffer, pH 7.0 (14). $\alpha_2^{Mmet}\beta_2^{deoxy}$ and $\alpha_2^{Mmet}\beta_2^{CO}$ of Hb M Boston were prepared by repetition of deaeration followed by flushing with pure N_2 and flowing with CO.

EPR Measurements

EPR measurements were carried out at X-band (9.35 GHz) microwave frequency using a Varian E-12 spectrometer with 100 kHz field modulation (15). An Oxford flow cryostat Dewar (ESR-900) was used for measurements at 5 K. The microwave frequency was calibrated with a microwave frequency counter (Takeda Riken, model TR5212). The magnetic field strength was determined by a NMR field meter EFM-2000AX (ECHO Electronic Co. Ltd. Japan). EPR spectra were recorded with a microwave power of 5 mW and a field modulation width of 0.5 mT (tesla). EPR signal intensity was directly proportional to the amounts of the Fe(III) hemes in Hbs under these conditions.

Visible Resonance Raman Measurements

Visible resonance Raman spectra were excited with the 413.1 nm line of a Kr laser (Model 2060, Spectra Physics) and the 488.0 nm line of an Ar laser (Model GLG3200, NEC) and detected with a liquid nitrogen cooled CCD detector (Model CCD3200, Astromed and Model LN/CCD-1300-PB, Princeton Instruments) attached to a 100 cm single polychromator (Model MC-100DG, Ritsu Oyo Kogaku). The slit width and slit height were set to be 200 μm (488 nm) or 150 μm (413.1 nm) and 20 mm, respectively. The spectral slit-widths are 6.6 cm^{-1} (488 nm) and 7.1 cm^{-1} (413.1 nm). A wavenumber width per one channel (resolution) of the detector is 0.73 cm^{-1} (488

nm) and 0.82 cm^{-1} (413.1 nm) under this condition. The laser power was made as low as possible and practically they were 50 mW (488 nm) and 0.25 mW (413.1 nm) at the sample point. For the experiments with the 488.0 and 413.1 nm excitation, 600 μl and 150 μl, respectively, of the 200 μM (heme) Hb solution were put into a spinning cell. Dissociation of CO by the probe laser was monitored by the ν_4 band, which appears at ~1355 and ~1370 cm^{-1} for photodissociated and non-dissociated forms, respectively. All measurements were carried out at room temperature with a spinning cell (1000 rpm). Raman shifts were calibrated with indene and accuracy of the peak positions of Raman bands was ±1 cm^{-1}. Integrity of each form was confirmed with visible absorption spectrum after RR measurements.

Ultraviolet Resonance Raman Measurements

UVRR spectra were excited by a XeCl excimer laser-pumped dye laser (EMG103MSC/LPX105 and FL2002/SCANMATE, Lambda Physik) as shown in CHAPTER 1.3 Apparatus (16). Approximately 150 μl of Hb sample (200 μM in heme) in Tris-Cl buffer was put into a spinning cell made of a synthetic quartz EPR tube with a diameter of 5 mm (17). Just before the measurement of UVRR spectra, Na_2SO_4 was added to the samples with the final concentration of 0.1 M as an internal intensity standard for Raman spectra. It was confirmed that the addition of sulfate did not cause any apparent Raman spectral change for the states examined in this study, although its use in Raman experiments was warned against due to possible tertiary structure change (18). Other details of UV Raman measurements were described previously (19).

Circular Dichroism Spectra Measurements

CD spectra were measured with a Jasco J-725 spectropolarimeter at 25 °C with a cell path-length of 2 mm. The instrument was calibrated with (+)-10-camphorsulfonic acid. Spectra were recorded with a scan speed of 50 nm/min , a slit-width of 1 nm, and a detector response time of 1

s, and 20 scans were averaged into a single spectrum. The observed spectra were corrected by subtraction of the solvent spectrum obtained under the identical condition. The results are represented with the unit of $\Delta\varepsilon$ ($M^{-1}cm^{-1}$) per mole of protein (in heme basis). The spectrum of Hb A was measured in individual series of measurements as a control. All samples used were 50 μM (in heme) in 0.05 M Tris-Cl buffer.

Absorption Spectra Measurements

Absorption spectra of Hb A and Hb M Boston were measured for both deoxy and CO forms at pH 7.5 and 9.0 with a Hitachi U-3210 spectrophotometer. The sample concentration was 10 and 200 μM for the B and Q band regions, respectively.

Oxygen Equilibrium Measurements

Oxygen equilibrium curves were determined by a spectroscopic method according to Sugita and Yoneyama (20) for the Hb solution with the concentration of 50-60 μM (in heme) in 0.05 M Tris-Cl buffer containing 0.1 M NaCl. Hb was deoxygenated by repetition of alternate evacuation and flushing with the Q gas (helium/isobutane = 99.05/0.95) in a Thunberg-type cell with 1-cm light path. A pH value of the Hb solution was determined at the end of experiment.

4.4 Result

Figure 4.1 shows the $g_{\perp}$ region of EPR spectra of metHb A (A), $\alpha_2^{Mmet}\beta_2^{deoxy}$ and $\alpha_2^{Mmet}\beta_2^{CO}$ of Hb M Boston at pH 7.5 (B) and those at pH 9.0 (C). The EPR spectra of Fe(III) high-spin hemes generally give rise to the pattern of axial symmetry with peaks at $g_{\perp} = 6$ and $g_{/\!/} = 2$. In fact, the $g_{\perp}$ spectrum of met Hb A gives a single peak at g=6, but that of Hb M Boston exhibits splitting into $g_1 = 6.32$ and $g_2 = 5.76$ at pH 7.5. It means the presence of anisotropy in the α heme plane in Hb M Boston. The anisotropy of the α heme in the $\alpha_2^{Mmet}\beta_2^{deoxy}$

state is almost the same between pH 7.5 (B, solid line) and at pH 9.0 (C, solid line). Upon binding of CO to the β heme, the splitting is almost the same between $\alpha_2^{Mmet}\beta_2^{deoxy}$ (B, solid line) and $\alpha_2^{Mmet}\beta_2^{CO}$ (B, broken line) at pH 7.5, but additional new rhombic signals with larger splitting (g_1 = 6.60 and g_2 = 5.53) appeared at pH 9.0 (C, broken line). Anisotropy of g-value is generally represented in terms of rhombicity, that is, $[(g_1 - g_2)/16 \times 100]$. In this case the rhombicity is changed from 3.50 ($\alpha_2^{Mmet}\beta_2^{deoxy}$) to 6.69 ($\alpha_2^{Mmet}\beta_2^{CO}$) by binding of CO to the β heme at pH 9.0. The Fe(III) low-spin signal was not detected for neither $\alpha_2^{Mmet}\beta_2^{deoxy}$ nor $\alpha_2^{Mmet}\beta_2^{CO}$ both at pH 7.5 and 9.0.

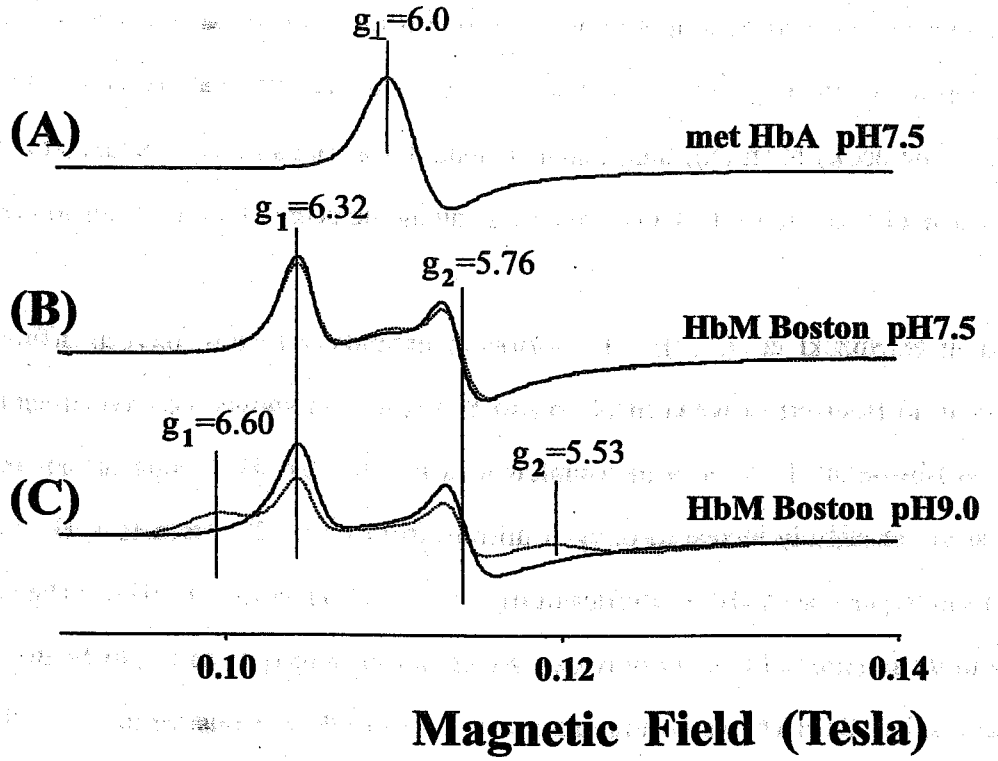

Figure 4.1: **EPR spectra of metHb A at pH 7.5 (A), Hb M Boston $\alpha_2^{Mmet}\beta_2^{deoxy}$ (solid line) and $\alpha_2M^{Mmet}\beta_2^{CO}$ (broken line) at pH 7.5 (B), and Hb M Boston $\alpha_2^{Mmet}\beta_2^{deoxy}$ (solid line) and $\alpha_2^{Mmet}\beta_2^{CO}$ (broken line) at pH 9.0 (C).**

Figure 4.2 shows the absorption spectra of Hb M Boston at pH 7.5 and 9.0. The deoxy form (A and B) has a Soret peak at 406 nm with a shoulder at 425 nm, and the CO form (C and D) has a main peak at 420 nm with a shoulder at 406 nm, while the spectra in the Q band region are in agreement with the previous measurements (21). The spectral change is due to the contribution of the ferrous β-heme upon the change from the deoxy (425 nm shoulder) to the CO form (420 nm). The pH difference spectra between pH 7.5 and pH 9.0 observed for $\alpha_2^{Mmet}\beta_2^{deoxy}$ (E) and $\alpha_2^{Mmet}\beta_2^{CO}$ (F) indicate that their patterns are alike but magnitude is larger for $\alpha_2^{Mmet}\beta_2^{CO}$ than for $\alpha_2^{Mmet}\beta_2^{deoxy}$. The inset shows the same set of spectra in the Q band region obtained with more concentrated solutions. One broad peak appeared for the deoxy form (A and B), but two peaks (β and α bands) appeared for the CO form (C and D), and their pH difference is larger for the CO form (F) than for the deoxy form (E), although their magnitudes are so small. Note that a positive peak is present around 520 nm for the CO form (F), meaning the decrease of a CT absorption at pH 9.0 than pH 7.5.

According to Suzuki et al. (2), Hb M Boston exhibits very low oxygen affinity, low cooperativity, and no Bohr effect between pH 6 and 8. Figure 4.3 shows the oxygen equilibrium curves of Hb M Boston at pH 7 and 9 in comparison with Hb A at pH 7. Raising pH for Hb M Boston resulted in the slightly increased oxygen affinity from P_{50} = 27.5 mmHg (pH 7) to 21.5 mmHg (pH 9) and the increased Hill's coefficient from n = 1.2 (pH 7) to 1.4 (pH 9). The values at pH 7 agree with those reported (2). As only two subunits can bind oxygen in Hb M Boston, the maximal value of n is 2.0 for Hb M Boston rather than 4.0 for Hb A. Considering n = 2.8 for Hb A, the increase in the n value of Hb M Boston from 1.2 to 1.4 seems to be significant, reflecting some change in the α1-β2 contacts.

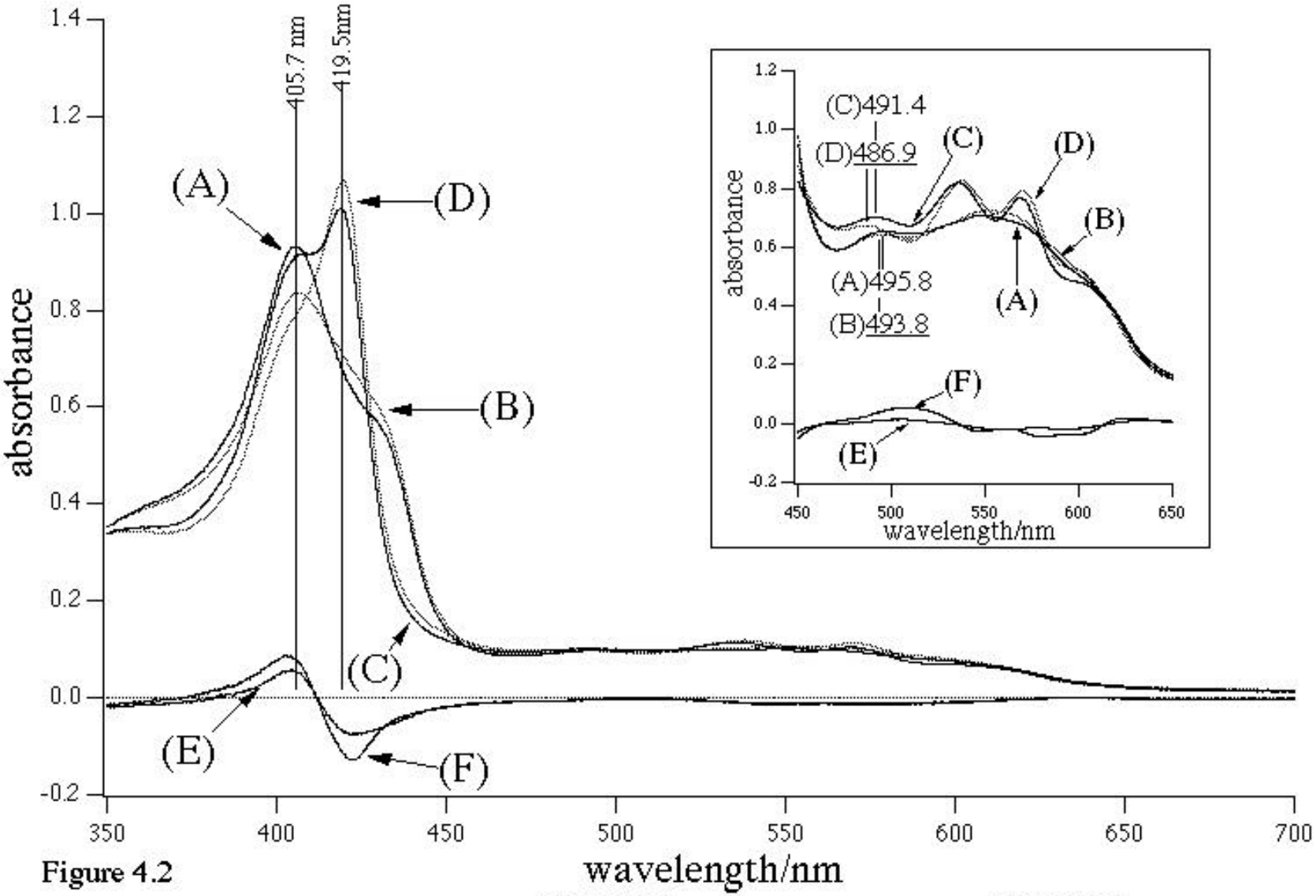

Figure 4.2

Absorption spectra of Hb M Boston $\alpha_2^{Mmet}\beta_2^{deoxy}$ at pH 7.5 (A, —) and $\alpha_2^{Mmet}\beta_2^{deoxy}$ at pH 9.0 (B, ···), $\alpha_2^{Mmet}\beta_2^{CO}$ at pH 7.5 (C, —), and $\alpha_2^{Mmet}\beta_2^{CO}$ at pH 9.0 (D, ···), and their difference spectra; E [(A) minus (B)], and F [(C) minus (D)].

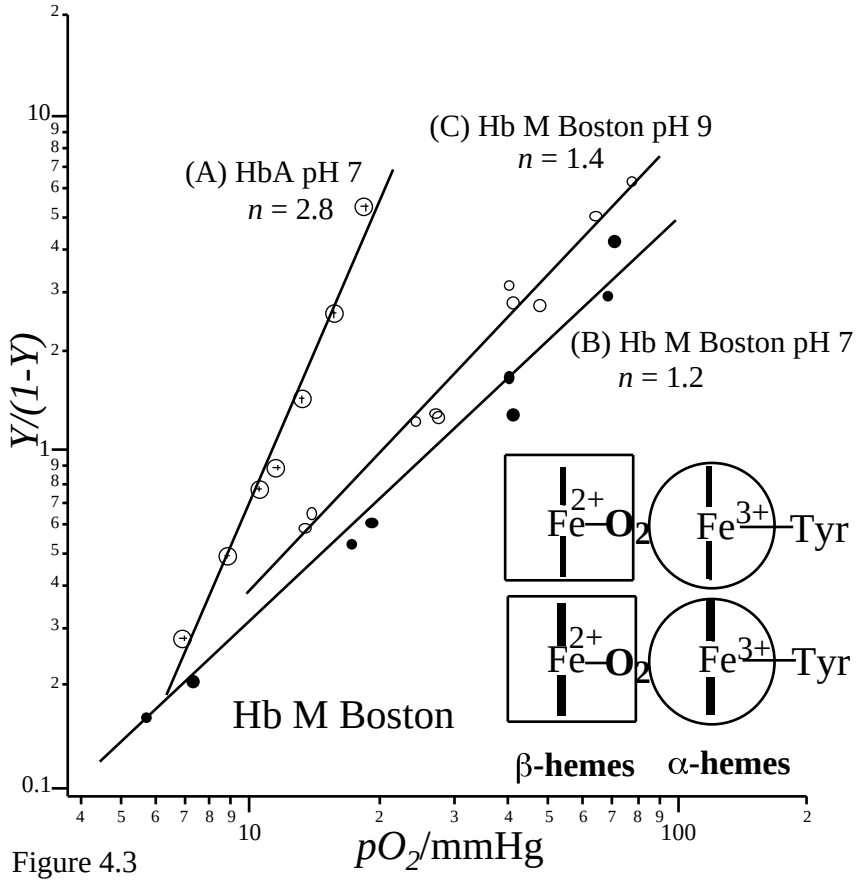

Figure 4.3

Oxygen equilibrium curves of Hb A at pH 7 (A) and Hb M Boston at pH 7 (B) and pH 9 (C). The ratio of the population of the oxy- to deoxy-hemes (Y: fractional oxygen saturation) is plotted against the partial pressure of oxygen (pO_2), both in logarithmic scales.

Figure 4.4 shows the 413.1 nm excited resonance Raman (RR) spectra of Hb M Boston at pH 7.3 (A and C) and pH 9.1 (B and D) for the deoxy- (A and B) and the CO-forms (C and D),

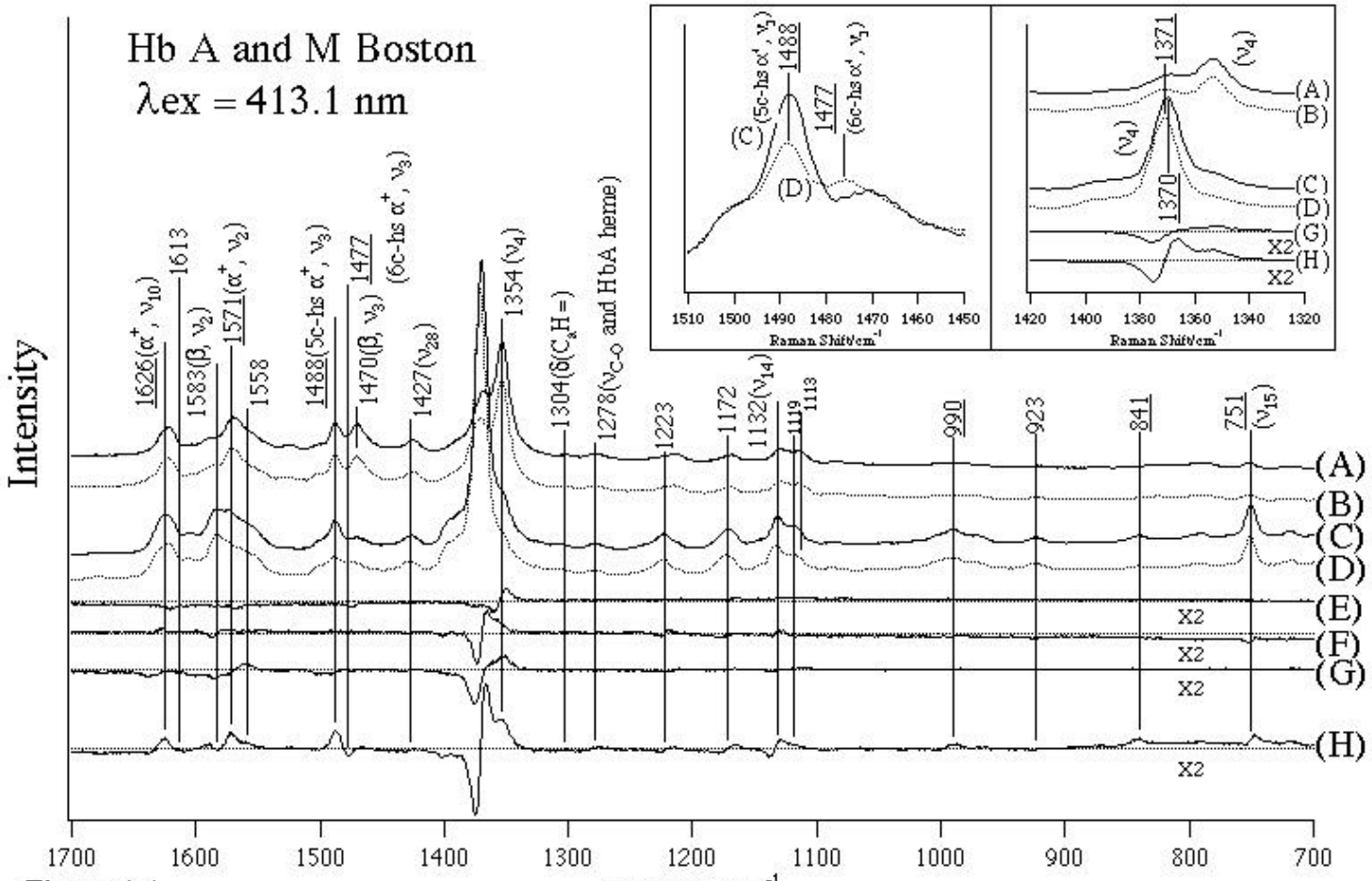

Figure 4.4

The 413.1 nm excited RR spectra of $\alpha_2^{Mmet}\beta_2^{deoxy}$ at pH 7.3 (A), $\alpha_2^{Mmet}\beta_2^{deoxy}$ at pH 9.1 (B), $\alpha_2^{Mmet}\beta_2^{CO}$ at pH 7.3 (C), $\alpha_2^{Mmet}\beta_2^{CO}$ at pH 9.1 (D), and their difference spectra; G [(A) minus (B)], and H [(C) minus (D)]. Similar pH difference spectra (pH 7.1 minus pH 9.1) of deoxyHb A and COHb A are displayed by traces E and F, respectively. The inset shows the expanded illustration of the spectra between 1320 and 1420 cm^{-1} (right) and 1450 and 1510 cm^{-1} (left). The marker, a+ means the aMmet heme throught the figures.

and their pH difference spectra (G and H). As spectra of Hb M Boston include the contributions from the ferric α- and ferrous β-hemes, it is difficult to distinguish between the two contributions.

Since the contribution of the normal β subunit to the spectra of Hb M Boston would be similar to that of Hb A, the RR spectra of Hb A were examined at the same conditions and their pH difference spectra (pH 7 minus pH 9) were calculated for the deoxy- and CO-forms as shown by spectra E and F, respectively. The pH difference peak appeared only for the ν_4 mode in the case of Hb A (E and F) in contrast with the case of Hb M Boston which gave many difference peaks particularly for the CO-form (H). The additional difference peaks include those at 751, 1132, 1370, 1488(1477), 1571, and 1626(1613) cm^{-1} (Parentheses mean negative peaks). The last four bands can be assigned to ν_4, ν_3, ν_2, and ν_{10} of a ferric heme, respectively (21-24). Among them, the ν_3 and ν_{10} frequencies are sensitive to the coordination number of a heme, and the peak positions at 1477 and 1613 cm^{-1} at pH 9.0 are indicative of the six-coordinate high-spin (6c-hs) heme. The differences of the bands at 751 and 1132 cm^{-1} (Fig. 4H), which are also weakly present in the spectrum of Hb A (Fig. 4F), are assignable to ν_{15} and ν_{14}, respectively (25). It is known that the abnormal subunit of Hb M Boston yields resonance enhanced Raman bands associated with the coordinated tyrosine upon excitation at 488.0 nm (21). Therefore, Raman spectra excited at 488.0 nm were examined in this study again.

Figure 4.5 shows the raw RR spectra $\alpha_2^{Mmet}\beta_2^{deoxy}$ (A) and $\alpha_2^{Mmet}\beta_2^{CO}$ (B) of Hb M Boston and deoxyHb A (C) and COHb A (D) all at pH 7.5 excited at 488.0 nm, and the corresponding pH 7.5-minus-pH 9 difference spectra (E, F, G, and H). In the spectra of Hb M Boston there are several bands which are absent in the spectra of Hb A. These include the bands at 602, 795, 829, 876, 1278, and 1503 cm^{-1}. Some of them have been already assigned in the previous studies (21, 26); the 602 cm^{-1} band to the Fe(III)-O (tyrosinate) stretching ($\nu_{Fe\text{-}O}$) (26), the 1278 cm^{-1} band to the C-O stretching mode ($\nu_{C\text{-}O}$) of Tyrα58 (21), and the 1503 cm^{-1} band to Y19a (27). The bands at 829 and 876 cm^{-1}, newly found in this experiment, are assignable to internal modes (possibly Y1

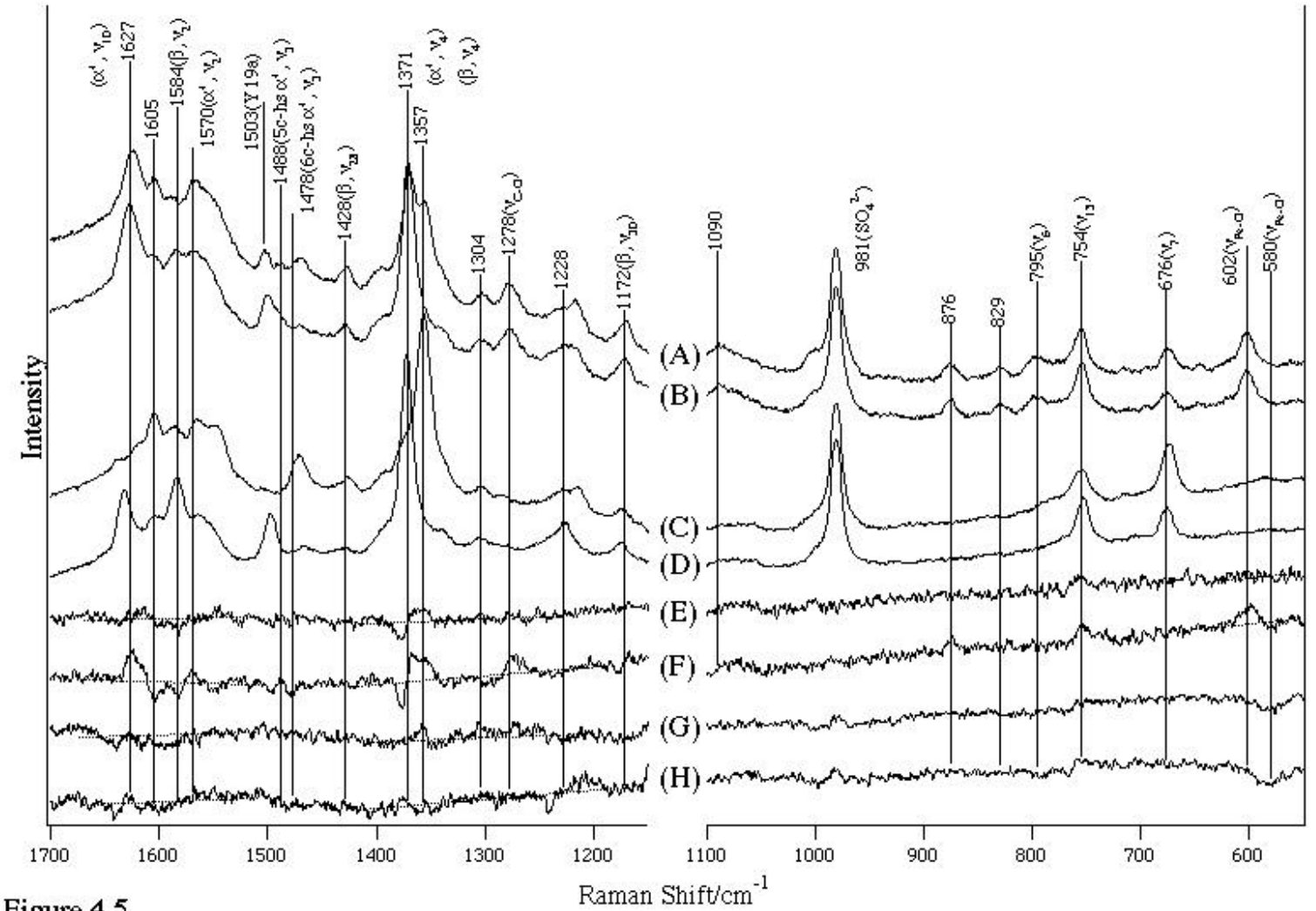

Figure 4.5

The 488 nm excited RR spectra of Hb M Boton $\alpha_2^{Mmet}\beta_2^{deoxy}$ at pH 7.5 (A), and $\alpha_2^{Mmet}\beta_2^{CO}$ at pH 7.5 (B), and of deoxyHb A at pH 7.5 (C), and COHb A at pH 7.5 (D), and their difference spectra;
(E) = $\alpha_2^{Mmet}\beta_2^{deoxy}$ at pH 7.5 (A) minus $\alpha_2^{Mmet}\beta_2^{deoxy}$ at pH 9.0,
(F) = $\alpha_2^{Mmet}\beta_2^{CO}$ at pH 7.5 (B) minus $\alpha_2^{Mmet}\beta_2^{CO}$ at pH 9.0,
(G) = deoxyHb A at pH 7.5 (C) minus deoxyHb A at pH 9.0, and (H) = COHb A at pH 7.5 (D) minus COHb A at pH 9.0.

and overtone of Y16a) of the coordinated tyrosinate. The pH difference spectra for deoxy- (Fig. 4.5G) and COHb A (Fig. 4.5H) yield no peak, indicating that the heme moiety undergoes no pH-dependent structural change. As to Hb M Boston, on the other hand, the RR spectra are little different between pH 7 and 9 for $\alpha_2^{Mmet}\beta_2^{deoxy}$ (E) but are clearly different for $\alpha_2^{Mmet}\beta_2^{CO}$ (F). The differences are prominent for the bands at 602(580), 754, 876, 1278, 1371, 1570 (1584), and 1627 (1605) cm^{-1} (Parentheses mean the position of negative peaks). Most of these differences seem to appear from the ferric heme but it is caused by CO binding to the ferrous β-heme. The low frequency shift of ν_{Fe-O} from 602 to 580 cm^{-1} means that the Fe(III)-O (tyrosinate) bond is somewhat weakened in $\alpha_2^{Mmet}\beta_2^{CO}$ at pH 9 than at pH 7 and would be compatible if Hisα87 is coordinated to the *trans* position of the Fe-O bond of the ferric α heme, giving rise to the 6c-hs structure. The decrease of Raman intensity of the ν_{C-O} mode at 1278 cm^{-1} at pH 9 also suggests some change in the Fe(III)-tyrosinate moiety. The differences at 1371, 1570 and 1627 cm^{-1} are considered to arise from the ν_4, ν_2 and ν_{10} modes of ferric α-heme similar to the case of 413.1 nm excitation. While the ν_4 frequency is sensitive to π electron delocalization between Fe and the macrocycle, the ν_2 and ν_{10} frequencies are sensitive to the core size of the porphyrin and thus to the coordination number of Fe. Thus, the 488.0 nm excited Raman spectra as well as the 413.1 nm excited spectra support the idea that the coordination of axial ligands in the α heme is influenced by CO binding to the β heme through the subunit contacts.

Figure 4.6 shows the 235 nm excited UVRR spectra for $\alpha_2^{Mmet}\beta_2^{deoxy}$ at pH 7.3 (A), $\alpha_2^{Mmet}\beta_2^{CO}$ at pH 7.3 (B), $\alpha_2^{Mmet}\beta_2^{deoxy}$ at pH 9.0 (C), $\alpha_2^{Mmet}\beta_2^{CO}$ at pH 9.0 (D), deoxyHb A at pH 7.3 (E), COHb A at pH 9.0 (F) in the frequency region from 1700 to 700 cm^{-1}, and their differences, G (A minus B), H (C minus D), and I (E minus F). The 981 cm^{-1} band of SO_4^{2-} ions was used to normalize the intensity of the spectra (28). In the spectrum of deoxyHb A, RR bands of tyrosine residues (Tyr) are seen at 1619 (Y8a), 1208 (Y7a), 1177 (Y9a) and 854 cm^{-1} (Y1), and those of tryptophan residues (Trp) are seen at 1558 (W3), 1360-1340 (W7; tryptophan doublet),

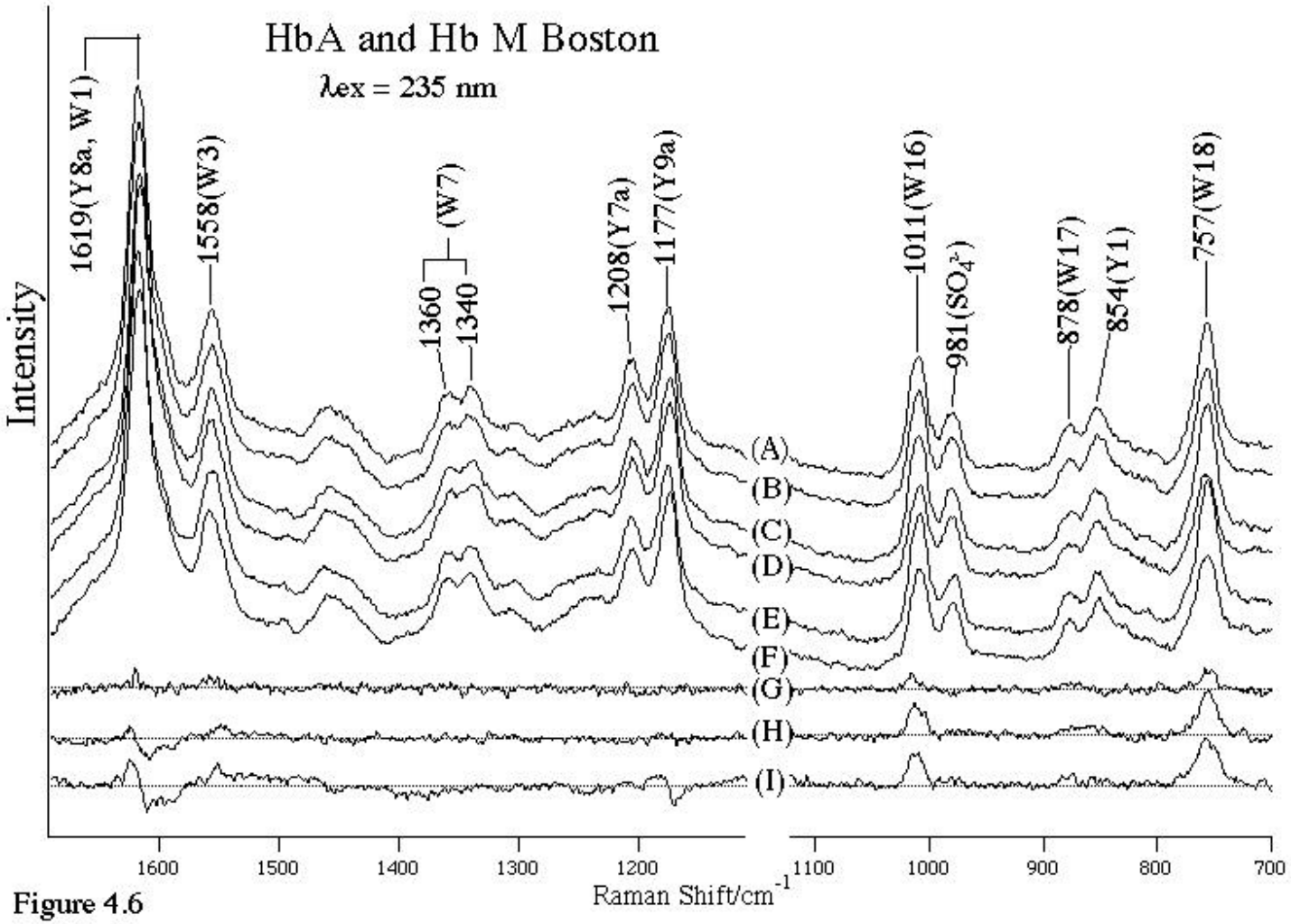

Figure 4.6

The 235-nm excited UVRR spectra of Hb M Boston $\alpha_2^{Mmet}\beta_2^{deoxy}$ at pH 7.3 (A), $\alpha_2^{Mmet}\beta_2^{CO}$ at pH 7.3 (B), $\alpha_2^{Mmet}\beta_2^{deoxy}$ at pH 9.0 (C), $\alpha_2^{Mmet}\beta_2^{CO}$ at pH 9.0 (D), deoxyHb A (E) at pH 7.3, and COHb A (F) at pH 9.0, and their difference spectra; G [(A) minus (B)], H [(C) minus (D)], and I [(E) minus (F)].

1011 (W16), 878 (W17), and 757 cm^{-1} (W18). The assignments are based on Harada and coworkers (27, 29, 30). These UVRR spectra of Hb A excited at 235 nm are essentially the same as those excited at 229 nm (31), although relative intensities of bands are slightly different between them due to differences in resonance conditions. The difference spectrum between deoxyHb A and COHb A indicates that the intensities of the W3, W16, W17, and W18 bands of Trp are much weaker for COHb A than for deoxyHb A, while the peak positions remain unaltered and that the frequencies of the Y8a and Y9a bands of Tyr are lower for COHb A than for deoxyHb A. These differences arise mainly from Trpβ37, Tyrα42, Tyrα140 and Tyrβ145 due to the quaternary structure change (13,32). The difference spectrum between $\alpha_2^{Mmet}\beta_2^{deoxy}$ and $\alpha_2^{Mmet}\beta_2^{CO}$ of Hb M Boston is very small at pH 7.3. Magnitudes of the changes of Trp bands for Hb M Boston are 10-20% of those of Hb A, and the change of Tyr was negligible at pH 7.3. The change of Trp bands of Hb M Boston becomes a similar size to that of Hb A at pH 9.0, but the change of Tyr bands are still very small. This demonstrates that the quaternary structure change due to CO binding to the β heme is extremely small at pH 7.3 but becomes appreciable at pH 9.0 regarding Trp residues.

Figure 4.7 shows the near-UV CD spectra of Hb A in the CO-, deoxy-, and met-forms (A), Hb M Boston in the CO- and deoxy-forms of the normal β subunit and in the met-form of the abnormal α subunit at pH 7 (B) and at pH 9 (C). As shown in Fig. 4.7A, deoxygenation is accompanied by a large decrease in the CD band of heme near 260 nm (33). The band becomes further smaller in the met form. The 260 nm band of CO-bound Hb M Boston ($\alpha_2^{Mmet}\beta_2^{CO}$) was smaller than that of COHb A and it becomes further smaller in the deoxy Hb M Boston ($\alpha_2^{Mmet}\beta_2^{deoxy}$) at both pH 7 and 9 (Fig. 4.7B and 4.7C).

Hb A shows a pronounced change in the CD spectrum around 280~300 nm upon the T → R transition. The T-state Hb (deoxyHb A) exhibits a distinctive negative CD band, whereas the R-state Hb (oxy-, CO-, or met-Hb A) gives weak positive CD bands. The change of ellipticity upon the T → R transition is considered to arise from local environmental changes of Tyrα42, Trpβ37,

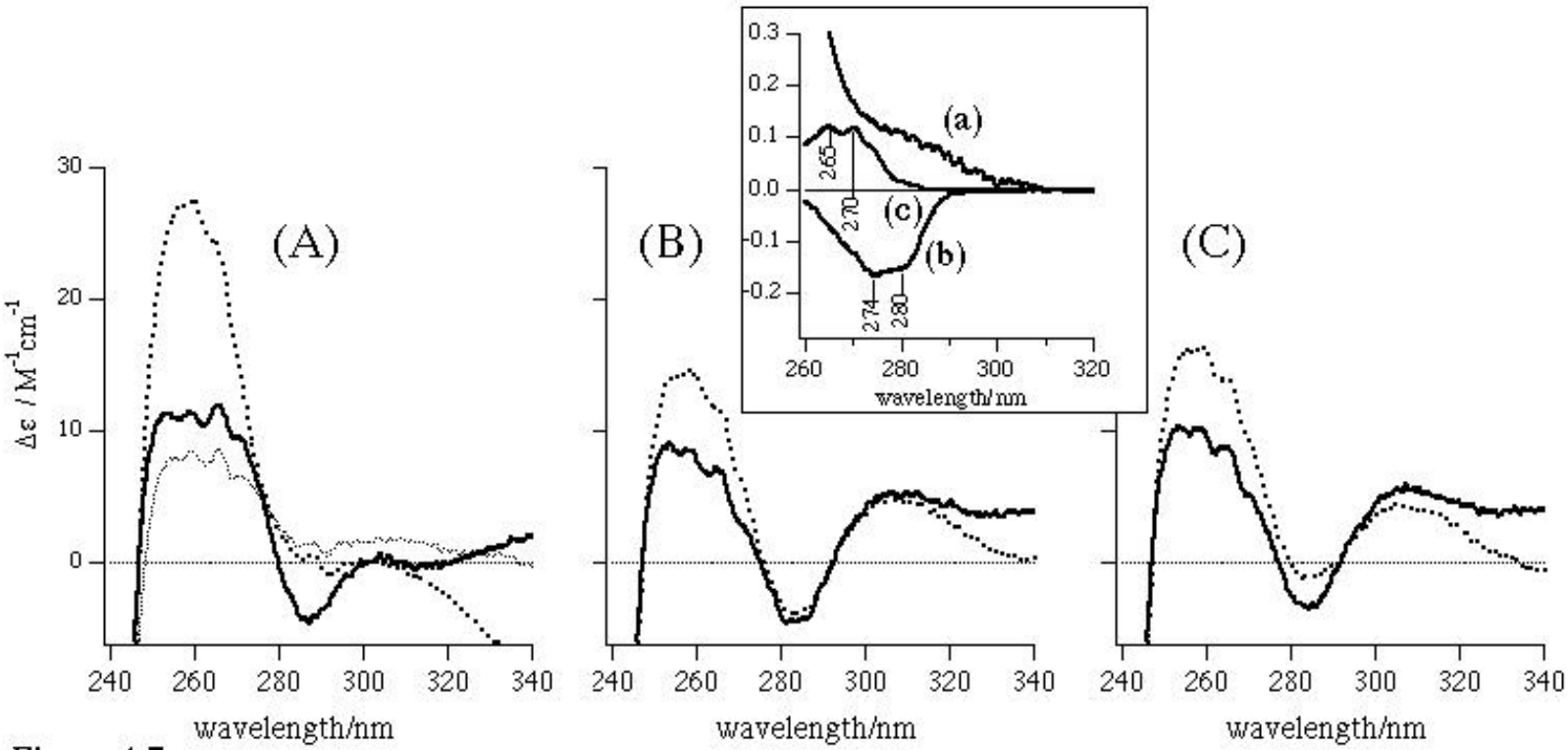

Figure 4.7

Near-UV CD spectra of Hb A (A), Hb M Boston at pH 7 (B) and at pH 9 (C). Hb solution was 50 μM (in heme) in 0.05 M Tris-Cl buffer containing 0.1 M NaCl. Dotted line: CO-form, Solid line: deoxy form. Thin dotted line in (A): met-form. For Hb M Boston, the deoxy and CO-forms mean $\alpha_2^{Mmet}\beta_2^{deoxy}$ and $\alpha_2^{Mmet}\beta_2^{CO}$, respectively. The inset shows the near-UV CD spectra of N-acetyl-L-tyrosinamide in 0.1 N NaOH (a), that in water (b) and O-phospho-L-tyrosine (Tyr-P) in 0.05 M Tris-Cl buffer, pH 7.2 (c). The sample concentrations are 0.9 mM for N-acetyl-L-tyrosineamide and 0.75 mM for O-phospho-L-tyrosine. CD spectra were acquired for a light path of 1 cm, and 40 scans were averaged.

and/or Tyrα140 (33-35). Hb M Boston at pH 7 shows a distinctive negative CD band at 287 nm irrespective of CO binding to the normal β subunit, indicating that the quaternary structure of Hb M Boston is frozen in the T-state even for the ligand bound form of the normal β subunit. However, at pH 9, the negative band at 287 nm of deoxyHb M Boston ($\alpha_2^{Mmet}\beta_2^{deoxy}$) decreased markedly upon CO binding to the normal β subunit (Fig. 7C). This indicates that a quaternary structure does not change at pH 7 but appreciably changes at pH 9 upon ligand binding to the normal β subunit of Hb M Boston.

The inset of Figure 4.7 shows the CD spectra of a model compound of tyrosine (N-acetyl-L-tyrosinamide) in water, that in 0.1 N NaOH, and O-phospho-L-tyrosine in 0.05 M Tris-Cl buffer, pH 7.2. Tyrosine in water gave a negative CD band at 274 and 280 nm whereas deprotonated tyrosine (in alkaline) gave a positive CD band. The CD bands of phosphorylated tyrosine (Tyr-P) are also positive. These features remind us that Hb M Boston gives a broad positive band near 310 nm in Figure 4.7(B-C). Although there are some differences in CD spectra between the model compounds and Tyr residue in the protein, it is likely that the positive CD band at 310 nm of Hb M Boston is due to Tyrα58 coordinated to the heme iron. The positive CD band of Hb M Boston at 310 nm did not change upon CO binding to the normal β subunit at pH 7 but decreased significantly at pH 9 (Fig. 4.7B and 4.7C), suggesting that Tyr coordination to the α heme was somehow perturbed by CO binding to the normal β subunit at pH 9.

4.5 Discussion

Quaternary Structure of $\alpha_2^{Mmet}\beta_2^{CO}$ at pH 7.5 and pH 9

We pointed out a local structure change around the ferric α-heme in $\alpha_2^{Mmet}\beta_2^{CO}$ of Hb M Boston. This change occurs in the CO bound form of β-heme and its magnitude is larger at pH 9.0 than at pH 7.5. This means that the intersubunit interactions are larger under alkaline conditions. Oxygen affinity of Hb M Boston is low and there is no cooperativity in the pH region between pH

6.5 and 7.9 (2). Accordingly, it is considered that ligand binding does not induce the quaternary structure change for Hb M Boston in the pH region between pH 6 and pH 8. However, the oxygen affinity of Hb M Boston became higher above pH 8 and cooperativity appeared as demonstrated by Fig. 4.3. This new finding suggests melting of the frozen T structure upon deprotonation of some residue(s) at pH 9. UVRR spectra reflect a higher order structure of protein. Here, the deoxy-minus-CO difference spectrum of Hb A (Fig. 4.6I) is used as the standard of the T-minus-R difference spectrum (13,19,32). In the 235 nm-excited UVRR spectra, the quaternary structure change appears as the spectral changes of Trp and Tyr residues. Figure 4.6G reflects the quaternary structure change on CO binding to the ferrous β heme of Hb M Boston at pH 7.3. The difference intensities of Trp bands are significantly weak and no peak is observed for Tyr bands, indicating little change of a quaternary structure. However, the difference spectrum at pH 9 (Fig. 4.6H) is close to that of Hb A (Fig. 4.6I) except for Y9a band. The quaternary structure dependent UVRR spectral changes of Trp residues mainly (~70%) arise from Trpβ37 (13,36,37). Accordingly, Trpβ37 changes toward a less hydrogen-bonding structure upon CO binding to the ferrous β-heme in a similar way to that in Hb A. Similar changes are also observed for other Hbs which cannot bind CO to the α heme, such as $\alpha_2^{NO}\beta_2^{deoxy}$ Hb (19) and $\alpha_2^{Ni}\beta_2^{deoxy}$ Hb (38). The Y9a band did not change upon CO binding to Hb M Boston. The absence of Y9a difference peak is also similar to the case of $\alpha_2^{Ni}\beta_2^{deoxy}$ Hb (38), in which a ligand cannot bind to the α heme. Thus, it is reasonable to conclude that the quaternary structure change occurs to Hb M Boston at pH 9 in a similar manner to that in ligand binding to β heme of Hb A. It is well known in the CD spectra that the negative band near 287 nm (Fig. 4.7A) serves as a T structure marker of Hb A (33). As to Hb M Boston at pH 7, $\alpha_2^{Mmet}\beta_2^{CO}$ gives the T-structure marker in the same way as $\alpha_2^{Mmet}\beta_2^{deoxy}$, but the T structure marker of $\alpha_2^{Mmet}\beta_2^{CO}$ becomes significantly weaker at pH 9. This is consistent with the UVRR result in the sense that binding of CO to Hb M Boston yields a significant amount of R quaternary structure at pH 9.

What Does Occur in the α-Heme upon CO Binding to the β Heme?

(I) Absorption Spectra

The pH difference in the absorption spectra shown in Fig. 4.2 indicate that pH dependence is larger for the CO-form than that for the deoxy form, although the spectral changes are qualitatively alike; the absorbance of the α ferric heme (406 nm) is larger at pH 7.5 than at pH 9.0 but that of the β ferrous heme (~420 nm) is opposite, and this trend is promoted by binding of CO to the β heme. In contrast, the pH difference spectra in the 480 to 620 nm region are qualitatively different between the deoxy and CO forms, although their magnitudes are small. The absorbance of $\alpha_2^{Mmet}\beta_2^{CO}$ around 520 nm decreases at pH 9 than at pH 7.0, suggesting the decrease of the charge transfer interaction from the oxygen of Tyrα58 to Fe(III) at pH 9.0, while the interaction scarcely changes with pH for $\alpha_2^{Mmet}\beta_2^{deoxy}$. Plausible origins of this include elongation of the Fe(III)-O(Tyrα58) bond and an angle change of this bond with regard the heme normal. The former results in a decrease of the D parameter of EPR rhombicity whereas the latter results in an increase of the E parameter. Whichever occurs, EPR rhombicity would increase.

(II) Visible Resonance Raman Spectra

Excitation of Raman spectra at 413.1 nm gave the ferric heme modes more favorably than ferrous heme modes. The frequencies of ν_3 and ν_{10} are known to be sensitive to the core size of porphyrin. The bands at 1488(ν_3) and 1626(ν_{10}) cm^{-1} are considered to reflect the five-coordinate high-spin (5c-hs) state (22-24). This is also consistent with the fact that the corresponding marker bands of Fe(III)(PPIXDBE)($OC_6H_4NO_2$), a model compound of tyrosinate-coordinate heme, are observed at 1494 and 1630 cm^{-1}, respectively (unpublished results). In the case of ferric hemes, the increase of core size occurs when the high-spin Fe atom is accommodated into the porphyrin plane by a change of the coordination number, and then the ν_3 and ν_{10} frequencies are expected to shift toward lower frequencies. The shift of ν_3 from 1488 to 1477 cm^{-1} and that of ν_{10} from 1626 to 1613 cm^{-1} in Fig. 4.4H is compatible to this idea. When the spin state is changed to a low spin

upon a change of coordination number, then the core size becomes smaller, because the core size is in the order of 6c-hs > 5c-hs > 6c-ls (39).

The visible resonance Raman spectra excited at 488.0 nm provide information different from those excited at 413 nm, since there is a CT absorption from tyrosinate to Fe(III) near 488.0 nm (21). The 488.0 nm excited Raman spectra of Hb M Boston showed obvious differences between pH 7.5 and 9.0 for $\alpha_2^{Mmet}\beta_2^{CO}$ as illustrated by Fig. 4.5F but little difference for $\alpha_2^{Mmet}\beta_2^{deoxy}$ (Fig. 4.5E). The differences appeared mainly for the bands associated with the coordinated tyrosinate. The most important is the frequency shift of the ν_{Fe-O} band from 602 to 580 cm^{-1}, meaning appreciable weakening of the Fe(III)-O(Tyrα58) bond at pH 9. Although either a movement of the oxygen of Tyrα58 or of Fe(III) can induce it, the movement of high-spin Fe atom toward the porphyrin plane and the accompanied change of iron coordination number seems more likely judging from the core expansion mentioned above.

About the ν_{C-O} mode of tyrosinate at 1278 cm^{-1}, the Raman intensity for $\alpha_2^{Mmet}\beta_2^{CO}$ decreased at pH 9, but its frequency remained unchanged. A similar phenomenon occurs to the 876 cm^{-1} band of $\alpha_2^{Mmet}\beta_2^{CO}$, which presumably arises from the Y1 mode of the coordinated Tyr. Since Raman intensity reflects the electronic excited state and is roughly proportional to a square of absorbance at the wavelength of Raman excitation but Raman frequencies reflect the electronic ground state, this observation conforms with the fact that the CT band becomes weaker at alkaline pH due to a change of the CT excited state. The difference peak around 1370 cm^{-1} may mean that delocalization of d_π electrons of Fe(III) to the e_g orbital of porphyrin ring decreases even in the ground state and thus ν_4 frequency is slightly raised at pH 9 than pH 7. All these observations imply appreciable reduction in the Fe(III)-tyrosinate interactions of the α heme at alkaline pH for the CO-bound form of β heme.

Thus, the Raman results suggest that the increased rhombicity (E/D) of the α heme of $\alpha_2^{Mmet}\beta_2^{CO}$ at pH 9 is caused by a decrease of the D parameter rather than an increase of the E

parameter, and the decrease of the D parameter is originated in weakening of the Fe(III)-O (Tyrα58) CT interactions and coordination of Hisα87 to its *trans* position. Since this is associated with binding of CO to the β heme, it should be regarded as an appearance of quaternary structure changes, although a route of communication remains to be clarified.

(III) EPR Spectra

The EPR spectral changes of the ferric α heme upon CO binding to the ferrous β-heme were clearly observed at pH 9.0 but not so clear at pH 7.5. The changes include the increase of anisotropy. The EPR anisotropy is usually represented in terms of E/D value (rhombicity = 3 × E/D), where D and E parameters reflect the axial (z) and the in-plane (x and y) ligand-field strengths, respectively, of the ferric α heme (40-42). Increase of E means more degradation of tetragonal symmetry, while the decrease of D means weakening in electronic interactions of axial ligand(s) with Fe. Two sets of EPR signals with different values of rhombicity (6.7 and 3.5) were observed for $\alpha_2^{Mmet}\beta_2^{CO}$ at pH 9.0. The latter was the same as that for $\alpha_2^{Mmet}\beta_2^{CO}$ at pH 7.5. Since the in-plane vibrations of the α heme change little between pH 7.5 and 9.0, it is reasonable to ascribe the rhombicity change to a change of D rather than E.

Among Tyr-coordinated Fe(III) hemes, one may expect that H64Y mutant Mb is closest to the abnormal α-chain of Hb M Boston. However, the H64Y mutant of horse heart Mb (hhMb) adopts the 6c-hs state (43), different from the Hb M Boston in which the ferric α heme adopts the 5c-hs state (44). Furthermore, for H64Y hhMb, were observed two sets of EPR signals with different values of rhombicity, 8.1 (main) and 3.0 (minor)(43). In Hb M Saskatoon having abnormal β-chains, the 6c-hs heme gives the rhombicity of 8.1 ~ 8.7 whether the normal α-heme adopts the deoxy, ferrous-CO or ferric form (10,14). Bovine liver catalase having a 5c-hs heme also gives rise to a similar value of rhombicity (= 7.5) (45). In contrast, Hb M Iwate, which has a 5c-hs heme in $\alpha_2^{Mmet}\beta_2^{deoxy}$ (21) and its fully oxidized form, $\alpha_2^{Mmet}\beta_2^{met}$ (26), gave the rhombicity of

2.4 for its CO form (46). Thus, the coordination number of iron has no direct correlation with a value of rhombicity.

The Fe(III)-axial ligand distance may have some correlation with EPR anisotropy. According to the X-ray structural analysis of H64Y hhMb, the Fe-O(Tyr64) and the Fe-His bond-lengths are 218 pm and 229 pm, respectively, and the Fe atom is displaced toward Tyr64 from the plane of the pyrrole nitrogen atoms by 39 pm (43). However, the EXAFS study of H64Y hhMb (47) gave the Fe-O distance of 188 pm, the value significantly shorter than the crystallographic value (218 pm), and inferred that the iron atom is displaced out of the heme plane by 47 pm. These observations suggest that the heme structure is slightly different between in a crystal and solution. In the case of H64Y mutant of sperm whale Mb (swMb), two kinds of Fe-O stretching bands have been observed at 578 and 600 cm^{-1} with nearly equal intensities in a solution state (48), and the former and latter bands were assigned to the 6c-hs and 5c-hs hemes, respectively. In this case, the 578 cm^{-1} component was correlated with the EPR minor component with rhombicity of 3.0, although differences between swMb and hhMb were noted there. Thus, interpretations are not always consistent. It seems to us more likely that the differences in temperatures are essential to make the population changes of the species in an equilibrium, and thus yields the accompanied differences in apparent observations. Namely, temperatures at which EPR, EXAFS, and Raman, were measured, are 4, 170, and 300 K, respectively, and seemingly the 6c-hs structure is more favorable at lower temperatures. The out-of-plane displacement of Fe atom would also depend on temperature. When the Fe atom comes into the heme plane, the Fe-O and Fe-His distances become longer and shorter, respectively, and the Fe-O stretching frequency as well as the D parameter of EPR would be altered even within the same coordination number.

The out-of-plane displacement of Fe(III) might determine rhombicity of heme EPR signals. It is generally thought that the Fe atom is displaced from the heme plane by *ca.* 50 pm in the N-bound 5c-hs hemes (49) and rhombicity is small(~3). This is also applicable to the O-coordinate 5c-

hs hemes like Hb M Iwate and Hb M Boston. In bovine liver catalase with 5c-hs heme, rhombicity is 7.5 (45) and the displacement of the Fe(III) atom from the mean plane of all ring atoms is at most 20 pm (50-52). This value of the out-of-plane displacement of Fe is smaller compared with those of many 5c-hs model compounds (49) and also than 47 pm of H64Y Mb (47). If the coordination number of the main species is determined by a temperature-dependent equilibrium and the smaller values of the out-of-plane displacement of Fe give rise to the larger value of EPR rhombicity even in the five coordinate state, then all the existing data seem to be explained satisfactorily. Accordingly, we propose that the difference in rhombicity of the α ferric heme between pH 7.5 and 9.0 for the CO bound form of β-heme arises from differences in the out-of-plane displacement of Fe(III), that is, the Fe atom in the ferric α subunit is pushed into the heme plane by Tyr64 and/or pulled by Hisα87 more at pH 9.0 than at pH 7.5 due to the larger intersubunit interactions.

Communication Pathway from the β-Heme to the α-Heme

Combination of information obtained from the measurements on oxygen equilibrium, EPR, CD, and visible and UV resonance Raman, demonstrated that the frozen T structure of Hb M Boston is molten at pH 9 and that ligand binding to the β heme causes a quaternary structure change toward R. Upon this change, some structural change takes place in the α heme. Thus, the α heme has an interaction with the β heme through subunit interface as illustrated in Figure 4.8. Similar phenomena occur on CO binding to β-heme of $\alpha^{Ni}\beta^{deoxy}$ (38) and $\alpha^{NO}\beta^{deoxy}$ (19). In both cases Trpβ37 undergoes a change upon binding of a ligand to the β heme (Fig. 4.8), although the size of change depends on pH.

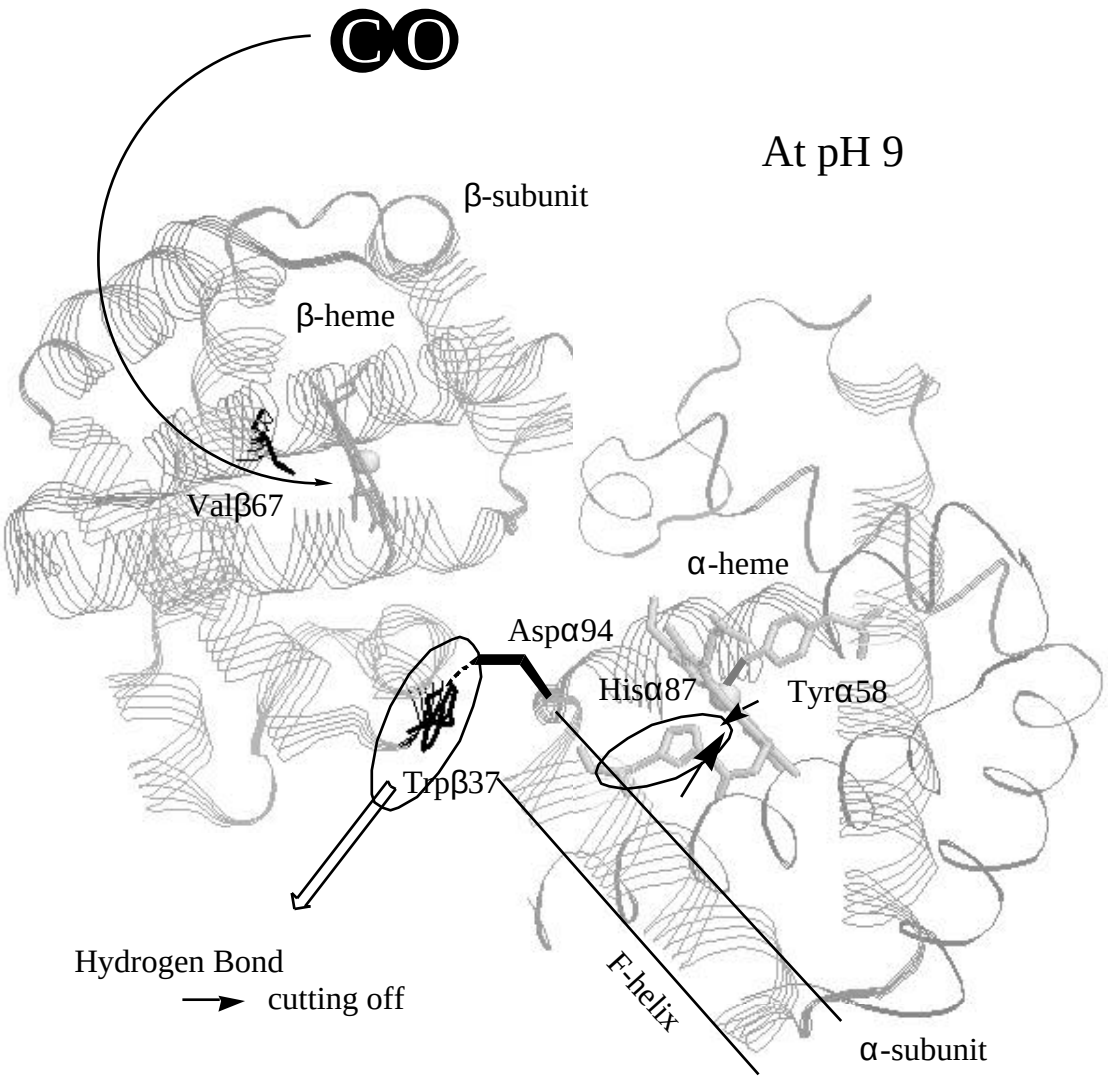

Figure 4.8 : Main chain arrangements in the α- and β subunits of deoxyHb M Boston. Important amino acid residues discussed in this paper including Tyrα58, Hisα87, Aspα94 and Trpβ37 are explicitly designated. X-ray crystallographic coordinates of the β subunit are taken from Hb A (54) but those of the α subunit are taken from the tyrosine mutant of horse myoglobin (43), registered in the Protein Data Bank and are rearranged partly. The thin broken line denotes the hydrogen bond between Trpβ37 and Aspα94, which is cleaved upon binding of CO to the β heme.

According to Perutz (6), CO binding to the α-heme pulls Fe(II) into the porphyrin plane and the F-helix of the α subunit is also pulled with the movement of the proximal His. The FG-corner of the α subunit connected to the F-helix of the α subunit has interaction with the C-helix of the β subunit through hydrogen bonds and electrostatic interactions. Trpβ37 belongs to the C-helix of the β subunit. Such a communication pathway of structural change from the α to β heme was previously suggested by Ho (53). The change in the coordination number in the α-heme of Hb M Boston would be induced by the inverse process of this, that is, the change of Trpβ37 causes finally the movement of Hisα87 of the F-helix of the α subunit. The amount of change is considered to be much smaller than that due to CO binding to the α heme in Hb A, but this small change of Hisα87 generates the 6c-hs ferric α-heme and thus EPR spectral change.

On the other hand, the UV spectral change of Tyr residues upon CO binding to the β heme of Hb M Boston is not so clear, and at least there is no change on Y7a and Y9a. This situation is similar to that in CO binding to the β heme of $\alpha_2^{Ni}\beta_2^{deoxy}$ (38) but not to that in CO binding to the β heme of $\alpha_2^{NO}\beta_2^{deoxy}$ for which the frequency shift toward R state was observed for Y9a (19). The Tyr residues which are responsible for UV Raman changes include Tyrα42, Tyrα140 and Tyrβ145 (32,38). It is highly likely that this difference arises from the local structure of distal side in the α-heme. The distal side of the α heme of $\alpha_2^{NO}\beta_2^{deoxy}$ contains a hydrogen bond between the heme-bound NO and Hisα58 (distal His). In contrast, the distal side in the α-heme of $\alpha_2^{Ni}\beta_2^{deoxy}$ involves no direct interaction between Ni and Hisα58. Hisα58 is contained in the E-helix and this residue is replaced by Tyr in the α subunit of Hb M Boston. Although Tyrα58 is coordinated to Fe(III), its ν_{CO} band was not affected by the quaternary structure change. Presumably, the E helix of the α subunit is little perturbed by binding of CO to the β heme similar to $\alpha_2^{Ni}\beta_2^{deoxy}$.

In conclusion, the α heme of Hb M Boston is influenced through the quaternary structure dependent movement of Hisα87 and as a result, the Fe(III)-O (Tyrα58) bond was weakened by binding of CO to the β heme.

4.6 Comprehensive Discussion: Similarity and Dissimilarity in the quaternary structural changes of three partially ligated Hb (NOHb, Ni-Fe Hybrid Hb, Hb M Boston)

Before detailed discussion on subject, the spectra of other Hb M are presented. Figures 4.9 and 4.10 show the UVRR spectra of Hb M Milwaukee and Hb M Iwate, respectively, together with those of HbA. There are four kinds of Hb Ms in which distal or proximal His is replaced by Tyr. In Hb M Iwate the proximal histidine (Hisα87) is replaced by tyrosine in the α subunit. Hb M Milwaukee is other kind of Hb Ms in which Valβ67 is replaced by glutamine in the β subunit. Schematic diagram for the structures of HbM Iwate, Hb M Milwaukee and Hb M Boston are given in Fig 4.11. Hb M Iwate binds ligands with the β heme only similar to Hb M Boston, while Hb M Milwaukee binds ligands with the α heme only.

The UVRR spectra of CO-bound Hb M Milwaukee at pH 7 (Figure 4.9) are similar to that of fully ligated Hb A, although intensities of Trp ands in the deoxy – minus - CO difference spectra, particularly W3, W16 and W18 bands are somewhat small and the amount of low wavenumber shifts of Tyr are also somewhat small. In the case of Hb M Milwaukee, the Fe-His bond in α heme is present. This situation is analogous to that in Ni-Fe Hybrid Hb of $\alpha^{CO}\beta^{Ni}$. In the case of $\alpha^{CO}\beta^{Ni}$, ligand binding to α heme brought about the changes of both tyrosine and tryptophan except for the condition of pH 6.7 in the presence of IHP.

The UVRR spectra of Hb M Iwate at pH 6.7 in the absence of IHP are similar to that of Hb M Boston at pH 7.1 in the absence of IHP. The characteristic feature in the spectra of Hb M Iwate is that ligand binding to β heme brings about no low wavenumber shift of Tyr bands but appreciable intensity changes of Trp bands, though in this pH condition the changes of tryptophan, especially W3, W16 and W18, are small. In the spectra of Hb M Iwate in the presence of IHP at pH 6.4 the change of tryptophan intensity is smaller. This phenomenon is observed in Hb M

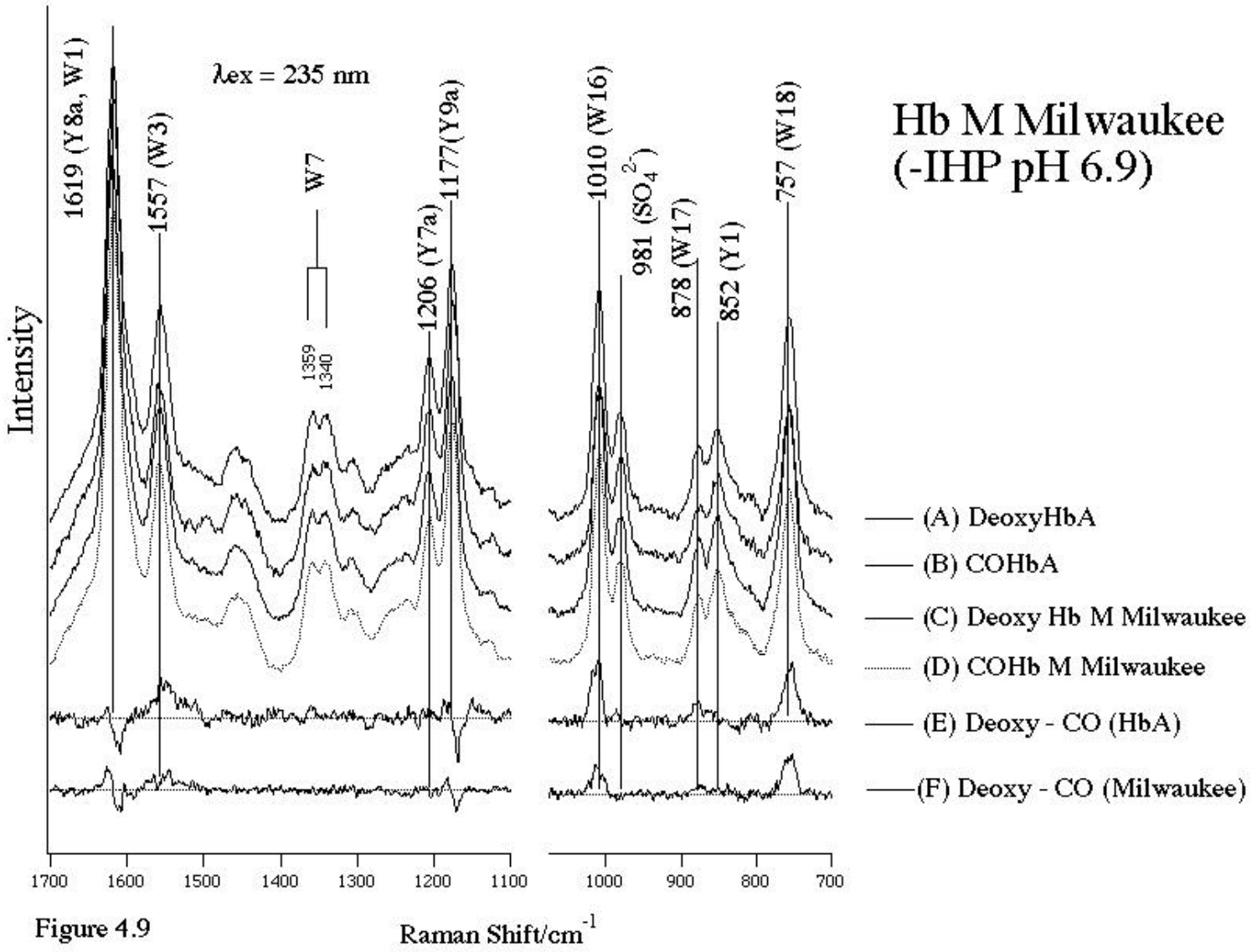

Figure 4.9

UVRR spectrum of DeoxyHbA (A) and COHbA (B) at pH 6.9 and of DeoxyHb M Milwaukee (C) and COHb M Milwaukee (D) at pH 6.9 and the difference spectra of (E) = (A) - (B) and (F) = (C) - (D).

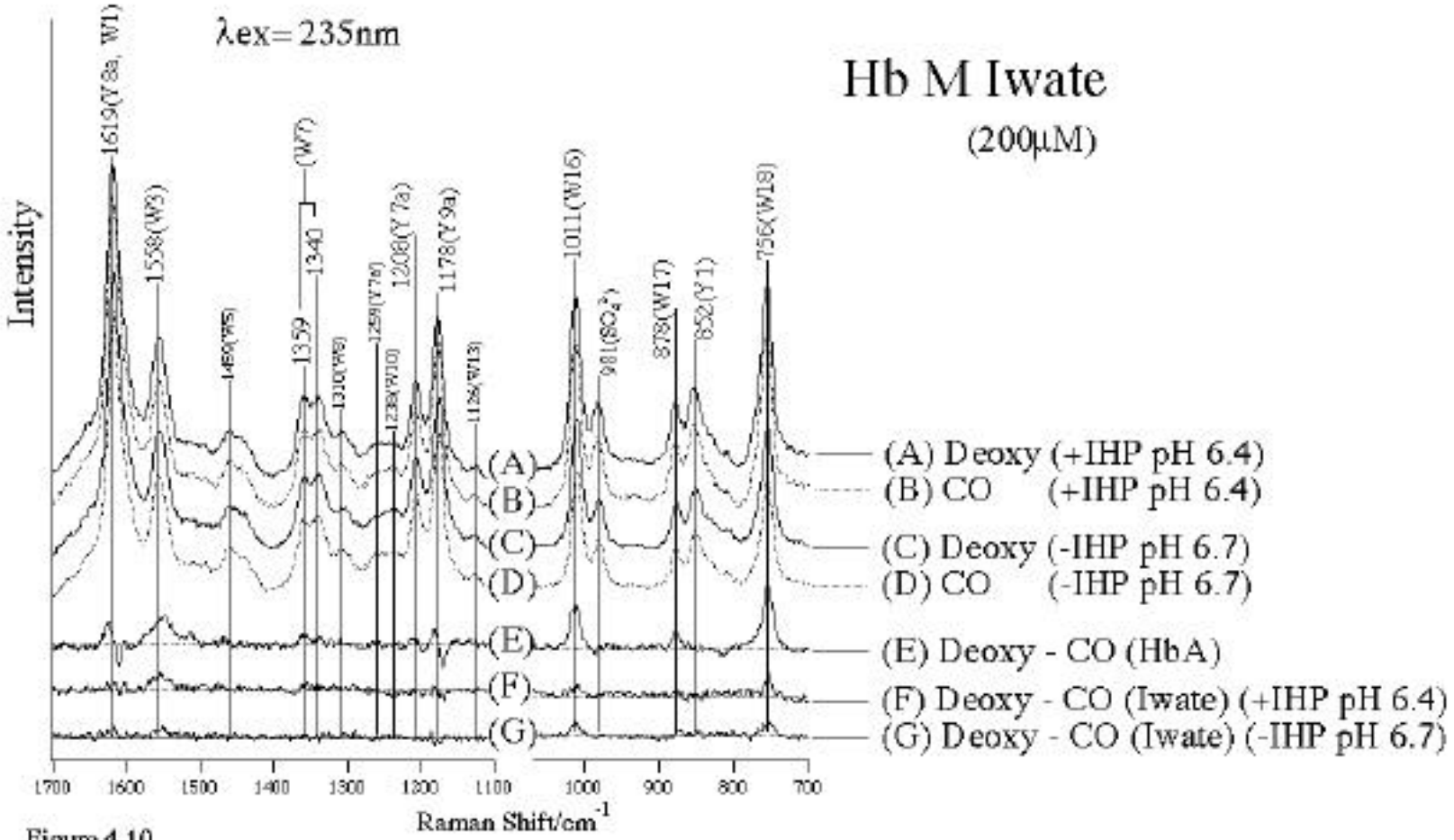

Figure 4.10

UVRR spectrum of DeoxyHb M Iwate (A) and COHb M Iwate (B) at pH 6.4 in the presence of IHP and of DeoxyHb M Iwate (C) and COHb M Iwate (D) at pH 6.4 in the absence of IHP and the difference spectra of (E) = DeoxyHbA - COHbA (pH 6.7), (F) = (A) - (B) and (G) = (C) - (D).

Boston at pH 6.4 in the presence of IHP (Figure 4.12). This situation is also analogous to Ni-Fe Hybrid Hb of $\alpha^{Ni}\beta^{CO}$. At lower pH (pH=6.7, 7.2) ligand binding to β heme brings about the intensity change of tryptophan bands. At pH 9 the low frequency shifts of tyrosine bands are observed, though in Hb M Boston at pH 9 lower shifts of tyrosine bands are somewhat obscure regarding Y9a, Y7a bands. Thus the behaviors of Hb M (Iwate, Boston, Milwaukee) and Ni-Fe hybrid Hb upon ligand binding to heme are very alike.

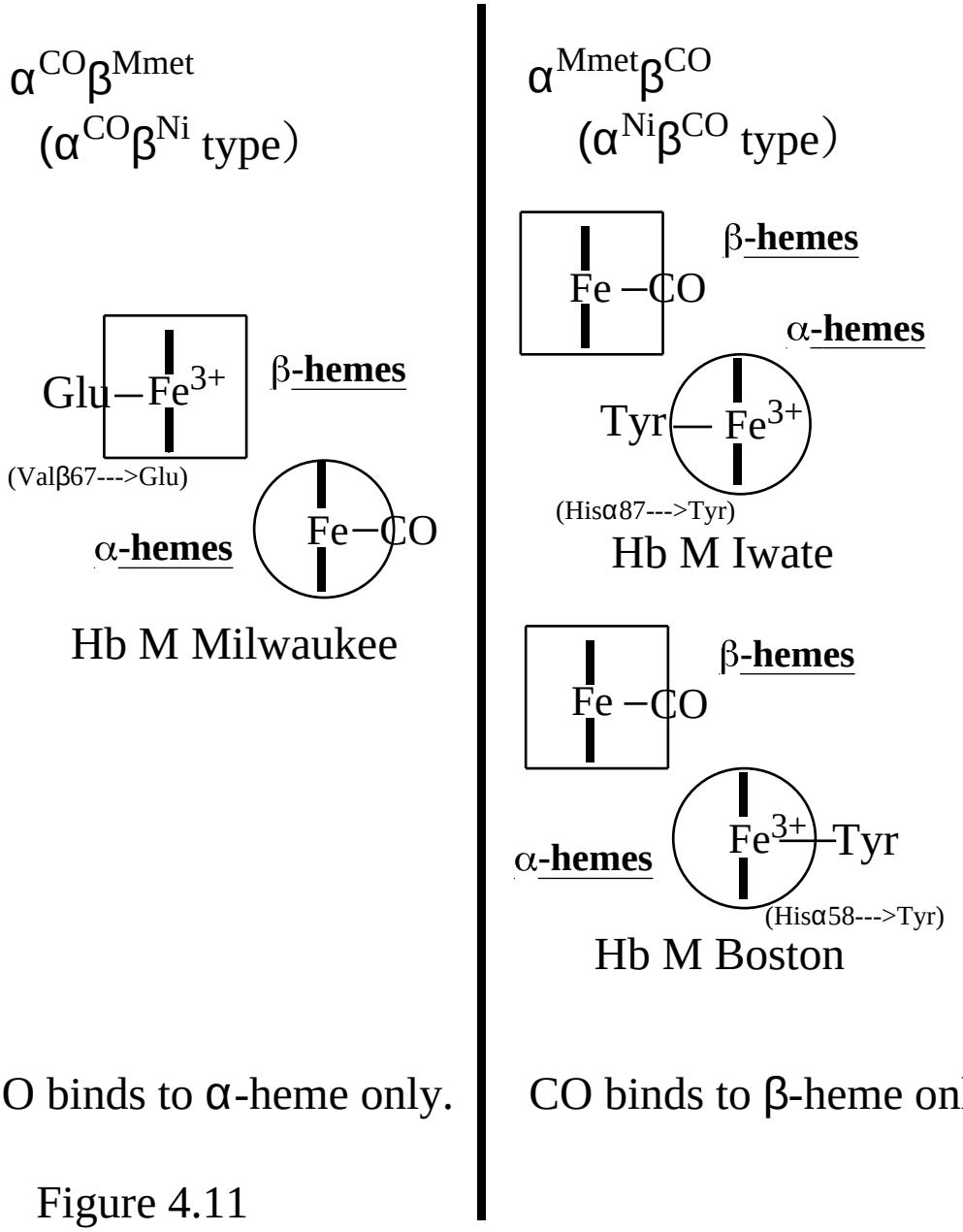

Figure 4.11

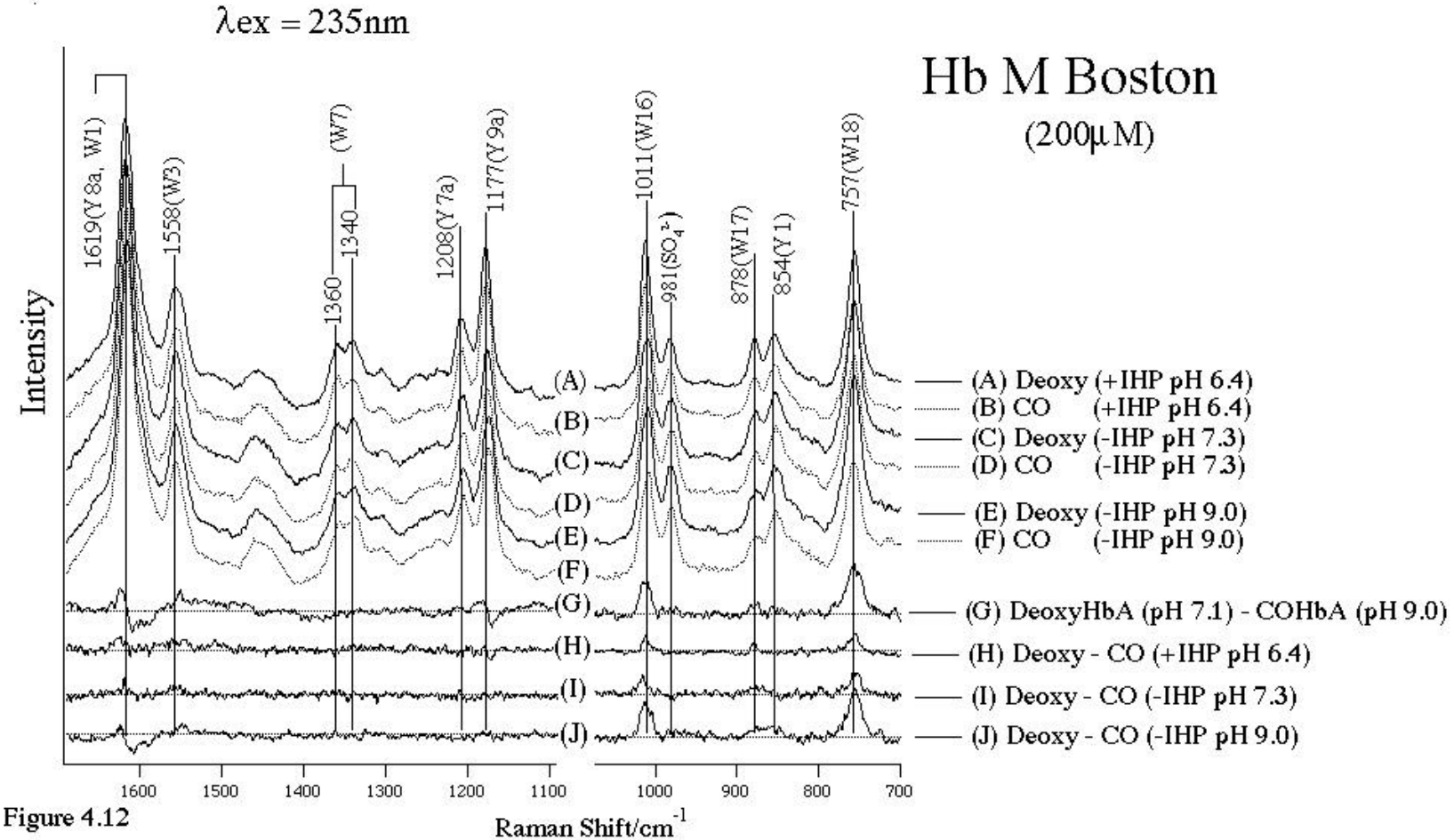

Figure 4.12

UVRR spectrum of DeoxyHb M Boston (A) and COHb M Boston (B) at pH 6.4 in the presence of IHP, of DeoxyHb M Boston (C) and COHb M Boston (D) at pH 7.3 in the absence of IHP and of DeoxyHb M Boston (E) and COHb M Boston (F) at pH 9.0 in the absence of IHP and the difference spectra of (G) = DeoxyHbA (pH 7.3) - COHbA (pH 9.0), (H) = (A) - (B), (I) = (C) - (D) and (J) = (E) - (F).

In the case of $\alpha^{NO}\beta^{deoxy}$, this type of binding to the α heme is apparently similar to $\alpha^{CO}\beta^{Ni}$. However, as pH is higher, the change of tryptophan and tyrosine bands in $\alpha^{CO}\beta^{Ni}$ occurs. In contrast, the changes of tryptophan and tyrosine bands in $\alpha^{NO}\beta^{deoxy}$ occur at neither lower pH (pH=5.5) nor higher pH (pH=8.8). In CHAPTER 3 and 4 it was pointed out that the coordination ability of NO is different from that of CO. The α-heme in $\alpha^{NO}\beta^{deoxy}$ adopts six-coordination at higher pH and this means the existence of the Fe-His bond. However, the Fe-His bond in the α heme might be was too weak to influence the F-helix in α-heme across the Fe-His bond. This point of $\alpha^{NO}\beta^{deoxy}$ is different from the cases of $\alpha^{CO}\beta^{Ni}$ and Hb M Milwaukee.

By the way, when we consider that $\alpha^{NO}\beta^{deoxy}$ is close to Hb such as $\alpha^{Ni}\beta^{deoxy}$, and Hb M Iwate and HbM Boston in which CO binds to β-heme, it would be worth to compare the change of CO binding to β-heme in $\alpha^{Ni}\beta^{Fe\text{-}deoxy}$ and Hb M Iwate and HbM Boston with that in $\alpha^{NO}\beta^{deoxy}$. In CHAPTER 3 and 4, the changes of tryptophan only were observed at lower pH and the low wavenumber shifts of tyrosine were observed at higher pH (pH = 9) for Hb M Iwate, HbM Boston and $\alpha^{Ni}\beta^{CO}$, although the low wavenumber shift is somewhat small. However, for $\alpha^{NO}\beta^{CO}$ the change of tryptophan and the low wavenumber shift of tyrosine were observed simultaneously at pH 5.5 in the presence of IHP. This point of $\alpha^{NO}\beta^{deoxy}$, especially the existence of the change of tyrosine, is different from other three ($\alpha^{Ni}\beta^{deoxy}$, and Hb M Iwate and HbM Boston) Hbs. Of course, at higher pH both change of tryptophan and tyrosine occurred in $\alpha^{NO}\beta^{NO}$. This suggests that quaternary structural change accompanied with CO (NO) binding to β-heme depends on the coordination state in α-heme. In the case of $\alpha^{NO}\beta^{NO}$, NO occupies the sixth coordination site in α-heme. There is no such a small molecule as NO in $\alpha^{Ni}\beta^{CO}$ and Hb M Iwate and Hb M Boston. As described in CHAPTER 3, the network involving distal histidine such as Fe-NO---His has a close connection with the change of tyrosine. In CHAPTER 4 the low wavenumber shift of tyrosine

band (Y8a) was observed for Hb M Boston at pH 9, though those of Y7a and Y9a are very small. This change of Hb M Boston at pH 9 might be caused by the increase of coordination number in α-heme, namely partial formation of proximal His-Fe bond, which was suggested from measurements of α-heme by visible resonance Raman spectroscopy. If this phenomenon occurs to $\alpha^{NO}\beta^{NO}$ at lower pH (pH 5.5), movement of Fe through the proximal His-Fe bond might move to E-helix through Fe-NO---distal His (E-helix) and causes the change of Tyrα42 through changes of C-helix from E-helix. Although it is practically difficult to pursue such a path which influences the environment of tyrosine (Tyrα42 and/or Tyrα140), it is likely that the change of tyrosine on CO binding to β-heme depends on the existence of the network involving distal histidine such as Fe-NO---His.

In conclusion the change of tryptophan and tyrosine accompanied by quaternary structural change due to ligand (CO) binding to α-heme or β-heme can be summarized in the following way. CO binding to α-heme causes a change of both tryptophan and tyrosine and the changes do not depend on the state of β-heme. On the other hand, CO binding to β-heme causes a change of tryptophan only basically, but the change of tyrosine strongly depends on the state of α-heme such as the case of Fe-NO---His. This suggests CO binding to α-heme than β-heme influences quaternary structural change more strongly

Acknowledgments

We thank Dr. R.Jagenburg for his courtesy of giving us blood containing Hb M Boston.

References

1. Hayashi, N., Motokawa, Y., Kikuchi, G. (1966*) J. Biol. Chem. 241,* 79-84.

2. Suzuki, T., Hayashi, A., Yamamura, Y., Enoki, Y., and Tyuma, I. (1965*) Biochem. Biophys. Res. Commun.* 19, 691-695.

3. Suzuki, T., Hayashi, A., Shimizu, A., and Yamamura, Y. (1966*) Biochim. Biophys. Acta 127,* 280-282.

4. Ranney, H.M., Nagel , R.L., Heller, P, and Udem, L. (1968) *Biochim. Biophys. Acta 160,* 112-115.

5. Monod, J., Wyman, J., and Changeux, J. P. (1965) *J. Mol. Biol. 12,* 88-118.

6. Perutz, M. F. (1970) *Nature 228,* 726-739.

7 Perutz, M. F., Fermi, G., and Luisi, B., Shaanan, B., and Liddington, R. C. (1987) *Acc.Chem.Res. 20,* 309-321.

8. Baldwin, J., and Chothia, C. (1979) *J.Mol.Biol. 129,* 175-220.

9. Inubushi, T., Ikeda-Saito, M., and Yonetani, T. (1983) *Biochemistry 22,* 2904-2907.

10. Hayashi, A. Suzuki, T., Shimizu, A., Morimoto, H., and Watari, H. (1967) *Biochim. Biophys. Acta 147,* 407-409.

11. Fung, L.W.-M., Minton, A.P., Ho, C. (1976) *Proc. Natl. Acad. Sci. U.S.A. 73,* 1581-1585.

12. Fung, L.W.-M., Minton, A.P, Lindstrom, T.R., Pisciotta A.V., and Ho, C. (1977) *Biochemistry 16,* 1452-1462.

13. Nagai, M., Kaminaka, S, Ohba, Y, Nagai, Y, Mizutani, Y., and Kitagawa, T. (1995) *J.Biol.Chem., 270,* 1636-1642.

14. Nishikura, K, Sugita, Y., Nagai, M., and Yoneyama, Y. (1975*) J. Biol. Chem. 250,* 6679-6685.

15. Nagai, K., and Hori, H. (1978) *FEBS Lett. 93,* 275-277.

16. Kaminaka, S., and Kitagawa, T. (1992) *Appl.Spectrosc., 46,* 1804-1808

17. Kaminaka, S., and Kitagawa, T. (1995) *Appl. Spectrosc. 49,* 685-687.

18. Song, S., and Asher, S. A. (1991) *Biochemistry 30,* 1199-1205.

19. Nagatomo, S., Nagai, M., Tsuneshige, A., Yonetani, T., and Kitagawa, T. (1999) *Biochemistry 38,* 9659-9666.

20. Sugita, Y., and Yoneyama, Y. (1971*) J. Biol. Chem. 246,* 389-394.

21. Nagai, K., Kagimoto, T., Hayashi, A., Taketa, F. and T. Kitagawa, T. (1983) *Biochemistry 22,* 1305-1311.

22. Spiro T.G., Stong, J.D., Srein, P. (1979*) J. Am. Chem. Soc. 101,* 2648-2655.

23. Teraoka, J., and Kitagawa, T. (1980*) J. Phys. Chem. 84,* 1928-1935.

24. Ozaki, Y., Iriyama, K., Ogoshi, H., Ochiai, T., Kitagawa, T. (1986*) J. Phys. Chem. 90,* 6105-6112.

25. Hu, S., Smith, K.M., Spiro, T.G. (1996*) J. Am. Chem. Soc. 118,* 12638-12646.

26. Nagai, M., Yoneyama, Y., and Kitagawa, T. (1989) *Biochemistry 28,* 2418-2422.

27. Harada, I., Miura, T., and Takeuchi, H. (1986) *Spectrochim.Acta, 42A,* 307-312.

28. Dudik, J. M., Johnson, C. R., and Asher, S. A. (1985) *J.Chem.Phys., 82,* 1732-1740.

29. Miura, T., Takeuchi, H., and Harada, I. (1988) *Biochemistry, 27,* 88-94.

30. Miura, T., Takeuchi, H., and Harada, I. (1989) *J.Ranan Spectrosc., 20,* 667-671.

31. Dick, L.A., Heibel, G., Moore, E.G., and Spiro, T.G. (1999) *Biochemistry 38,* 6406-6410.

32. Nagai, M., Wajcman, H., Lahary, A., Nakatsukasa, T., Nagatomo, S., and Kitagawa, T. (1999) *Biochemistry, 38,* 1243-1251.

33. Perutz, M.F., Ladner, J.E., Simon, S.R., Ho, C. (1974) *Biochemistry 13,* 2163-2173.

34. Perutz, M.F, Fersht, A.R., Simon, S.R, and Roberts G.C.K. (1974) *Biochemistry 13,* 2174-2186.

35. Li, R., Nagai, Y., and Nagai, M. (2000*) Chirality 12,* 216-220.

36. Rodgers, K. R., Su, C., Subramaniam, S., and Spiro, T. G. (1992) *J.Am.Chem.Soc., 114,* 3697-3709.

37. Nagai, M., Imai, K., Kaminaka, S, Mizutani, Y., and Kitagawa, T. (1996) *J. Mol. Struct., 379,* 65-75.

38. Nagatomo, S., Nagai, M., Shibayama, N., and Kitagawa, T. (2002) *Biochemistry, 41***,** 10010 –10020.

39. Boffi, A., Das T.K., della Longa, S., Spagnuolo, C., and Rousseau, D.L. (1999) *Biophysical Journal 77,* 1143-1149.

40. Mizuhashi, S. (1969) *J. Phys. Soc. Japan 26,* 468-492.

41. Kotani, M. (1963) *Rev. Mod. Phys. 35,* 717-720.

42. Palmer, G. in The Porphyrins (Dolphin, D., Ed.) Vol. IV, p 313-354, Academic Press, New York, 1979.

43. Maurus, R., Bogumil, R., Luo, Y., Tang, H.-L., Smith, M., Mauk, A.G., Brayer, G.D. (1994*) J. Biol. Chem. 269,* 12606-12610.

44. Pulsinelli, P.D., Perutz, M.F., Nagel, R.L (1973) *Proc. Natl. Acad. Sci. U.S.A. 70,* 3870-3874.

45. Torii, K., and Ogura, Y. (1969*) J. Biochem. 65,* 825-827.

46. Hayashi, A. Shimizu, A., Yamamura, Y., and Watari, H. (1965*) Biochim. Biophys. Acta 102,* 626-628.

47. Tang, H.-L., Chance, B., Mauk, A.G., Powers, L.S., Reddy, K.S., and Smith, M. (1994) *Biochim. Biophys. Acta 1206,* 90-96.

48. Egeberg, K.D., Springer, B.A., Martinis, S.A., Sligar, S.G., Morikis, D., and Champion, P.M. (1990*) Biochemistry 29,* 9783-9791.

49. Hoard, J.L., Hamor, M.J., Hamor, T.A., and Caughey, W. S. (1965*) J. Am. Chem. Soc. 87,* 2312-2319.

50. Reid III, T.J., Murthy, M.R.N., Sicignano A., Tanaka, N., Musick, W.D.L., and Rossmann, M.G. (1981) *Proc. Natl. Acad. Sci. U.S.A. 78,* 4761-4771.

51. Fita, I., Silva, A.M., Murthy, M.R.N., and Rossmann, M.G. (1986) *Acta Crystallogr. Sec. B 42,* 497-515.

52 Fita, I., and Rossmann, M.G. (1985*) J. Mol. Biol. 185,* 21-37.

53. Ho, C. (1992*) Adv. Protein Chem. 43,* 152-312.

54. Fermi, G., Perutz, M.F., Shaanan B., and Fourme R. (1984*) J. Mol. Biol. 175,* 159-174.

Part II

CHAPTER 5

Resonance Raman Revisit to Influences of Strong Allosteric Effectors, on Quaternary Structure Changes of Hemoglobin

Paper in preparation

S. Nagatomo, M. Nagai, Y. Mizutani, T. Yonetani, and T. Kitagawa

5.1 Abstract

A strong allosteric effector, bezafibrate (BZF), seems to remove cooperativity in oxygen binding of Hb A in the low affinity limit, but the ^{1}H NMR spectrum of the fully liganded form exhibits the pattern of the R quaternary structure. To elucidate the apparent discrepancy, the quaternary structure change of Hb A has been investigated in the presence and absence of allosteric effectors including 2,3-bisphospho-glycerate (BPG), inositol(hexakis)phosphate (IHP), and BZF, with static and time-resolved resonance Raman (RR) spectroscopy. The quaternary structure sensitive Fe-His stretching ($\nu_{Fe\text{-}His}$) band and the UVRR bands arising from the α1-β2 subunit interface examined as function of the number (*m*) of CO molecules bound to Hb, in which the *m* number was varied by a pump laser power for photodissociation and monitored with the intensity of the ν_4 band. The results indicated that an allosteric effector influences the static structures of neither deoxy nor liganded forms but affects switching point and transition rate between the T and R quaternary structures. The $\nu_{Fe\text{-}His}$ frequency of a transient at 13 μs following CO photolysis in the presence of BZF at pH 6.4 was lower by 5 cm^{-1} than that in its absence under the conditions of 30% photodissociation. The frequency shift at the same delay time became larger with increase of photodissociation (with a higher power of pump laser). The R to T structural change was completed at 4 μs in the presence of BZF at pH 6.4 even if photodissociation was as small as 12%,

---

Footnotes

Abbreviations used are; Hb A, hemoglobin A; Mb, myoglobin; COHb A, carbonmonoxy hemoglobin A; COMb, carbonmonoxy myoglobin; BPG, 2,3-bisphospho-glycerate; IHP, inositol(hexakis)phosphate; BZF, bezafibrate; RR, resonance Raman; UVRR, ultraviolet resonance Raman;

but in its absence at pH 8.8, it was not completed at 13 μs even under increased photodissociation (30%). The present results suggest that the switching point between the T and R structures exists between the *m* numbers of 3 and 4 in the presence of BZF and IHP at pH 6.4 but between 2 and 3 in the absence of any effectors at pH 9. Thus, the apparent no cooperativity and the appearance of the R type ^{1}H NMR signal for the fully liganded form can be satisfactorily interpreted in the framework of two state model.

5.2 Introduction

Human hemoglobin A (Hb A) with $\alpha_2\beta_2$ tetramer structure, exhibiting positive cooperativity in oxygen binding, has been extensively investigated with various methods, since it serves as a basic model for general allosteric proteins (1) and currently, elucidation of a structural mechanism of cooperativity is a major subject of Hb studies. X-ray crystallographic studies have demonstrated the presence of two distinct quaternary structures, called T (tense) and R (relaxed) structures, which correspond to the low- and high-affinity states, respectively, and whose typical structures are seen for the deoxy and CO-bound forms of Hb A, respectively (2). The cooperative oxygen binding of Hb has been explained in terms of a reversible transition between the two quaternary structures, switching of which takes place at a certain number of bound ligands (3,4). However, recent more extensive examinations under various pH conditions in the presence of various allosteric effectors stressed importance of the tertiary structure change for oxygen binding rather than the quaternary structure (5), demonstrating that the T/R two state model is applicable only to limited conditions like stripped Hb, but not to general solution conditions containing various allosteric effectors including 2,3-bisphosphoglycerate (BPG), inositol(hexakis)phosphate (IHP), and bezafibrate (BZF) at wide range of pH. Phosphate ions of BPG and IHP are practically working in animal red cells to adjust oxygen affinity, while BZF is widely used to take care of high fat diseases.

These effectors do not affect oxygen affinity of proteins like myoglobin or isolated chains of Hb A. Thus, some specific subunits contacts are indispensable for these effectors to alter oxygen affinity of Hb even if the tertiary structure is essential to oxygen affinity. In the case of the simple two state model, X-ray crystallographic analysis (6) indicated that the largest structural differences between the T and R structures are present at the $\alpha 1$-$\beta 2$ subunit interface, where resets of hydrogen bonds and salt-bridges take place upon ligand binding to deoxyHb. The ^{1}H NMR signal of Tyrα42, which forms a hydrogen bond with Aspβ99 in the T state and thus yields a well defined peak but is free in the R state and therefore apparently disappears due to rapid exchanges, has served as a diagnostic marker for the quaternary structure (7,8). However, Yonetani et al. (5) observed the disappearance of the ^{1}H NMR signal for the fully liganded Hb A in the presence of BZF despite the fact that HbA in this solution condition exhibits extremely low oxygen affinity and no cooperativity and seems to be frozen in the T state even after fully liganded state. It is also found recently (9) that BZF binds to the globin near E-helix of the α subunit, which is distinct from the binding sites of IHP and BPG, which are known to bind at the $\beta_1 \cdots \beta_2$ subunit interface. Therefore, it became a fundamental problem to reexamine the relations among the quaternary structure, tertiary structure, oxygen affinity and cooperativity.

The practical question to be answered is whether the ordinary quaternary structure change occurs to Hb A in the presence of BZF and IHP at pH 6.4 in the process of oxygen binding. If the fully liganded form adopts the R structure as indicated by the ^{1}H NMR study but its oxygen binding is hardly cooperative (=1.3), then a quaternary structure would not be directly related with the oxygen affinity and its change may not be essential to cooperativity. This would lead to overthrow the established interpretation of Hb cooperativity. It is in general agreement that the strain in the Fe-His bond, monitored by visible RR spectroscopy, is one of main factors to determine the oxygen affinity (10) and that some changes at the subunit contacts are essential for appearance of cooperativity (3,11,12). The globin structures in the T and R states of Hb A can be

diagnosed by vibrational spectra of the interacting residues which are monitored by UV resonance Raman spectroscopy (13,14). Therefore, to explore structural influences of strong allosteric effectors, we revisited the quaternary structure changes of Hb A upon ligand dissociation with the new techniques of RR spectroscopy. Here we focused on intermediately ligand bound states ($m \neq 0$ or 4), which are practically difficult with ordinary static techniques. Quaternary structures of the intermediately ligand bound states can be explored with dynamical techniques like time-resolved measurements of the Fe-His stretching ($\nu_{Fe\text{-}His}$) RR band upon photolysis of CO, in which the m number after photolysis can be varied by variation of a laser power.

5.3 Experimental Procedures

Sample Preparation

HbA was purified from fresh human blood by a preparative isoelectric focusing electrophoresis (15). Approximately 150 μL of the 200 μM (in terms of heme) Hb A solution was put into a spinning cell made of a synthetic quartz EPR tube (diameter = 5 mm) (16). DeoxyHb and COHb were prepared by adding sodium dithionite (1 mg/mL) to oxyHb after replacement of the inside air of the sample tube with N_2 and CO, respectively. Five typical conditions of solvents as characterized in Table 1 were selected to compare; (I) pH 9, no effector, (II) pH 7.4, 5 mM BPG, (III) pH 6.4, 5 mM BZF, (IV) pH 6.4, 5 mM IHP, (V) pH 6.6, 1 mM BZF and 5 mM IHP. Influences of an allosteric effector are expected to become stronger as proceeding from condition (I) to (V). Solvents used were HEPES buffer for the pH range from 6.4 to 9 and a pH value in the presence of a selected allosteric effector was determined with a pH meter (BECKMAN Φ720 pH Meter).

Table 5.1 Solution Conditions Oxygen affinity and Cooperativity

Number	Solution Conditions	K_T/torr^{-1}	K_R/torr^{-1}	n_{max}
(I)	pH 9, no effector	0.25	10	2.5
(II)	pH 7.4, 5mM BPG	0.04	8	3.0
(III)	pH 6.4, 5mM BZF	0.016	0.8	2.1
(IV)	pH 6.4, 5mM IHP	0.008	0.16	1.9
(V)	pH 6.6, 1mM BZF + 5mM IHP	0.006	0.02	1.3

The value of K_T, K_R and Hill coefficient were adopted by ref.(5).

$n_{\max}$: Hill coefficient

$$K = \frac{[HbO_2]}{[Hb][O_2]}$$

*Visible Resonance Raman Measurement*s

Visible resonance Raman spectra were excited with the 441.6 nm line of a He/Cd laser (Kimmon electrics, Model KR1801C) and detected with a liquid nitrogen-cooled charge coupled device (CCD, Princeton instruments, Model LN/CCD-1100-PB) attached to a home-designed 100 cm single polychromator (Ritsu Oyo Kogaku, Model MC-100DG) (17). The slit-width and slit-height were set to be 200 μm and 20 mm, respectively. The corresponding spectral slit-width is 8 cm^{-1} and the wavenumber-width per one channel of the detector was 0.7 cm^{-1}. The laser power used was 5.4 mW for deoxyHb and 0.2 ~ 2.0 mW for COHb at the sample point for steady state measurements. The fully deoxy state was measured with a constant rate (1000 rpm) spinning cell at an ambient temperature, while intermediately liganded states of COHb were measured with a variable rate (180, 600, and 1800 rpm) spinning cell. Raman shifts were calibrated with indene or carbon tetrachloride, and the accuracy of the peak position of well defined Raman bands was ±1 cm^{-1}.

Ultraviolet Resonance Raman Measurements

UVRR spectra were excited by a XeCl excimer laser-pumped dye laser (Lambda Physik, Model, LPX120I and SCANMATE). The 308 nm line from the XeCl excimer laser (operated at 100 Hz) served as a pump to excite coumarine-480 in the dye laser, and its 470 nm output was frequency-doubled with a β-BaB_2O_4 crystal to generate 235 nm pulses. Details of the measurement system were described separately (18).

Time Resolved Resonance Raman Measurements (for R-structure of COHbA)

Picosecond time-resolved RR spectra were obtained using a homemade pump/probe system, in which wavelengths of the probe and pump beams were set to be 442 and 540 nm, respectively. Details of apparatus are described previously (19,20).

5.4 Results

Figure 5.1 shows the 441.6 nm excited RR spectra of deoxyHb A in the presence of 0.5 mM BZF and 2 mM IHP at pH 6.3 (A), 5 mM BZF at pH 6.3 (B), 2 mM BPG at pH 7.5 (C) and no effector at pH 8.9 (D). The oxygen affinity becomes higher by a factor of 50 within the category of T as going from (A) to (D). Nevertheless, the four RR spectra were closely alike. If the strain exerted by a globin on a heme is larger in the case of low affinity extreme, the Fe-histidine (F8) bond should involve the strain and its stretching frequency should become lower. Unexpectedly, the quaternary structure sensitive Fe-histidine stretching mode ($\nu_{Fe\text{-}His}$) observed around 215 cm^{-1} exhibits only 0.7 cm^{-1} difference. The value of $\nu_{Fe\text{-}His}$ (215.1 cm^{-1}) for (A) is typical among the T-state deoxy Hb A (23), indicating that even the strongest allosteric effector, BZF, hardly changes the heme structure of deoxyHb. The vibrations involving the vinyl bending mode around 429 and 401 cm^{-1} and propionate bending mode around 363 cm^{-1}, the assignments of which are based on Spiro and coworkers (21,22), yield practically the same frequencies for the four different conditions, meaning that the side-chain geometry is little altered by the allosteric effectors.

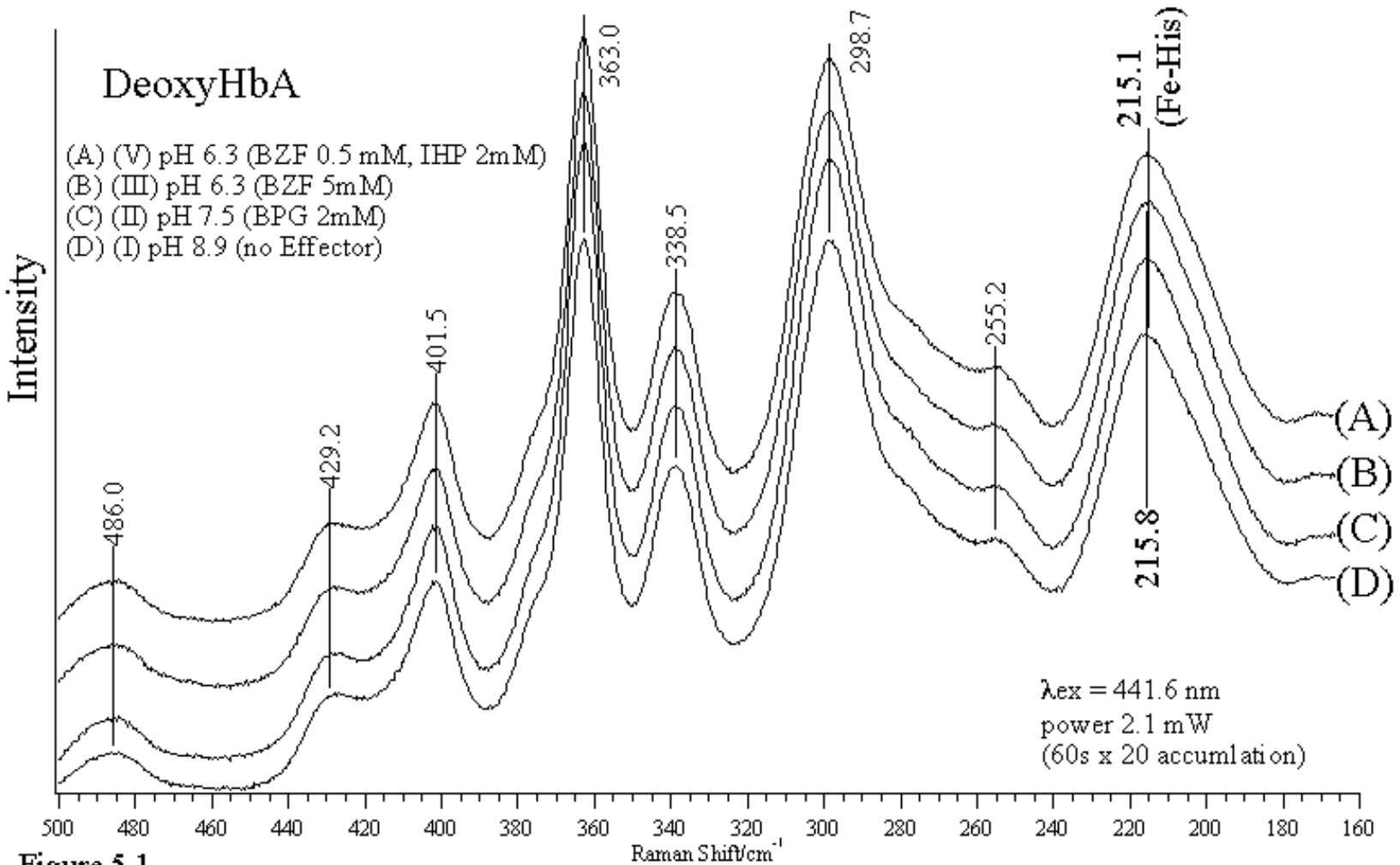

Figure 5.1 The 441.6-nm excited RR spectra of deoxyHb at pH 6.3 (BZF 0.5 mM and IHP 2 mM) (A), at pH 6.3 (BZF 5mM) (B), at pH 7.5 (BPG 2 mM) and at pH 8.9 (no effector). All samples are equilibrated with 0.05 M HEPES buffer, containing 0.1 M Na_2SO_4, and protein concentrations were 200 μM in heme. Laser power at the sample point was 2.1 mW and the spectra are sum of 20 exposures of 60 s.

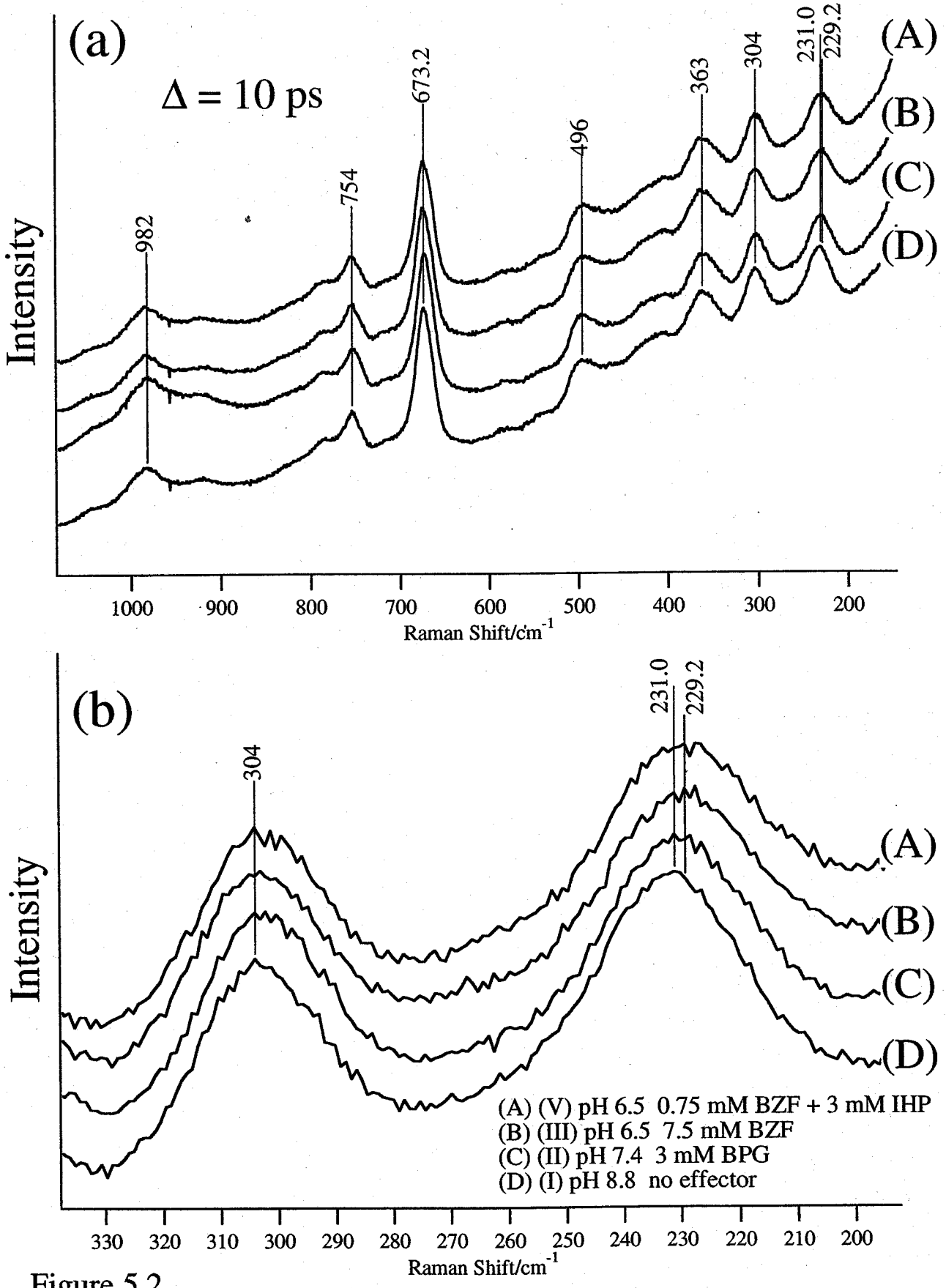

Figure 5.2

The 442-nm excited RR spectra at 10 ps after photodissociation of COHb upon pumping at 540 nm for the solution conditions of pH 6.5 with 0.75 mM BZF and 3 mM IHP (A), pH 6.5 with 7.5 mM BZF (B), pH 7.4 with 3 mM BPG (C), and pH 8.8 with no effectors (D). All samples are equilibrated with 0.05 M HEPES buffer, containing 0.1 M Na_2SO_4, and protein concentrations were 300 μM in heme. Panel (a) shows the spectral region between 150 and 1050 cm^{-1}, while panel (b) shows their expansion for the frequency region between 190 and 330 cm^{-1}.

Figure 5.2 shows the photodissociated transient RR spectra of COHb A observed at 10 ps following photolysis of CO, in which the pump power is adjusted to photodissociate at most 10 % of the sample in one event and the probe power is set so low that it does not cause photodissociation at all. Although the $\nu_{Fe\text{-}His}$ mode has no Raman intensity for the CO bound form, the photodissociated transient five-coordinate species exhibits time dependent intensity change. In the case of COMb, the intensity increases with time, in which 90 % of the intensity change occurs within 1 ps but the remaining 10 % in 10-20 ps (24). This intensity increase matches with the time dependence of a band center shift of the near IR CT band (25) and is considered to reflect the time dependence of the out-of-plane displacement of the Fe atom (26). On the other hand, the frequency shift of the $\nu_{Fe\text{-}His}$ mode of the transient deoxyMb takes place with a time constant of 100 ps, reflecting a tertiary structure change of globin (26) and its rate depends on the viscosity of solvent.

It is known that the relaxation of the $\nu_{Fe\text{-}His}$ frequency is extremely slow for Hb due to quaternary structure changes (27,28). Therefore, the $\nu_{Fe\text{-}His}$ frequency of the early transient species vibrational assignments are based on Harada and coworkers (21). The intensities of spectra (A,B) are normalized with the band of SO_4^{2-} ions at 982 cm^{-1}. Generally the T/R quaternary structure in the picosecond time regime is considerably higher than those for the equilibrium deoxy species, indicating the unrelaxed five-coordinate deoxy heme with the Fe atom on the porphyrin plane. Due to this feature, the RR spectra shown in Figure 5.2(A) are appreciably different from the equilibrium spectra shown in Figure 5.1 regarding individual peak frequencies and intensities. The 982 cm^{-1} band in Figure 5.2(A) appears from SO_4^{2-} ions commonly present as an internal intensity standard. The 338 cm^{-1} band in Figure 5.1, which was noted to exhibit time-dependent intensity changes for COHb after photolysis by Friedman (27), is absent in Figure 5.2(A).

The $\nu_{Fe\text{-}His}$ frequency at 10 ps after photolysis is inferred to reflect the CO-bound form and therefore, the $\nu_{Fe\text{-}His}$ spectral region is expanded in Figure 5.2(b). The transient $\nu_{Fe\text{-}His}$ frequencies of

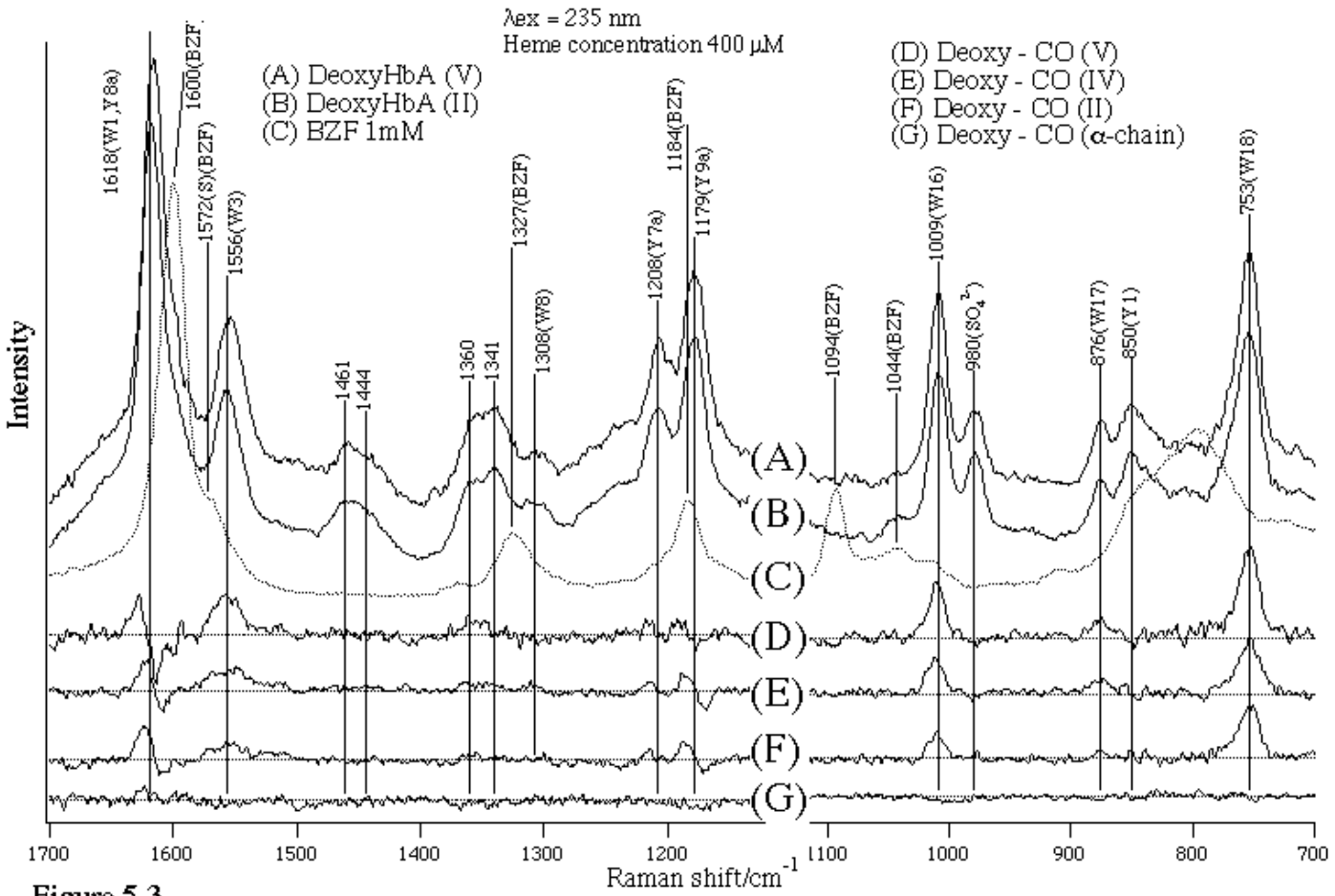

Figure 5.3

The 235-nm excited UVRR spectra of deoxyHbA at pH 6.6 with 1 mM BZF and 5 mM IHP (A), and at pH 7.5 with 5 mM BPG (B), and their deoxyHb-minus-COHb difference spectra; (D) and (F) are for A and B respectively, while (E) is the corresponding difference for the solution at pH 6.4 with 5 mM IHP and (G) denotes the corresponding difference of isolated α chain (at pH 6.7, phosphate buffer). The 235-nm excited UVRR spectrum of BZF (1 mM) in the same buffer is also included as spectrum (C). The assignments of bands are marked besides the wavenumber, in which Y and W denote the modes of Tyr and Trp residues, respectively. The band at 980 cm^{-1} arises from SO_4^{2-} ions contained as an internal intensity standard. All samples of Hb are equilibrated with 0.05 M HEPES buffer, containing 0.2 M Na_2SO_4, and the protein concentrations were 400 μM in heme.

all the four cases are, in fact, distinctly higher than those of equilibrium deoxyHb and little differ with solvent conditions; the highest is 231.0 cm^{-1} for (D) of typical R state and the lowest is 229.2 cm^{-1} for (A) of the lowest affinity extreme, while the frequency of the out-of-plane skeletal mode (γ_7) is identical among the four. Anyway, the maximum frequency difference of $\nu_{Fe\text{-}His}$ ($\Delta\nu$ = 1.8 cm^{-1}), which would be due to structural differences in the CO-bound forms, is much smaller than the general T/R frequency difference of deoxyHb (6 cm^{-1}) (18) as well as those between the unrelaxed and relaxed deoxyHbs (~15 cm^{-1}) (20). Consequently, we concluded that the heme structures of the CO-bound Hb A under these four different solvent conditions are alike.

Figure 5.3 shows the 235-nm excited UVRR spectra of deoxyHb A (A,B) under three typical solvent conditions (II,V) and the corresponding deoxy-minus-CO difference spectra (D-G). The difference spectra of (E) and (G) are deoxy-minus-CO difference spectra for the solution at pH 6.4 with 5 mM IHP (IV) and for isolated α chain (at pH 6.7, phosphate buffer), respectively. Since BZF itself gives strong UVRR bands, whose spectrum is delineated by spectrum (C), the contribution from BZF was subtracted from the spectrum observed for the condition (V) and the resultant spectrum is represented as spectrum (A). The UVRR spectra of Hb A contain mainly the bands of Trp and Tyr residues, which are designated by W and Y followed by a mode number, respectively, and the differences are sensitively indicated by the UVRR bands of W3, W7, W16, W17 and W18 of Trp resides and Y8a, Y7a, Y9a, and Y1 of Tyr residues (11-14,30-32). The difference peak intensities of spectrum (D) are larger than those of spectra (E) and (F) but the spectral patterns remain unchanged. If a quite different globin structure is generated by BZF, some bands of Tyr and Trp residues might be shifted and the spectral pattern would be altered. Since there was effectively no difference among their CO-bound forms under the conditions of II, IV, and V, these spectral differences are ascribed to the deoxy state. Accordingly, these UVRR difference spectra indicate that the T structures are of similar type but strongest for solution (V) and weakest for solution (II).

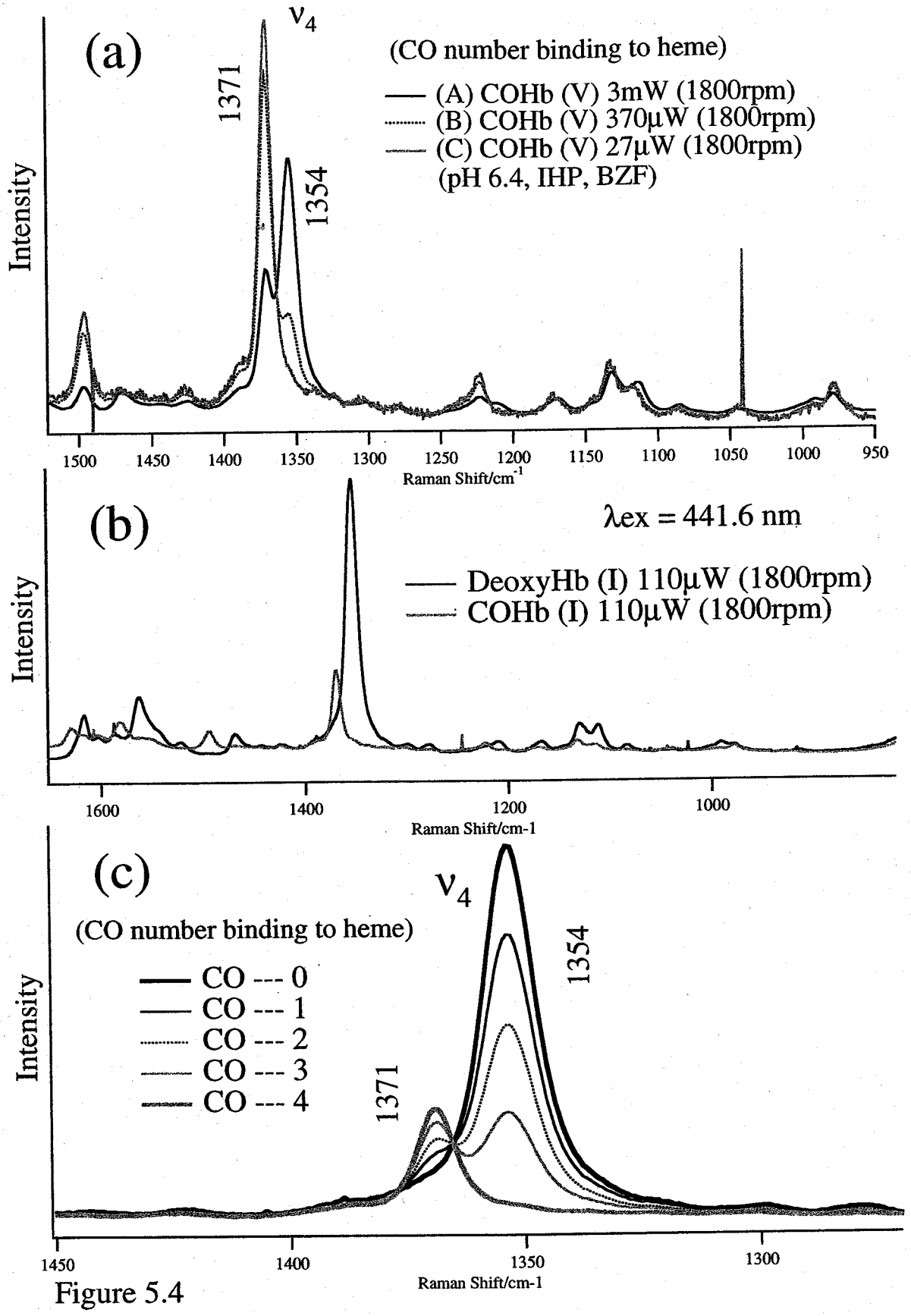

Figure 5.4

Panel (a): The 441.6-nm excited RR spectra of COHb in a steady state at pH 6.6 with 1 mM BZF and 5 mM IHP measured with a spinning cell of constant rate (1800rpm). Laser power used was 3.0, 0.37 and 0.027 mW for A, B, and C, respectively.
Panel (b): The 441.6 nm excited RR spectra of fully deoxyHbA and fully CO-bound HbA at pH 8.8 with no effector measured with a spinning cell of 1800 rpm. The two spectra were observed under the same experimental conditions with a laser power of 110 μW at the sample point. All samples are equilibrated with 0.05 M HEPES buffer, containing 0.1 M Na_2SO_4, and protein concentrations were 200 μM in heme.
Panel (c): Simulated ν_4 bands for different numbers (m = 1~4) of CO molecules bound to Hb, which were calculated from the spectra shown in the middle panel.

The amount of photodissociated species can be changed by a laser power. Here, 100% and 50% photolysis mean that the number (m) of CO molecules remaining on Hb after photolysis is 0 and 2 in average, respectively. Figure 5.4 explains how to determine the m number in the steady state experiment. In this measurement, the probe light works also as a pump light, that is, a given molecule is irradiated by laser light twice during a single stay in the laser beam, in which the first irradiation induces photodissociation of CO and the second irradiation yields a Raman spectrum. The maximum delay time of the probe light from the pump light is the residence time of a molecule in the laser beam. Since the diameter of the irradiation beam is adjusted to be 0.5 mm and velocity (v mm/s) of a given molecule can be calculated from the spinning rate (p rpm) and diameter ($2d$ mm) of the cell to be $2dp\pi/60$, the residence time is given by $0.5/v$ s. In one turn of the cell, all the photodissociated deoxyHb molecules are recombined with CO under the present pressure of CO. Since it is well established that the ν_4 band appears at 1371 and 1354 cm^{-1} for CO- and deoxy-hemes, respectively, we can monitor a proportion of photodissociated hemes from the relative area intensity of the ν_4 bands. Panel (a) displays the spectra of COHb in the solvent condition (V) observed with a spinning cell of constant rate (1800 rpm) and with different laser powers. Spectra (A) and (C) were obtained with the highest (3 mW) and the lowest (27 μW) laser powers, respectively. It is apparent that intensity of the 1354 cm^{-1} band (ν_4 band of photodissociated species) increases with increase of laser power at the expense of intensity of the 1371 cm^{-1} band (ν_4 band of CO-bound form). The intensities of 100% deoxyHb (m = 0) and 100% COHb (m = 4) excited at 441.6 nm with the present experimental conditions are delineated in panel (b). Due to closer proximity of the Raman excitation wavelength to the Soret band of the deoxy species than to that of the CO-form, the 1354 cm^{-1} band is much stronger than the 1371 cm^{-1} band. By combining the two spectra with an appropriate ratio, the expected spectra for a given average m number could be synthesized as shown by panel (c). These curves could be used as the calibration curves for determining the m number, that is, the extent of photodissociation under a laser power used.

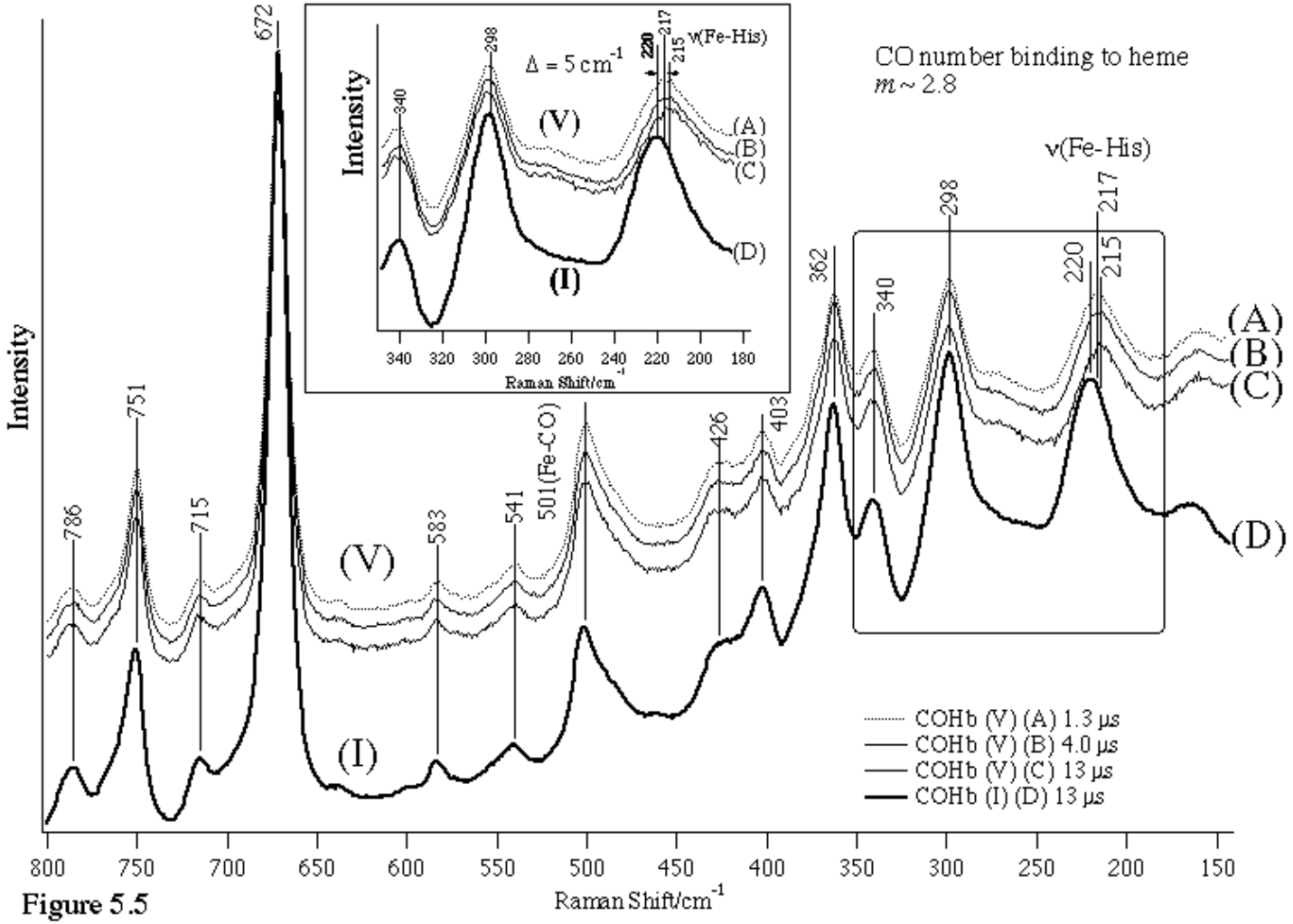

Figure 5.5

The 441.6-nm excited RR spectra of COHb for a certain fixed number of CO molecules bound to Hb under the solution conditions of (V) and (I). The spinning rate of the cell is 1800 rpm (A), 600 rpm (B), and 180 rpm (C) all for (V) and 180 rpm for (I). All samples are equilibrated with 0.05 M HEPES buffer, containing 0.1 M Na_2SO_4. Protein concentrations were 200 μM in heme.

Figure 5.5 shows the 441.6 nm excited RR spectra of COHb observed with a spinning cell of variable rates. A rate of spinning was 1800, 600, and 180 rpm for spectra (A), (B) and (C), respectively, and accordingly, the residence time of a given molecule in the laser beam was 1.3 (A), 4.0 (B) and 13 μs (C). For the spectra (A~C) shown in Figure 5.5, the *m* number was adjusted to be 2.8 under the solvent condition of V (containing 1 mM BZF and 5 mM IHP at pH 6.4). Spectrum (D) was observed for COHb for the condition (I) at pH 8.8 in the absence of any allosteric effectors with the same *m* number as those for (A~C). The overall spectral patters of (A)~(D) are alike but the $\nu_{Fe\text{-}His}$ band position is slightly different; it is 217, 215, 215 and 220 cm^{-1} for spectra (A)~(D), respectively. This part of spectra is expanded in the inset with regard to the abscissa axis. The frequency of γ_7 band at 298 cm^{-1} do not differ among the four spectra but the band positions of $\nu_{Fe\text{-}His}$ meaningfully differ among them.

Recalling that the $\nu_{Fe\text{-}His}$ frequency of transient deoxyHb at 10 ps after photolysis was 229-231 cm^{-1} in Figure 5.2, these frequencies in Figure 5.5 are fairly close to that of the static deoxyHb. However, the relaxation of the Fe-His bond may not be finished at 1.3 μs. It seems to be almost finished at 4.0 μs for the solvent condition (V), because the frequencies for 4.0 and 13 μs are identical. On the other hand, the $\nu_{Fe\text{-}His}$ frequency at 13 μs after photolysis for the solvent condition (I) is still higher than that of the static (spectrum (D) in Figure 5.1). This means that the structural relaxation is much faster for the solvent conditions (V) than for (I), presumably due to the fact that the T structure is greatly stabilized in solution (V) than in (I).

Figure 5.6 displays typical RR spectra in the $\nu_{Fe\text{-}His}$ region observed under two different solvent conditions (I and V) with different spinning rates together with the simultaneously observed spectra in the ν_4 region. It is noted that the *m* number was varied by changing the spinning rate with the constant laser power in this experiment, because the reproducibility of spinning rate is much more precise than that of a laser power. Panels (a) and (b) show the spectra observed for the solvent conditions (I) and (V), which are expected to yield the normal R and T-like quaternary

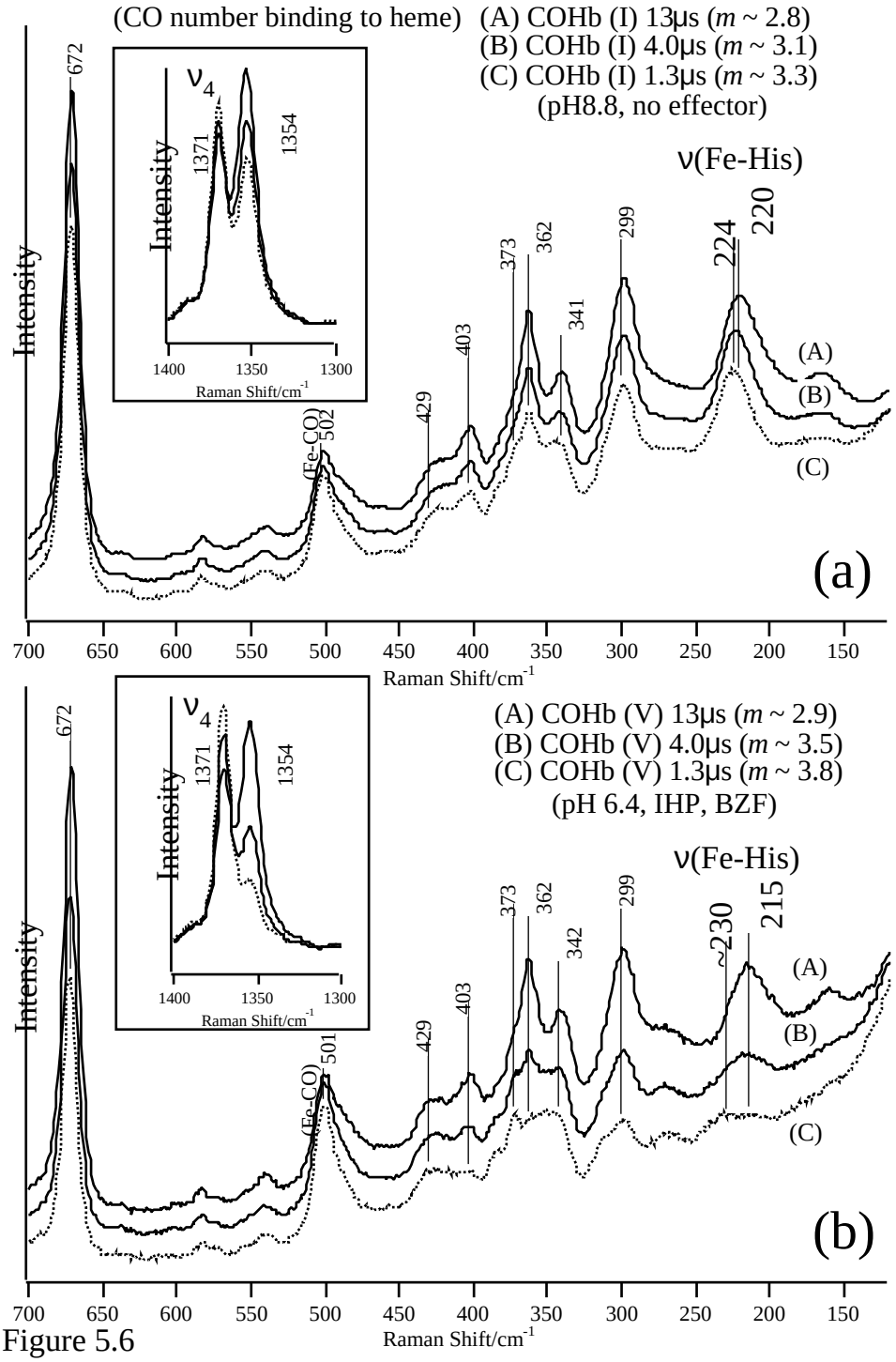

Figure 5.6

The 441.6-nm excited RR spectra of COHb in the solution conditions (I) (panel a) and (V) (panel b) observed with a fixed laser power but different spinning rates; 180 rpm (A), 600 rpm (B) and 1800 rpm (C). The inset shows the ν_4 band region observed with the same experimental conditions as those of the corresponding lower frequency region. All samples are equilibrated with 0.05 M HEPES buffer, containing 0.1 M Na_2SO_4. Protein concentrations were 200 μM in heme. The *m* numbers were calculated from the corresponding ν_4 spectra in the inset figures and Figure 5.4 (panel c).

structures in the CO-bound form, respectively. Since the *m* number and the residence time of a molecule in the laser beam are changed at the same time, discussion becomes somewhat vague, but we can compare the spectra for similar conditions.

The $\nu_{Fe\text{-}His}$ frequency becomes lower for longer residence time, but it is stressed that there is a qualitative difference between the results shown in panel (a) and (b). The $\nu_{Fe\text{-}His}$ band is clearly seen for all cases in panel (a) and the frequency little changes (from 224 to 220 cm^{-1}) as the residence time is changed from 1.3 to 13 μs. These $\nu_{Fe\text{-}His}$ frequencies are categorized into that of R deoxyHb (18). Spectral patterns of the porphyrin modes are little altered with time. Although the Fe-CO stretching mode at 502 cm^{-1} seems to exhibit somewhat broadening for smaller *m* number, this is caused by relatively larger contribution from the porphyrin band around 500 cm^{-1} upon weakening of the Fe-CO band for smaller *m* numbers. In contrast, in panel (b), the $\nu_{Fe\text{-}His}$ band is obscure in spectrum (C) and the $\nu_{Fe\text{-}His}$ frequency changes considerably (from ~230 to 215 cm^{-1}) as the residence time is changed from 1.3 to 13 μs. The intensity of the $\nu_{Fe\text{-}His}$ band also grows with time. The intensities of the $C_\beta C_c C_d$ bending mode of propionic acid side chain at 378-368 cm^{-1} and the $C_\beta C_a C_b$ bending mode of vinyl side chain at 424-405 cm^{-1} (21,22) as well as the Fe-CO stretching band at 502 cm^{-1} are different between spectra (A) and (C). When the spectra at 13 μs of the residence time are compared between the two solution conditions in Fig. 5.6, for which the *m* numbers are alike (2.8 and 2.9), their $\nu_{Fe\text{-}His}$ frequencies are different, indicating that Hb adopts the R-like deoxyHb for solution (I) but T-like deoxyHb for solution (V). In the case of solution (V), the $\nu_{Fe\text{-}His}$ frequency suggests that the Hb adopts the T quaternary structure even for $m = 3.5$, while it adopts the R structure for $m = 3.8$, for which the frequency at 1.3 μs is practically the same as that at 10 ps after photolysis (Figure 5.2(A)). It is noted that the $\nu_{Fe\text{-}His}$ band in spectrum (C) in Figure 5.6(b) seems to consist of two bands at 233 and 215 cm^{-1}, and their relative intensities appeared to change with the *m* number. This means that there are two stable quaternary structures even for COHb in solution (V) and their relative population changes with the number of CO

molecules bound to Hb. If the frequency changes are caused by the tertiary structure change, the frequency change should appear as continuous shift of a single band, but the present observation disfavors such an idea.

5.5 Discussion

Structural Influences of Allosteric Effectors

Cooperativity and oxygen affinity of Hb A changes greatly with solution conditions including the presence and absence of an allosteric effector (5,33). BPG and IHP can be regarded as more moderate effectors than BZF. Their binding sites to Hb A are different between BZF (within the α chain) and BPG (and IHP) which are between two β chains. However, the visible RR spectra reflecting the heme structure and UVRR spectra reflecting the globin structure are qualitatively categorized into a few distinct groups, that is, deoxy-T, deoxy-R, liganded-T, and liganded-R, although there are some distributions within a given group. The visible RR spectra shown in Figure 5.1, which are all deoxy-T type, indicate that allosteric effectors hardly influence the static structure of deoxy heme. It is emphasized that the low affinity extreme as seen for solution V does not involve stronger strain in the Fe-His bond.

The 10-ps transient RR spectra shown in Figure 5.2, which were obtained for average 10% photodissociation of COHb but do not contain the contribution from the remaining COHb, are deduced to reflect the structure of CO-bound form, because the relaxation time of quaternary structure is not so fast. Even for a monomer COMb, the earliest tertiary structure change of globin takes place with a time constant of 100 ps (24-26). The similarity of spectra among (A)~(D) in Figure 5.2 implies that the heme structures of transient deoxyHb in the four different solution conditions are alike. This means that structures of COHb in four different solution conditions are also alike.

The UVRR spectra shown in Figure 5.3, which contain mainly the side chain vibrations of aromatic residues, exhibit rather typical T-minus-R difference spectra for all four different solution conditions despite the fact that oxygen affinity and cooperativity are greatly different as indicated in Table 5.1; Hill coefficients for the conditions (I-V) are 2.5, 3.0, 2.1, 1.9, and 1.3. Cooperativity for the condition (V) is almost nothing (=1.3). The static UVRR spectral difference between deoxyMb and COMb is present though small, and were previously ascribed to Tyr146 (sperm whale) and Trp7 (horse and sperm whale) (34). The UVRR spectral differences between deoxyHb and COHb are ascribed to the quaternary structure changes of Tyrα42, Tyrα140, Tyrβ145 and Trpβ37 (13,14). Accordingly, the UVRR spectral changes of globin due to the tertiary structure change are distinguished from those of the quaternary structure change for Hb A. These Raman results suggest that the structures of complete deoxy- and CO-bound forms of Hb are hardly altered by the presence of allosteric effectors. This is compatible to the disappearance of the T maker band in the ^{1}H NMR spectrum that demonstrated the formation of the R quaternary structure for the fully liganded form of Hb A in the presence of BZF and IHP (5). Regarding UVRR spectra, the peak intensities in the deoxy-minus-CO difference spectra were slightly influenced by the presence of BZF and IHP as clearly demonstrated in Figure 5.3, while their spectral patterns are little altered. In addition, appreciable effects also appeared in the Fe-His stretching band in Figure 5.6, which suggested that the influences of effectors would be present in the intermediate states ($m \neq 0$ or 4) rather than the initial ($m = 0$) and final ($m = 4$) states of ligand binding.

Figure 5.5 shows the time dependence of photodissociated deoxyHb A in the presence of BZF and IHP with a certain fixed number of CO molecules bound to Hb, which is 2.8 in this case. To keep the m number constant, a laser power was changed in the measurements for different periods of illumination time. The $\nu_{Fe\text{-}His}$ frequency is 217 cm^{-1} at Δt = 1.3 μs and 215 cm^{-1} at 13 μs. This frequency difference is much smaller than that between the presence and absence of BZF and IHP at the same Δt value (13 μs), which is 5 cm^{-1} for m = 2.8. If these frequencies represent a

nearly relaxed state for *m* = 2.8, the results mean that deoxyHb stays in the T-like and R-like states in solution conditions (V) and (I), respectively. It is noted that the Fe-CO stretching band is observed at 501 cm^{-1} in common to all spectra of Figure 5.5. This means that the distal structure of globin is hardly altered in the relaxation process and also by the presence of effectors. The structural influences of the effectors seem to appear most sensitively in the Fe-histidine(F8) bond.

Since the fact that the $\nu_{Fe\text{-}His}$ frequency for *m* = 2.8 was 217 cm^{-1} at Δt = 1.3 μs means that a temporal change of the $\nu_{Fe\text{-}His}$ frequency in the time interval between Δt = 1.3 to 13 μs is relatively small, the differences in the $\nu_{Fe\text{-}His}$ frequencies obtained with a constant laser power but with different spinning rates as shown in Figure 5.6, would be attributed to differences in the *m* number. Comparison of the two spectra for Δt = 1.3 μs in the upper and lower panels of Figure 5.6 demonstrates that the $\nu_{Fe\text{-}His}$ frequency is distinctly higher for in the presence of BZF + IHP but that for Δt = 13 μs is reversed. This demonstrates that the quaternary structure of COHb differs from that of deoxyHb even in the presence of BZF and IHP. Since the *m* number and Δt are simultaneously changed in this experiment, it is difficult to determine exclusively which of them directly causes the differences in the $\nu_{Fe\text{-}His}$ frequencies of transient deoxy hemes. For the solution condition (I), the $\nu_{Fe\text{-}His}$ frequency is 224 cm^{-1} for *m* = 3.3 and 220 cm^{-1} for *m* = 2.8. These frequencies belong to the category of R type deoxyHb (18). For the solution condition (V), however, the $\nu_{Fe\text{-}His}$ frequency is 215 cm^{-1} for *m* = 3.5 and 2.9, meaning that the deoxyHb adopts the T structure for both. For Δt = 1.3 μs, the band exhibits inhomogeneous broadening due to coexistence of two kinds molecules. This suggests us that the T and R structures are coexistent for *m* = 3.8 but the T structure gains in strength for *m* = 3.5 and becomes dominant for *m*= 2.9. In other words, the dependence of T and R populations on the *m* number is distinctly different between solutions (V) and (I); it is mainly T for *m* = 3.5 in the presence of BZF and IHP (V) but is R even for *m* = 2.8 in the absence of any effectors (I).

Relation between Cooperativity and Oxygen Affinity

One of effects of allosteric effectors of Hb A is to decrease oxygen affinity (5). A binding scheme of effector molecules to Hb is not always universal. BPG and IHP decreases the oxygen affinity of the deoxy form but scarcely affects the ligand bound form. As a result, Hill coefficient increases slightly in the presence of effectors. In contrast, BZF and IHP lower the oxygen affinity of both the deoxy and ligand-bound forms and as a result Hill coefficient is almost unity. This feature may indicate that the T to R quaternary structure change does not take place upon oxygen binding, while only the tertiary structure changes (9). However, the ^{1}H NMR study demonstrated a change of spectral pattern to that of the R structure for the fully liganded Hb in the presence of BZF and IHP (5). The present Raman results are rather compatible with the ^{1}H NMR results. The subunit interface contacts as well as the heme structure for complete deoxyHb were not altered by the presence of IHP, BPG or BZF. They are of ordinary T-type. On the other hand, the contacts in the subunit interface as well as the heme structure of the fully liganded form, which were distinct from those of deoxyHb, were also hardly influenced by the presence of IHP, BPG or BZF. Judging from the $\nu_{\text{Fe-His}}$ frequency, the T to R transition takes place when the average number of bound ligands is 3.5 in the presence of BZF and IHP but below 2.8 in the absence of any allosteric effectors. This switching *m* number would depend on the molecular species of effectors. It is evident that in the case of solution condition (I) the structural relaxation has not been finished within 13 μs yet and therefore, the $\nu_{\text{Fe-His}}$ frequency at $\Delta t = 13$ μs is not exactly the same as that of the fully relaxed state and the relaxation time would also be different between the presence and absence of effectors.

The conclusion from the present experiments can be interpreted in Figure 5.7, where free energy levels for T_m and R_m are schematically drawn. Here, ΔG_T and ΔG_R mean the free energy decrease upon binding of a ligand within the T and R quaternary structures, respectively, and the subscript *m* denotes the *m* number, which is the number of ligand molecules bound to Hb. It is assumed that solution conditions change the energy of the T system relative to that of the R system.

If the T_3 level is significantly higher than the R_3 level as indicated by black lines, the quaternary transition is expected to occur in the intermediate state around m = 2~3 and cooperativity would be observed for ligand binding. This corresponds to the solution condition (I). In contrast, if the T_3 level is significantly lower than the R_3 level as indicated by gray lines, the quaternary structure change occurs upon binding of the fourth ligand and in this case cooperativity would not be apparently observed for ligand binding. Since ΔG for the last step would be slightly larger than other ΔG_T, the binding constant would increase in the final stage of ligand binding, but the affinity for ligand would remain low until the final stage of ligand binding. This means that cooperativity is apparently lost despite the fact the fully liganded form adopts the R structure. Presumably this corresponds to the solution condition (V) of the present case. This interpretation is not compatible to the note that the quaternary structure transition occurs between T_2 and R_3 in the presence of BZF and IHP at pH 6.6 (5), but there is no experimental evidence in structure for the presence of R_3. The present study demonstrated that Hb adopts the T structure in the stage of m = 3.5.

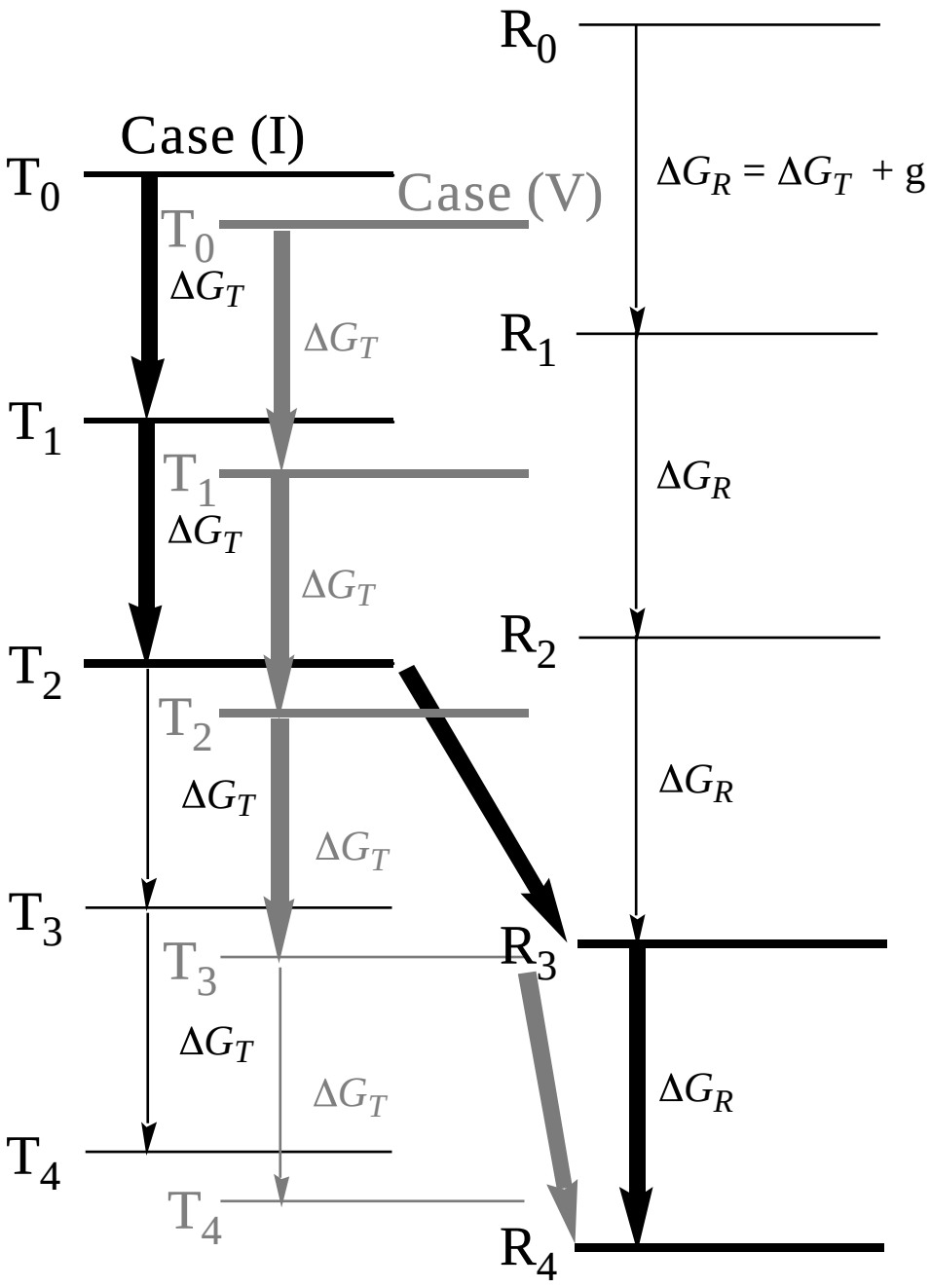

Figure 5.7 Schematic free energy diagram of Hb for oxygen binding. Gibbs free energy level of $T_0 - T_4$ and $R_0 - R_4$ are represented by horizontal bars, in which subscripts denote the *m* number. It is assumed that the $T_0 - T_4$ system is changed relative to the $R_0 - R_4$ system by solvent conditions (I-V). When T_3 is higher than R_3 (black), the system crossing occurs between T_2 to R_3 transition. When T_3 is lower than R_3 (gray), the system crossing occurs between T_3 to R_4 and as a result cooperativity is apparently lost.

References

1. Monod, J., Wyman, J., and Changeux, J. P. (1965) *J. Mol. Biol. 12,* 88-118.

2. Perutz, M. F. (1970) *Nature 228,* 726-739.

3. Perutz, M. F. (1979) *Annu. Rev. Biochem. 48,* 327-386.

4. Perutz, M. F., Fermi, G., Luisi, B., Shaanan, B., and Liddington, R. C. (1987) *Acc. Chem. Res. 20,* 309-321.

5. Yonetani, T., Park, S. I., Tsuneshige, A., Imai, K., and Kanaori, K. (2002) *J. Biol. Chem., 277,* 34508-34520.

6. Baldwin, J., and Chothia, C. (1979) *J. Mol. Biol. 129,* 175-220.

7. Fung, L. W.-M., and Ho, C. (1975) *Biochemistry 14,* 2526-2535.

8. Ho, C. (1992) *Adv. Protein Chem. 43,* 152-312.

9. Shibayama, N., Miura, S., Tame, R. H. J., Yonetani, T., and Park, S-Y. (2002) *J. Biol. Chem. 277,* 38791-38796.

10. Kitagawa, T. in Biological Applications of Raman Spectroscopy, Spiro, T. G. ed., Vol. 3, Chapter 3, John Wiley & Sons, 1988, New York, USA.

11. Rodgers, K. R., and Spiro, T. G. (1994) *Science, 265,* 1697-1699.

12. Hu, X., Rodgers, K. R., Mukerji, I., and Spiro, T. G. (1999) *Biochemistry 38,* 3462-3467.

13. Nagai, M., Kaminaka, S., Ohba, Y., Nagai, Y., Mizutani, Y., and Kitagawa, T. (1995) *J. Biol. Chem. 270,* 1636-1642.

14. Nagai, M., Wajcman, H., Lahary, A., Nakatsukasa, T., Nagatomo, S., and Kitagawa, T. (1999) *Biochemistry, 38,* 1243-1251.

15. Nagai, M., Nishibu, M., Sugita, Y., Yoneyama, Y., Jones, R. T., and Gordon, S. (1975) *J. Biol. Chem. 250,* 3169-3173.

16. Kaminaka, S., and Kitagawa, T. (1995) *Appl. Spectrosc. 49,* 685-687.

17. Ogura, T., Takahashi, S., Hirota, S., Shinzawa-Itoh, K., Yoshikawa, S., Appelman, E. H., and Kitagawa, T. (1993) *J. Am. Chem. Soc. 115*, 8527-8536.

18. Kaminaka, S., and Kitagawa, T. (1992) *Appl. Spectrosc. 46*, 1804-1808.

19. Uesugi, Y., Mizutani, Y., and Kitagawa, T. (1997) *Rev. Sci. Instrum. 68*, 4001-4008.

20. Mizutani, Y., and Kitagawa, T. (2001) *Chem. Rec. 1*, 258-275.

21. Hu, S., Smith, K. M., and Spiro, T. G. (1996) *J. Am. Chem. Soc. 116*, 12638-12646.

22. Hu, S., Morris, I. K., Singh, J. P., Smith, K. M., and Spiro, T. G. (1993) *J. Am. Chem. Soc. 115*, 12446-12458.

23. Nagai, K., Kitagawa, T., and Morimoto, H. (1980) *J. Mol. Biol. 136*, 271-289.

24. Mizutani, Y., and Kitagawa, T. (2001) *J. Phys. Chem. B 105*, 10992-10999.

25. Lim, M., Jackson, T. A., and Anfinrud, P. A. (1993) *Proc. Natl. Acad. Sci. U.S.A. 90*, 5801-5805.

26. Kuczera, K., Lambry, J.-C., Martin, J.-L., and Karplus, M. (1993) *Proc. Natl. Acad. Sci. U.S.A. 90*, 5805-5809.

27. Friedman, J. M., Rousseau, D. L., Ondrias, M. R., and Stepnoski, R. A. (1982) *Science, 218*, 1244-1246.

28. Friedman, J. M., Rousseau, D. L., and Ondrias, M. R. (1982) *Ann. Rev. Phys. Chem. 33*, 471-491.

29. Harada, I., and Takeuchi, H. (1986) in Spectroscopy of Biological Systems (Clark, R. J. H., and Hester, R. E., Eds.) pp. 113-175 John, Wiley & Sons, Ltd. New York.

30. Nagatomo, S., Nagai, M., Tsuneshige, A., Yonetani, T., and Kitagawa, T. (1999) *Biochemistry 38*, 9659-9666.

31. Nagatomo, S., Nagai M., Shibayama, N., and Kitagawa, T. (2002) *Biochemistry, 41*, 10010 –10020.

32. Nagai, M., Aki, M., Li, R., Jin, Y., Sakai, H., Nagatomo, S., and Kitagawa, T. (2000)

Biochemistry 39, 13093-13105.

33. Imai, K., “Allosteric Effects in Haemoglobin” Cambridge University Press, Cambridge (1982).

34. Haruta, N., Aki, M., Ozaki, S., Watanabe, Y., and Kitagawa, T. (2001) *Biochemistry 40,* 6956-6963.

Acknowledgement

I would like to express my sincere thanks to Professor Teizo Kitagawa for his kind guidance, many valuable suggestions, and encouragement, as well as for critical reading of this thesis.

I am also deeply indebted to Dr. Takashi Ogura (Assistant Professor: the University of Tokyo) and Dr. Yasuhisa Mizutani (Assistant Professor: Kobe University) for their kind introduction of practical resonance Raman measurements to me and for their helpful suggestions and valuable discussions.

I would like to thank Professor Masako Nagai for her advice and helpful suggestions, especially, about preparation of hemoglobin which is a base of my thesis.

I wish to thank Dr. Hiroshi Hori (Osaka University) for his valuable suggestions and discussion, especially about EPR measurement, and Dr. Naoya Shibayama (Jichi Medical School) for his valuable advice about preparation of Ni-Fe hybrid Hemoglobin.

I also wish to thank all members of Kitagawa's laboratory for their useful discussions and kindness.

I also would like to thank Emeritus Professor Hideaki Chihara, Professor Nobuo Nakamura and Dr. Sadamu Takeda (Professor: Hokkaido University) for leading me to physical-chemistry.

Finally, I express my great thanks to my parents.